PhD Thesis
Electroweak phenomenology in standard model and extra dimensions

Takuya Kakuda

Graduate school of science and technology, Niigata University,Japan

February 24, 2014

Abstract

We study constraints on the Universal Extra Dimension (UED) by taking into account current results of the Large Hadron Collider (LHC). We focus on three types of phenomennological issues, namely Higgs production and decay processes at the LHC, the electroweak precision measurement, and the vacuum stability. We studied seven types of six-dimensional UED models as well as five-dimensional one. We have found that the Higgs signal strength gives typical lower bounds on compactification scale of extra dimension(s) as 650 GeV for the five-dimensional model and 800–1400 GeV for the six-dimensional models, respectively. The electroweak S, T parameters also give 700 GeV for the five-dimensional model and 900–1500 GeV for the six-dimensional models, respectively. We have estimated the ultraviolet cutoff scale in higher dimensional theory by vacuum stability bound by using four-dimensional effective theory approach.

Contents

1 Introduction **7**

2 Review on the Standard Model **9**
2.1 Higgs mechanism in electroweak symmetry 9
2.1.1 Higgs potential 9
2.1.2 Electroweak symmetry breaking 11
2.1.3 Yukawa sector 11
2.2 Renormalization 12
2.3 Renormalization group equation 15
2.3.1 Scale invariance and renormalization group 15
2.3.2 RGE for the SM gauge couplings 18
2.3.3 Gauge fixing 21
2.3.4 RGE for λ and Yukawa interaction 21

3 Phenomenology in electroweak sector **27**
3.1 Vacuum stability bound 27
3.1.1 Effective potential 27
3.1.2 RGE improvement on effective potential 29
3.2 Higgs production at the LHC 30
3.2.1 Higgs production and decay process at the LHC 30
3.2.2 Signal strength of Higgs boson decay 31
3.3 Electroweak S, T parameters 33
3.3.1 The ρ parameter 34
3.3.2 Custodial symmetry 35
3.3.3 S, T parameters 37
3.3.4 Analysis of S,T parameters 38

4 Extra dimensions and their electroweak phenomenology **41**
4.1 RGE and vacuum stability bound in UEDs 42
4.1.1 RGE in six-dimensional UED models 42
4.1.2 Running of Higgs quartic interaction and Vacuum Stability 45
4.2 Higgs signals at Large Hadron Collider in UEDs 48
4.2.1 Feature of Higgs signals in UED models 48

4.2.2 Strategy to constrain the KK mass scale . . . 49
4.2.3 Bound on KK scale from the current data . . . 52
4.2.4 S, T parameters in UEDs . . . 53
4.2.5 Numerical result of S, T parameters analysis . . . 57
4.3 Five-dimensional limits . . . 59

5 Summary and overview **63**

A RGE for SM and UEDs **65**
A.1 UEDs in orientable space . . . 65
A.2 Projective Sphere case . . . 66
A.3 RP^2 case . . . 67
A.4 mUED case . . . 68

B A, B functions **69**
B.1 A function . . . 69
B.2 B functions . . . 70
B.2.1 B_0 (scalar integral) . . . 70
B.2.2 B_1 (vector integral) . . . 71
B.2.3 B_{21} and B_{22} (tensor integral) . . . 73
B.3 Fermion loop . . . 74

C Two-point functions of gauge bosons in six-dimensional UEDs **77**
C.1 Notations . . . 77
C.2 Gauge boson two-point function in six-dimensional UEDs and mUED : Bosonic contribution . . . 78
C.2.1 UEDs on oriented geometry case . . . 79
C.2.2 RP^2, PS, mUED cases . . . 79

D Loop functions in single Higgs production and decay **81**

Chapter 1

Introduction

The standard model (SM) of elementary particles [1] is one of the masterpieces in theoretical physics. The SM is based on quantum field theory with three important concepts, gauge principle, renormalization, and the mechanism of spontaneous symmetry breaking. The gauge principle is a fundamental idea of interacting field theory. The renormalization fixes physical values. The mechanism of spontaneous symmetry breaking tells us what is our vacuum. The $SU(2)_L \times U(1)_Y$ gauge symmetry breaking occurs by non-zero vacuum expectation value of the Higgs doublet [2]. The SM was constructed based on these ideas, and it turn out to be very successful model today for explaining the results of collider experiments below ~ 100 GeV scale [3, 4].

The extra dimensional theory is one of a candidate of new physics. It was first suggested by Kaluza and subsequeutly developed by Klein in early 20th century [20, 21]. In late 20th century, Antoniadis [22] pointed out a possibility of realizing TeV scale extra dimension. After that, various types of extra dimensional models have been suggested. The Universal Extra Dimension (UED) models are a type of extra dimensional models. The UED assumes that all the SM particles can propagate in the extra dimensional bulk. The virtue of UED is that the lightest Kaluza-Klein particle (LKP) can be a dark matter. It is based on a symmetry of extra dimension, Kaluza-Klein (KK) parity [23, 24]. The minimal five-dimensional UED (mUED) based on orbifold extra dimension S^1/Z_2, was first suggested by Ref. [25]. The mUED and phenomenological constraints on it are well studied: electroweak S, T parameters gives a lower bound on KK scale as about 700 GeV [26], flavor changing neutral current detection experiment of $b \to s\gamma$ gives 600 GeV [27], the prospects of the mUED at the LHC and future linear collider has also been discussed in Ref. [28–43].

The UED has been extended by introducing more than one extra spacial dimension. We can construct six-dimensional models with various geometry of extra spacial dimensions. The models have been proposed based on two-torus, T^2/Z_2 [44], T^2/Z_4 [45, 46], $T^2/(Z_2 \times Z_2')$ [47], on two-sphere, S^2/Z_2 [48], on two-sphere with Stueckhelbarg field [49, 50], and on non-orientable manifold: the real projective plane RP^2 [51] and the projective sphere PS [52]. An advantage of six-dimensional models is that the number of generation is required to be three by the cancellation of six-dimensional gravitational and $SU(2)_L$ global anomaly [53]. The collider phenomenology in six-dimensional models has been proposed

for T^2/Z_4 [54–59], and for RP^2 [60–63]. As another way to extend the mUED, it has been considered introducing five-dimensional mass terms or brane localized interaction terms on five-dimensional bulk [64–66].

In this thesis, we study not only the mUED but also all the known six-dimensional UED models and their phenomenology cyclopaedically [67].

The vacuum stability is one of the most important phenomenology in this LHC era. In the SM case, Froggatt and Nielsen predicted Higgs and top masses to be 135 ± 9 GeV and 173 ± 5 GeV by assuming the electroweak vacuum must be stable up to Planck scale [68]. Currently it is suggested that the electroweak vacuum can be stable up to Planck scale with Higgs mass $m_H \sim 125$ GeV by using three-loop RGE [69, 70]. Unlike the SM case, the electroweak vacuum in UED models cannot be a stable up to such a high scale because KK tower accelerates an RG evolution. The ultraviolet (UV) cutoff scale Λ is most important to discuss an extra dimensional model. We need an upper bound on KK summation in loop processes. We estimate the highest possible UV cutoff Λ_{max} of six-dimensional UED models by discussing electroweak vacuum stability. In the mUED case, Λ_{max} is $\Lambda \lesssim 5M_{KK}$ [71]. We have newly analyzed an RGE of Higgs quartic interaction and top Yukawa for five and six-dimensional UED models without resorting to the approximation employed in the analysis of gauge coupling running proposed in [50].

By using Λ_{max} that we estimated from vacuum stability, we study collider phenomenology in five and six-dimensional UED models. The Higgs production at the LHC is mostly by the gluon fusion process through a top loop. In general UED models, the KK top loops enhance the cross section of the gluon fusion process. Since the Higgs production cross section is enhanced, the signal strength of Higgs to dibosons $H \to ZZ, WW$ and fermionic decays $H \to f\bar{f}$ are enhanced. Higgs decay to diphoton $H \to \gamma\gamma$ is a loop induced process, and thus sum of KK top and KK W loop contributions gives small suppression of $H \to \gamma\gamma$ decay cross section [72]. Due to this small suppression, the enhancement $H \to \gamma\gamma$ is smaller than other channels. Originally six-dimenaional case was proposed in [48], and diphoton decay rate was studied in [50]. Here we take into account more thorough data of Higgs production channels for each event category. We can find the details of production channels and event category from data of ATLAS collaboration [73–75] and CMS [76, 76, 77]. We also estimate constraints from electroweak S and T parameters [78, 79]. The contributions from KK Higgs boson and KK top were discussed [25, 26]. In addition to these, we take into account the contributions from KK gauge bosons as was first done in [67].

The thesis is organized as follows. First, we review the electroweak sector in the SM. Spontaneous symmetry breaking, renormalization, and RGE in the SM is core ideas to discuss electroweak phenomenology. We review these topics in Chapter 2. Next, in Chapter 3, we show basic issues on electroweak phenomenology that we focus on in this thesis. In Chapter 4, we show the results of our analysis, constraints from Higgs signal strength, electroweak S, T parameters, and upper bounds on Λ by RGE. Finally, we summarize our work and discuss our future prospects. The details of formula that we use in our analysis are summarized in Appendices.

Chapter 2

Review on the Standard Model

The SM has three types of gauge symmetry $SU(3)_c \times SU(2)_L \times U(1)_Y$, and the Higgs doublet field breaks $SU(2)_L \times U(1)_Y$ symmetry into $U(1)_{e.m.}$ spontaneously [2, 80]. When we consider radiative corrections in quantum field theory, we face divergences in loop integrals. Renormalization is the method that can remove such a divergence from the original Lagrangian. After the renormalization formulation, we can consider the effective Lagrangian taking into account radiative corrections. The renormalization technique need a renormalizaton scale, and thus physical parameters depend on renormalization scale. We can analyze the scale dependence of physical parameters by renormalization group equation (REG). In this chapter, we review the spontaneous symmetry breaking mechanism in the SM, renormalization formula, and the RGE of the coupling constants in the SM. Our notation is based on Ref [1].

2.1 Higgs mechanism in electroweak symmetry

2.1.1 Higgs potential

In order to consider spontaneous symmetry breaking in the SM, we start with $SU(2)_L \times U(1)_Y$ symmetric Lagrangian with gauge kinetic terms and Higgs Lagrangian,

$$\mathcal{L} = -\frac{1}{4} W^a_{\mu\nu} W^{a\mu\nu} - \frac{1}{4} B_{\mu\nu} B^{\mu\nu} + (D_\mu \Phi)^2 - V(\Phi), \tag{2.1}$$

$$V(\Phi) = \frac{\mu^2}{2} |\Phi|^2 + \frac{\lambda}{4} |\Phi|^4, \tag{2.2}$$

where $W^a_{\mu\nu} = \partial_\mu W^a_\nu - \partial_\nu W^a_\mu + f_{abc} W^b_\mu W^c_\nu, B_{\mu\nu} = \partial_\mu B_\nu - \partial_\nu B_\mu$ are field strength of gauge bosons. $SU(2)_L \times U(1)_Y$ gauge covariant derivative is

$$D_\mu = \partial_\mu - i g_2 I^a_W W^a_\mu + i g_Y \frac{Y}{2} B_\mu \tag{2.3}$$

with Pauli matrix $I^a_W = \frac{1}{2}\sigma^a$, hyper charge Y. μ^2 is mass parameter of the Higgs doublet Φ which can be negative, and λ is self interaction of Higgs sector. The electricmagnetic

charge Q is defined by the Gell-Mann Nishijima relation

$$Q = I_W^3 + \frac{Y}{2}. \tag{2.4}$$

The Higgs doublet field is defined by

$$\Phi = \frac{1}{\sqrt{2}} \begin{pmatrix} \phi_1 + i\phi_2 \\ \phi_4 + i\phi_3 \end{pmatrix} = \begin{pmatrix} \phi^+ \\ \phi^0 \end{pmatrix}, \tag{2.5}$$

where $\phi_{1,2,3,4}$ are component field of spin 1/2 representation of the $SU(2)_L$ $\phi^{+/0}$ are charged/neutral Higgs field. Φ has hyper charge Y =1. After the electroweak symmetry breaking we can write the ground state of Higgs doublet as

$$\langle \Phi \rangle = \begin{pmatrix} 0 \\ \frac{1}{\sqrt{2}} v \end{pmatrix}, \tag{2.6}$$

with v =246 GeV is non-zero vacuum expectation value of phsical Higgs field H. We can write the Higgs doublet by v and quantum fluctuation around v as

$$\Phi = \begin{pmatrix} \phi^+ \\ \frac{1}{\sqrt{2}}(v + H + i\chi) \end{pmatrix}. \tag{2.7}$$

The vacuum condition

$$\frac{dV(\Phi = \langle \Phi \rangle)}{d\langle \Phi \rangle} = 0 \tag{2.8}$$

gives the relation,

$$\mu^2 = -\frac{1}{2}\lambda v^2, \tag{2.9}$$

and then we can write the Higgs potential for physical Higgs field H as

$$\begin{aligned} V(H) = \frac{1}{2}\mu^2 H^2 &+ \frac{\lambda}{4}\left((\phi^+\phi^-)^2 + 2vH(\phi^+\phi^-) + H^2(\phi^+\phi^-) - \chi^2(\phi^+\phi^-)\right) \\ &+ \frac{\lambda}{16}\left(H^4 + 6v^2H^2 + 4v^3H + 4vH^3\chi^4 - 4vH\chi^2 - 2H^2\chi^2\right). \end{aligned} \tag{2.10}$$

We find the physical Higgs mass in the SM as a quadratic term of H, thus

$$m_H^2 = \frac{1}{2}\lambda v^2. \tag{2.11}$$

2.1.2 Electroweak symmetry breaking

Now we turn to Higgs-gauge interaction which comes from the kinetic term of the Higgs doublet,

$$\begin{aligned}
&\left| \left[-i\frac{g_2}{2} \begin{pmatrix} W_\mu^3 & \sqrt{2}W_\mu^+ \\ \sqrt{2}W_\mu^- & -W_\mu^3 \end{pmatrix} + i\frac{g_Y}{2}B_\mu \right] \begin{pmatrix} \phi^+ \\ \frac{1}{\sqrt{2}}(v+H+i\chi) \end{pmatrix} \right|^2 \\
&= \left[-i \begin{pmatrix} \frac{g_2^2-g_Y^2}{2g_Z}Z_\mu - eA_\mu & \frac{g_2}{\sqrt{2}}W_\mu^+ \\ \frac{g_2}{\sqrt{2}}W_\mu^- & g_Z Z_\mu \end{pmatrix} \begin{pmatrix} \phi^+ \\ \frac{1}{\sqrt{2}}(v+H+i\chi) \end{pmatrix} \right]^2 \\
&= \left| \left(\frac{g_2^2-g_Y^2}{2g_Z}Z_\mu - eA_\mu \right)\phi^+ + \frac{g_2}{2}W_\mu^+(H+v+i\chi) + \frac{g_2}{\sqrt{2}}W_\mu^-\phi^+ + g_Z Z_\mu \frac{1}{\sqrt{2}}(H+v+i\chi) \right|^2,
\end{aligned} \tag{2.12}$$

where g_2, g_Y are gauge coupling constant in $SU(2)_L \times U(1)_Y$ gauge symmetry, $g_Z^2 = g_Z^2 + g_Y^2$, $e = \frac{g_2 g_Y}{g_Z}$, $W^\pm, Z, A$ are defined by the weak mixing

$$\begin{aligned}
\begin{pmatrix} c_W & s_W \\ -s_W & c_W \end{pmatrix} \begin{pmatrix} W_\mu^3 \\ B_\mu \end{pmatrix} = \begin{pmatrix} Z_\mu \\ A_\mu \end{pmatrix}, \quad W_\mu^\pm = \frac{1}{\sqrt{2}}(W_\mu^1 \mp iW_\mu^2), \\
c_W = \frac{g_2}{g_Z}, \quad s_W = \frac{g_Y}{g_Z},
\end{aligned} \tag{2.13}$$

then we can find the masses of W, Z boson as

$$m_W = \frac{v}{2}g_2, \quad m_Z = \frac{v}{2}\sqrt{g_Y^2 + g_2^2}. \tag{2.14}$$

We used 't Hooft-Feynman gauge.

2.1.3 Yukawa sector

Next we turn to Yukawa sector. We write the doublet lepton and quark as

$$L_j^L = P_L L_j = \begin{pmatrix} \nu_j^L \\ l_j^L \end{pmatrix}, \quad Q_j^L = P_L Q_j = \begin{pmatrix} u_j^L \\ d_j^L \end{pmatrix}, \tag{2.15}$$

and right handed lepton and quarks as

$$l_j^R = P_R l_j, \quad u_j^R = P_R u^j, \quad d_j^R = P_R d_j, \tag{2.16}$$

where L_j, Q_j, l_j, u_j, d_j are Dirac spinor, and $P_L = \frac{1-\gamma_5}{2}$, $P_R = \frac{1+\gamma_5}{2}$ are projection operators. The index j explain generation of charged leptons l, neutrinos ν, up and down type quarks u and d. Electroweak charge assignment for these fermions is summarized in Table 2.1.

fields	L	l	Q	u	d
$SU(2)_L \times U(1)_Y$charge	(2,-1/2)	(1,-1)	(2,1/6)	(1,2/3)	(1,-1/3)

Table 2.1: Charge assignment for SM fermions.

The fermionic Lagrangian in electroweak sector is

$$\begin{aligned}\mathcal{L}_F = &\sum_j \left(\overline{L}_j^L \gamma^\mu D_\mu L_j^L + \overline{Q}_j^L \gamma^\mu D_\mu Q_j^L\right) \\ &+ \sum_j \left(\overline{l}_j^R \gamma^\mu D_\mu l_j^R + \overline{u}_j^R \gamma^\mu D_\mu u_j^R + \overline{d}_j^R \gamma^\mu D_\mu d_j^R\right) \\ &- \sum_{ij} \left(\overline{L}_j^L V_{ji}^l l_i^R \Phi + \overline{Q}_j^L V_{ji}^u u_i^R \overline{\Phi} + \overline{Q}_j^L V_{ji}^d d_i^R \Phi\right), \end{aligned} \tag{2.17}$$

where the covariant derivative D_μ acting on left-handed fermion L^L, Q^L with $SU(2)_L \times U(1)_Y$ gauge boson W_μ^a and B_μ, and the covariant derivative for the right-handed fermion involving only $U(1)_Y$ gauge boson B_μ since l^R, u^R, d^R are singlet for $SU(2)_L$. V_{ji}^l, V_{ji^u}, and V_{ji^d} are Yukawa coupling matrices, and $\overline{\Phi}$ is charge conjugate of Higgs doublet. Yukawa sector can give fermion masses with non-zero vacuum expectation value of Higgs field v. The femiron mass matrices are witten as

$$m_{ji}^f = \frac{v}{\sqrt{2}} V_{ji}^f. \tag{2.18}$$

and it is diagonalized by bilinear transformation for fermion generation.

2.2 Renormalization

When we calculate quantum corrections by integrating loop diagrams, we face divergences. The renormalization is the technique that we remove such a divergence. In order to remove divergence, we first stand on divergent bare tree level Lagrangian. Any bare parameters in the bare Lagrangian i.e. bare fields, bare masses and bare couplings, are divergent by themselves. We can divide the bare Lagrangian into finite with the physical part and unphysical divergent part, and after that, we calculate loop integral by using such a physical part of parameters. Finally, we cancel the divergences from loop diagrams by the bare parameters, and let only physical part survive. It is also important that we choose a renormalization scheme. There are various regularization schemes to isolate divergences from loop integrals. In this section, we apply a renormalization technique to two types of loop diagrams in ϕ^4 theory, and we use dimensional regularization and $\overline{\text{MS}}$ scheme.

Let us start with tree level Lagrangian for a real scalar boson ϕ as follow,

$$\mathcal{L} = \frac{1}{2}(\partial_\mu \phi)^2 - m^2\phi^2 - \frac{\lambda}{4!}\phi^4. \tag{2.19}$$

We can write 1-loop correction for 2-point function of scalar boson with (2.19) as

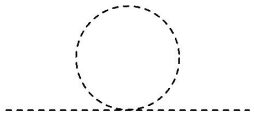

$$= \frac{1}{2}\lambda \int \frac{d^4k}{(2\pi)^4}\frac{1}{k^2-m^2}, \tag{2.20}$$

where the factor $\frac{1}{2}$ is the symmetric factor, k is the momenta in the internal leg. WHen we coose dimensional regularization scheme, we generalize our space-time dimensions as d-dimensions, and after calculation of the loop integral, we take $d \to 4$ limit. We can rewrite the 1-loop (2.20) as

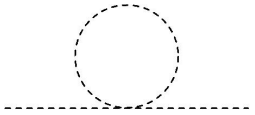

$$= \frac{1}{2}\lambda\mu^{4-d} \int \frac{d^dk}{(2\pi)^d}\frac{1}{k^2-m^2}. \tag{2.21}$$

The equation (2.21) is calculated in Appendix B, and we find

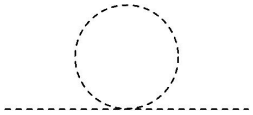

$$\begin{aligned} &= \lambda\mu^\epsilon A(m^2) \\ &= \lambda\mu^\epsilon \frac{i}{16\pi^2}m^2\left[\frac{2}{\epsilon}+1-\gamma+\log 4\pi+\log\frac{\mu^2}{m^2}+\mathcal{O}(\epsilon)\right] \\ &= \lambda\mu^\epsilon \frac{i}{16\pi^2}m^2\left[\tilde{\Delta}+\log\frac{\mu^2}{m^2}+\mathcal{O}(\epsilon)\right], \end{aligned} \tag{2.22}$$

where $\epsilon = 4-d$, $\gamma = 0.577$ is Eular-Madcheroni constant, and $\tilde{\Delta} = \frac{2}{\epsilon}+1-\gamma+\log 4\pi$. In $\epsilon \to 0$ limit($d=4$ limit), the first term in (2.22) is divergent. The form (2.22) means that the 1-loop correction for scalar 2-point function gives a divergent loop correction for scalar mass. In order to eliminate this divergence, let us reconsider the original Lagrangian (2.19).

We restart with the idea that the original Lagrangian (2.19) is divergent by itself. We call this original divergent Lagrangian as "bare" Lagrangian which is associated "bare" parameters;

$$\mathcal{L}_B = \frac{1}{2}(\partial_\mu\phi_B)^2 - m_B^2\phi_B^2 - \frac{\lambda_B}{4!}\phi_B^4. \tag{2.23}$$

We factorize the divergent part of bare field ϕ_B, bare mass m_B, and bare coupling λ_B as

$$\begin{aligned} \phi_B &= \sqrt{Z_\phi}\phi_R, \\ m_B &= Z_M Z_\phi^{-1} m_R, \\ \lambda_B &= Z_\lambda Z_\phi^{-2}\lambda_R, \end{aligned}$$

where ϕ_R, m_R, and λ_R are "re-normalized" field, mass, and coupling constant which are not divergent. The factors Z_ϕ, Z_m, and Z_λ are renormalization factors which cancel the divergence of bare parameters. From this factorization, we can rewrite (2.23) by renormalized

field, mass, and coupling, and we also can divide the bare Lagrangian into renormalized Lagrangian with divergent part as follow,

$$\begin{aligned}\mathcal{L}_B &= \frac{1}{2}Z_\phi(\partial_\mu\phi_R)^2 - Z_m m_R^2\phi_R^2 - Z_\lambda\frac{\lambda_R}{4!}\phi_R^4 \\ &= \frac{1}{2}(\partial_\mu\phi_R)^2 - m_R^2\phi_R^2 - \frac{\lambda_R}{4!}\phi_R^4 \\ &\quad + (Z_\phi - 1)\frac{1}{2}(\partial_\mu\phi_R)^2 - (Z_m - 1)m_R^2\phi_R^2 - (Z_\lambda - 1)\frac{\lambda_R}{4!}\phi_R^4. \end{aligned} \tag{2.24}$$

The first line is the renormalized Lagrangian which is not divergent and identified the physical parameters. The second line is counter terms of kinetic, mass, and coupling constant. When we start from divergent theory, we can formally divide the divergence from original theory as above, and now, let us cancel this counter terms with 1-loop divergence we saw above. We can only know the value of the renormalized parameters. We cannot know the bare theory, and thus we can freely choose the counter terms for easy calculation. As the simplest cancellation condition, we put a renormalization condition for scalar boson mass counter term as

$$(Z_m - 1) = \lambda\frac{i}{16\pi^2}\tilde{\Delta}, \tag{2.25}$$

where we have already put $\epsilon \to 0$. This renormalization scheme is $\overline{\text{MS}}$ scheme.

Next, let us calculate 1-loop correction for 4-point function using (2.24), that is related to be B_0 function defined in Appendix (B), as

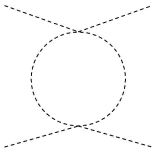

$$\begin{aligned} &= \mu^\epsilon\frac{3\lambda_R}{2}\int\frac{d^dk}{(2\pi)^d}\frac{1}{(k^2-m^2)\left((k-p)^2-m^2\right)} \\ &= \mu^\epsilon\frac{3\lambda_R}{2}B_0(p^2,m^2,m^2) \\ &= \mu^\epsilon\frac{3\lambda_R}{2}\frac{i}{16\pi^2}\int_0^1 dx\left(\tilde{\Delta} - \log\frac{\mu^2}{-p^2x(1-x)+m^2}\right), \end{aligned} \tag{2.26}$$

where x is the Feynman parameter. Since $\tilde{\Delta}$ does not depend on x, we can easily find the divergence in the vertex correction in $\epsilon \to 0$ limit, which is

$$\frac{3\lambda_R}{2}\frac{i}{16\pi^2}\left(\frac{2}{\epsilon}\right). \tag{2.27}$$

By a similar condition assign (2.25), we can cancel the divergence with counter term in $\overline{\text{MS}}$ scheme,

$$(Z_\lambda - 1)\frac{\lambda_R}{4!} = \frac{3\lambda_R}{2}\frac{i}{16\pi^2}\tilde{\Delta}. \tag{2.28}$$

2.3 Renormalization group equation

In this section, we review the idea of renormalization group equation (RGE) and RGE evolution of the SM. We have seen a renormalizable theory which contains kinetic terms, mass terms and dimensionless coupling terms of fields. In order to calculate a value of mass or coupling which contain loop corrections, we must choose an energy scale. This fact originate from the fact that we must introduce the regularization scale to regularize a loop divergence. RGE shows a scale dependence of running mass, coupling, and field. After we review some formula for RGE, we will calculate RGE for the SM coupling constants. We can find typical behavior of the SM gauge couplings, top Yukawa and Higgs quartic interaction, see for example [81]. The evolution of top Yukawa and Higgs quartic interaction is particularly an important information to estimate vacuum stability that we will review in the next chapter.

2.3.1 Scale invariance and renormalization group

We reviewed renormalization with dimensional regularization technique in section 2.2. We can write renormalized n-point function Γ^n_R without any divergences. Since we must introduce a scale μ in order to regularize bare n-point function Γ^n_B, renormalized n-point function Γ^n_R and its renormalization coefficient depend on the scale μ. Let us start with the theory of renormalized n-point coupling. When we write renormalization coefficient for field as

$$\sqrt{Z_\phi}\phi_R = \phi_B,$$

with renormalized field ϕ_R and bare field ϕ_B, the renormalized n-point coupling of ϕ_R generally written as

$$\frac{Z_g}{\sqrt{Z_\phi}^n} C_R = C_B$$

where C_R is renormalized coupling and C_B is bare coupling. We rewrite a renormalization coefficient of n-point function $Z_g/\sqrt{Z_\phi}^n = Z_n$. Let us write scale dependence explicitly,

$$\Gamma^n_B = Z_n(\mu)\Gamma^n_R(\mu), \tag{2.29}$$

where Γ^n_B is bare n-point function. The equation (2.29) impose

$$\mu\frac{d}{d\mu} Z_n(\mu)\Gamma^n_R(\mu, C_R, m_R, p) = 0. \tag{2.30}$$

We write renormalized mass and momentum of renormalized field of n-point function as m_R, p and a coupling as g_R explicitly. The scale invariance (2.30) written as

$$\left(-n\mu\frac{\partial}{\partial\mu}\sqrt{Z_n} + \mu\frac{\partial}{\partial\mu} + \mu\frac{\partial C_R}{\partial\mu}\frac{\partial}{\partial C_R} + \mu\frac{\partial m_R}{\partial\mu}\frac{\partial}{\partial m_R}\right)\Gamma^n_R(\mu, C_R, m_R, p) = 0, \tag{2.31}$$

and here we define

$$\gamma(g) \equiv \mu\frac{\partial}{\partial\mu}\log\sqrt{Z_n},$$
$$\beta(g) \equiv \mu\frac{\partial}{\partial\mu}g_R,$$
$$m_R\gamma_m(g) \equiv \mu\frac{\partial}{\partial\mu}m_R. \tag{2.32}$$

Then the equation (2.31) is written as

$$\left(\mu\frac{\partial}{\partial\mu}+\beta(g)\frac{\partial}{\partial g_R}-n\gamma(g)+m_R\gamma_m(g)\frac{\partial}{\partial m_R}\right)\Gamma_R^n\left(\mu,g_R,m_R,p\right)=0. \tag{2.33}$$

This equation is Renormalization Group Equation (RGE) and the coefficients (2.33) is β-function of field, coupling and mass. From β-function (2.33), we can find the scale dependence of field, coupling and mass.

Now, we consider a physical meanings of an RGE by solving them analytically. Let us start with RGE of an observable

$$A = A(g(\mu),\mu/Q), \tag{2.34}$$

where Q is a typical energy scale, for example, it is center of mass $\sqrt{s}$ when A is total cross section. In general, when we calculate A by renormalized perturbation theory, we can write A as

$$A(g(\mu),\mu/Q) = a_0 + a_1 g(\mu) + g(\mu)^2\left(a_2^{(1)}\log\frac{\mu}{Q}+a_2^{(0)}\right) + g(\mu)^3\left(a_3^{(2)}\log^2\frac{\mu}{Q}+a_3^{(1)}\log\frac{\mu}{Q}+a_3^{(0)}\right)+\cdots. \tag{2.35}$$

We can write scale invariance (2.31) for (2.34) as

$$\left(\mu\frac{\partial}{\partial\mu}+\mu\frac{\partial g(\mu)}{\partial\mu}\frac{\partial}{\partial g(\mu)}\right)A(g(\mu,\mu/Q))=0. \tag{2.36}$$

After a change of variable $t\equiv\log(\mu/Q)$, and $\frac{\partial}{\partial t}=\mu\frac{\partial}{\partial\mu}$, equation (2.36) is written as

$$\left(\partial/\partial t-\hat{H}\right)A(g(\mu),t)=0,\quad \text{where}\quad \hat{H}\equiv\mu\frac{\partial g(\mu)}{\partial\mu}\frac{\partial}{\partial g(\mu)}, \tag{2.37}$$

like as the form of Shrödinger equation and it can be solved as a linear differential equation. We can write $A(g(\mu),t)$

$$A(g(\mu),t) = e^{\hat{H}t}A(g(\mu),0) = \sum_{n=0}^{\infty}\frac{t^m\hat{H}^m}{n!}A(g(\mu),0)$$
$$= \sum_{n=0}^{\infty}\frac{\log^n(\mu/Q)}{n!}\left[-\beta(g(\mu))\frac{\partial}{\partial g}\right]^n\left(a_0+a_1 g+a_2^{(0)}g^2\cdots\right), \tag{2.38}$$

where we used $t = 0$ case of (2.35) in the second line in (2.38). Since β-function $\beta(g(\mu))$ can be expanded by order of coupling

$$\beta(g(\mu)) = -\beta_0 g(\mu)^2 - \beta_1 g(\mu)^3 - \beta_2 (\mu)^4 + \cdots . \tag{2.39}$$

Taking into account (2.38) (2.39), we can sort $A(g(\mu, t))$ by order of logarithms as

$$A(g,t) = a_0 + \sum_{n=0}^{\infty} \left(a_1 g \left[\beta_0 g \log\left(\mu/Q\right)\right]^n + \left(c_1 \frac{\beta_1}{\beta_0} g^2 + c_2 a_2^{(0)} g^2 \right) \left[\beta_0 g \log\left(\mu/Q\right)\right]^n + \cdots \right), \tag{2.40}$$

where $c_{1/2}$ are coefficient of order g^3 that we can count from n-th order derivative in (2.38), and we omitted the argument μ for coupling g. The first logarithm term of (2.40) is "Leading Log" (LL), the second one is Next to Leading Log (NLL), and so on. The LL terms have much larger contribution than NLL terms in low energy limit. The form (2.40) re-sorts all order of loop corrections (2.35) into order of LL, NLL, $\cdots$ by solving RGE. In other words, by solving RGE, we can calculate contributions of logarithm from quantum correction order by order.

We can calculate LL contribution just by taking into account 1-loop diagrams. Let us consider a real scalar ϕ^4 theory as an example. Since ϕ^4 theory does not have field renormalization at this order, we only have to take into account vertex correction diagram. Loop integral for vertex correction is

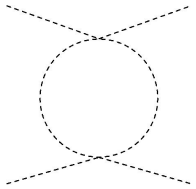

$$= \frac{3}{2}\lambda^2 \frac{i}{16\pi^2} \left(\tilde{\Delta} - \log \frac{\mu^2}{M^2} \right), \tag{2.41}$$

where g is coupling of ϕ^4 interaction, and M is mass of the scalar, coefficient $3/2$ is taking into account S, T, U channels and symmetric factor, $\tilde{\Delta}$ contains divergence and finite correction, and $g^2 \log\left(\mu^2/M^2\right)$ is LL in this theory. Two loop diagram in ϕ^4 theory contains not only LL but also NLL terms, as follow

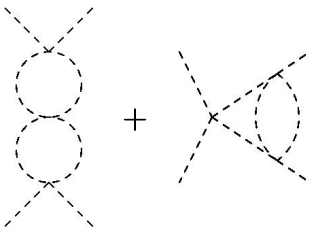

$$= i \frac{1}{16\pi^2} \lambda^2 \left(\tilde{\Delta} - C_1 g \log\left(\frac{\mu^2}{M^2}\right) - C_2 g^2 \log\left(\frac{\mu^2}{M^2}\right) \right), \tag{2.42}$$

where C_1, C_2 are coefficients which contain an information of loop factor, channels, symmetric factor and so on. The second term in (2.41) is LL, and the last term is NLL. On the other hand, we can diagrammatically draw any types of 2-loop diagram by replacing one of a tree level vertex in a 1-loop diagram by 1-loop diagram itself like Figure 2.1. In

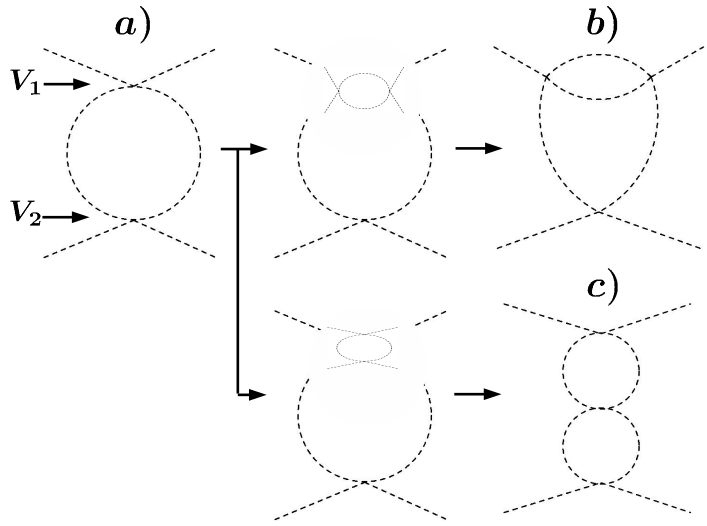

Figure 2.1: We can draw 2-loop diagram b) by replacing vertex V_1 by s-channel of 1-loop diagram a) itself. c) also can drawn by replacing V_1 by t-channel of a). The replacing also must apply to vertex V_2. By such a way, all order of loop diagrams can be drawn by replacing tree level vertex by 1-loop diagram.

such a way, we can count LL contributions from all order of diagrams by counting only LL in 1-loop diagrams. In other words, we can calculate all the LL in higher order loops by iteration of coupling by 1-loop diagram. This operation corresponds to replacing one of g in equation (2.41) by $g\log(\mu^2/M^2)$. Thus, in order to count contributions of LL, we just have to take into account only 1-loop diagrams. This "re-summation" of LL is called "1-loop RGE". The "2-loop RGE" is also known as re-summation of NLL terms. We will show the SM 1-loop RGE in the following subsections.

2.3.2 RGE for the SM gauge couplings

Now, we show 1-loop RGE running for the SM gauge couplings. In this thesis, we omit some details of derivation of gauge coupling RGE. The 1-loop gauge coupling β-functions in the SM are well known

$$\frac{d}{d\log\mu}\alpha_i = -\frac{\mathrm{b}_i}{2\pi}\alpha_i, \tag{2.43}$$

with

$$\begin{aligned}\mathrm{b}_{SU(N)} &= -\frac{11}{3}\sum_{\text{vector}} C_2(\text{Adjoint}) + \frac{2}{3}\sum_{\text{Weyl}} C(r) + \frac{1}{3}\sum_{\text{Scalar}} C(r)\\ \mathrm{b}_{U(1)} &= \frac{2}{3}\sum_{\text{Weyl}} Y_f^2 + \frac{1}{3}\sum_{\text{Scalar}} Y_H^2,\end{aligned} \tag{2.44}$$

gauge group	b_i
$SU(3)_c$	-7
$SU(2)_L$	-19/6
GUT normalization $U(1)_Y$	123/50
$U(1)_Y$	41/10

Table 2.2: Value of b_i in the SM gauge group with GUT normalization $U(1)_Y$ and non-GUT normalization $U(1)_Y$.

where $\alpha_i = g_i^2/4\pi$ is is fine structure constant for arbitrary type of gauge group with index i, C_2(Adjoint) is quadratic Casimir operator defined by

$$T_G^a T_G^a = C_2(\text{Adjoint}) \tag{2.45}$$

where T_G^a is a generator of G. The value of C_2(Adjoint) for $SU(N)$ gauge group is N . $C(r)$ is Dinkin index defined by

$$tr\left[T_r^a T_r^b\right] C(r)\delta^{ab}, \tag{2.46}$$

for representation r. The value of $C(r)$ for a $SU(N)$ gauge group is 1/2 for the fundamental representation. Y_f, Y_H are hypercharge of Weyl fermions and Higgs we reviewed in subsection 2.1.1, and 2.1.3.

Note that we can freely choose a overall coefficient of quantum numbers in $U(1)$ gauge group. Thus, when consider grand unified theory, we often choose a normalization for $U(1)_Y$ as

$$\frac{5}{3}{g_{Y.GUT}}^2 = {g_Y}^2. \tag{2.47}$$

We summarize β-function coefficient b_i in the SM case in Table 2.2. We must choose an input value of the RGE at the weak scale value of gauge couplings. These values are well measured [97];

$$g_Y(m_Z) = 0.343, \quad g_{Y\,\mathrm{GUT}}(m_Z) = 0.444, \quad g_2(m_Z) = 0.638, \quad g_s(m_Z) = 1.217. \tag{2.48}$$

The 1-loop RGEs of gauge couplings are closed by themselves, thus we can simply solve them as differential equations. Figure 2.3.2 shows RGE running of SM gauge couplings from the weak scale to Planck scale as a numerical result. The left figure of Figure 2.3.2 shows the RGE running in non-GUT normalization case of $U(1)_Y$ coupling. The right one is GUT normalization of $U(1)_Y$ case. The vertical axis is gauge coupling constant g_i corresponding to energy scale μ, and the horizontal axis is reference energy scale. Green, red and blue lines show runnings of strong coupling g_c, g_2, and g_Y. We can see that value of gauge coupling constants in right figure of 2.3.2 become close in high energy region around 10^{17} GeV compare with left figure. We are able to see not only high energy region but also a

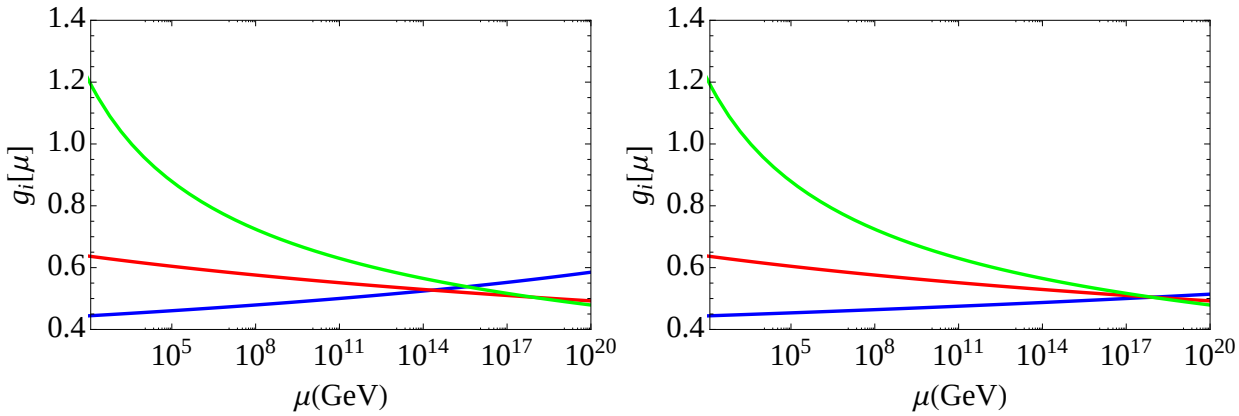

Figure 2.2: RGE evolution of the SM gauge couplings. Green line shows g_s running, red line is g_2 and blue is g_Y. Left figure using non-GUT normalized $U(1)_Y$ coupling g_Y, and right figure using GUT normalized g_Y.

region lower than weak scale. Figure 2.3 shows the running of g_s in the SM from MeV scale to 1 TeV scale in 1-loop RGE. We choose the boundary condition as same as (2.48) We can see that the strong coupling becomes very large compare with the high energy region case we can see in Figure . If coupling constants become larger than $\sqrt{4\pi}$ (sometime people takes 3 this value, however we take $\sqrt{4\pi}$). we cannot apply a perturbation theory to effective theory. In the SM, there is a sale that the strong coupling becomes larger than $\sqrt{4\pi}$ we can see in Figure 2.3. Such a scale is Λ_{QCD} and its value is near 220 MeV. It is known that such a running behavior can be explained by asymputotic freedom [82]. In the lower region from Λ_{QCD}, we need other effective theory than the SM. It is well known that, in such energy region, hadoronic theory is required to calculate several physical value.

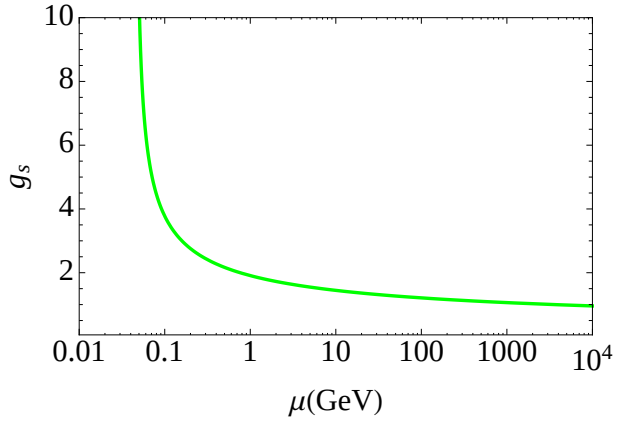

Figure 2.3: Asymptotic freedom of strong coupling g_s in the SM.

2.3.3 Gauge fixing

RGE running can be found from β-function that we reviewed in (2.33). In order to calculate 1-loop β-function of couplings, we must consider gauge fixing because the number of 1-loop diagrams are depend on gauge fixing. General 't Hooft gauge fixing term are written as

$$\mathcal{L}_{\rm GF} = -\frac{1}{2\xi^i}\left(\partial^\mu V_\mu + \xi M \phi_i\right)^2, \tag{2.49}$$

where ξ is a gauge fixing parameter, V_μ is arbitrary gauge field, M is mass parameter in gauge fixing, and ϕ_i are Goldstone mode comes from non physical component of Higgs field. We often choose this type of gauge fixing term to cancel quadratic transition term of gauge boson and Goldstone mode. In the case of the SM, we choose a concrete form of 't Hooft gauge as

$$\mathcal{L}_{\rm GF} = -\frac{1}{2}\left(F^{\gamma 2} + F^{Z 2} + 2F^+F^-\right)^2, \tag{2.50}$$

with gauge fixing functions

$$\begin{aligned} F^\pm &= \frac{1}{\xi^W}\partial^\mu W_\mu^\pm \mp i m_W \sqrt{\xi^W}\phi^\pm, \\ F^Z &= \frac{1}{\xi^Z}\partial^\mu Z_\mu - m_Z\sqrt{\xi^Z}\chi, \\ F^\gamma &= \frac{1}{\xi^\gamma}\partial^\mu A_\mu, \end{aligned} \tag{2.51}$$

where $\xi^{W,Z,\gamma}$ are gauge fixing parameter for W, Z, boson and photon. Since photon is massless and it does not 'eat' Goldstone mode, the photon gauge fixing term does not have mass term. We use the simplest 't Hooft gauge, $\xi^{W,Z,\gamma} = 1$ gauge, called 't Hooft-Feynman gauge.

2.3.4 RGE for λ and Yukawa interaction

Next let us turn to RGE running of Higgs quartic interaction and Yukawa couplings in the SM. A brief review on these RGEs in the SM is summarized in [81] for example. First, let us focus on the Higgs quartic interaction. Since we are using 't Hooft-Feynman gauge, we must take into account eight types of 1-loop diagrams that we summarize in Figure 2.4. The diagram 1 in Figure 2.4 simply comes from Yukawa coupling, diagram 2 generated by 3-point derivative coupling; Higgs-Goldstone-gauge, diagrams 3 and 4 are simply generated by 4-point interaction; Higgs quartic point, Higgs-Higgs-Goldstone-Goldstone, and Higgs-Higgs-gauge-gauge. The triangle diagrams 5 and 6 generated by one 4-point interaction and two 3-point derivative couplings. Diagram 7 is generated by four 3-point derivative coupling, and diagram 8 simply comes from Yukawa coupling. The other 1-loop diagrams are not divergent, and thus the diagrams we must take into account are fulfilled

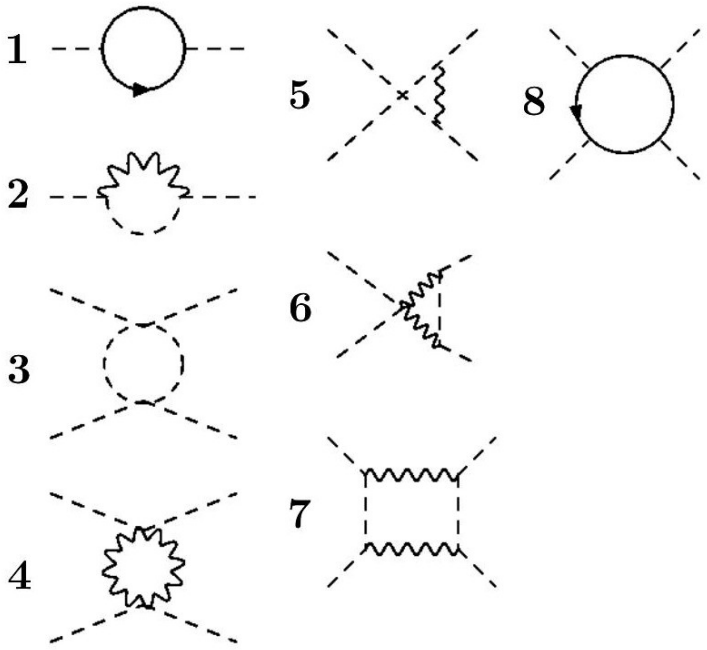

Figure 2.4: 1-loop diagrams for Higgs quartic interaction in 't Hooft-Feynman gauge.

by Figure 2.4. Self energy diagrams 1 and 2 affect λ through a field renormalization factor, like

$$\lambda_0 = Z_\lambda (Z_H)^{-2} \lambda_R, \tag{2.52}$$

where λ_0 is bare coupling of Higgs quartic interaction, Z_λ is vertex renormalization factor, Z_H is field renormalization factor, and λ_R is renormalized quartic interaction. The β-function for λ is found to be

$$\begin{aligned}\mu\frac{d}{d\mu}\lambda &= \beta_\lambda \\ &= \frac{1}{16\pi^2}\left\{6\lambda^2 - \left(3g_Y^2 + 9g_2^2\right) + \frac{3}{2}\left(g_Y^4 + 2g_Y^2 g_2^2 + 3g_2^4\right) + 4\lambda\sum_i N_{ci} y_{fi}^2 - 8\sum_i N_{ci} y_{fi}^4\right\},\end{aligned} \tag{2.53}$$

where the index i runs for of the SM fermions, N_{ci} is the color factor correspond to fermion f_i, and its value is for charged lepton N_{ci}=1 and for up type and down type quarks have N_{ci}=3.

Since β-function of λ contains Yukawa and gauge interactions, we must solve the RGE as simultaneous differential equations with gauge and Yukawa interactions to know an evolution of λ. We already know gauge coupling β-functions in subsection 2.3.2, and thus let us consider β-function of Yukawa interaction. The type of diagrams for Yukawa

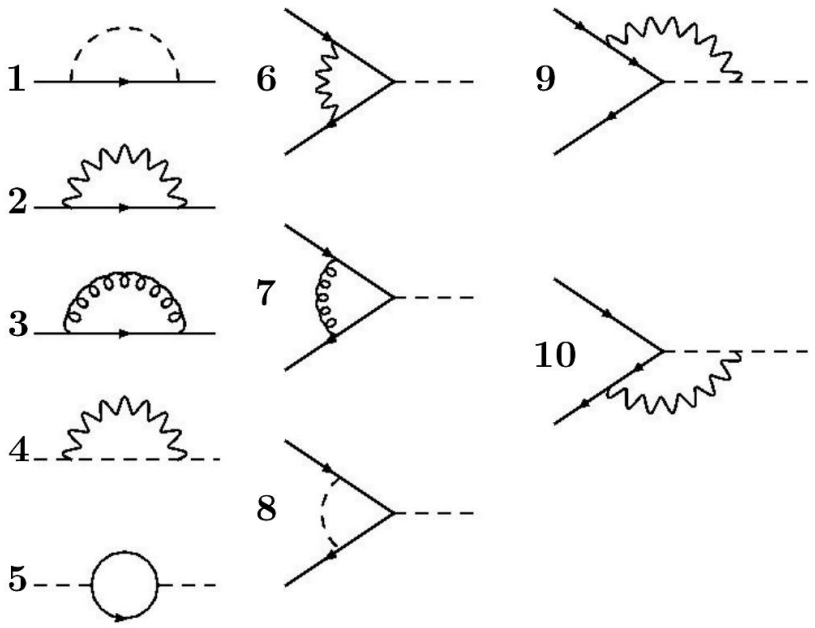

Figure 2.5: 1-loop diagrams for Yukawa interaction in 't Hooft-Feynman gauge.

interaction in 't Hooft-Feynman gauge is summarized in Figure 2.5. There are also ten types of diagrams. Fermion self energy 1, 2, 3, and Higgs self energy 4 and 5 affect Yukawa interactions through field renormalizations;

$$y_{fi0} = Z_{y_{fi}}(Z_{fiL})^{-1}(Z_{fiR})^{-1}(Z_H)^{-1/2}y_{fiR} \tag{2.54}$$

where $Z_{y_{fi}}$ is renormalization coefficient for Yukawa vertex correction, $Z_{fiL/R}$ is field renormalization coefficient for left/right handed fermion same as (2.52). Vertex corrections 6, 7 and 8 are simply generated by 3-point gauge and Yukawa couplings. 3-point interaction in diagrams 9 and 10 are derivative coupling which generates Higgs-Goldstone-gauge interaction. The diagrams 3 and 7 are generated by strong interaction, thus charged lepton Yukawa β-function does not contain their effects. β-functions for charged lepton, up type, and down type quarks are found to be

$$\beta_{y_{lk}} = \frac{1}{16\pi^2}\left\{-\frac{15}{4}g_Y^2 - \frac{9}{4}g_2^2 + \frac{3}{2}y_{lk}^2 + \sum_i N_{ci}y_{fi}^2\right\}y_{lk} \tag{2.55}$$

$$\beta_{y_{uk}} = \frac{1}{16\pi^2}\left\{-\frac{17}{12}g_Y^2 - \frac{9}{4}g_2^2 - 8g_s^2 + \frac{3}{2}y_{uk}^2 + \sum_j y_{dj}^2(V_{kj}V_{jk}^\dagger) + \sum_i N_{ci}y_{fi}^2\right\}y_{uk} \tag{2.56}$$

$$\beta_{y_{dk}} = \frac{1}{16\pi^2}\left\{-\frac{15}{12}g_Y^2 - \frac{9}{4}g_2^2 - 8g_s^2 + \frac{3}{2}y_{dk}^2 + \sum_j y_{uj}^2(V_{kj}^\dagger V_{jk}) + \sum_i N_{ci}y_{fi}^2\right\}y_{uk} \tag{2.57}$$

where the index $k = (1, 2, 3)$ shows generation of fermions. Since input values of light flavor Yukawa interactions are much smaller than top Yukawa, RG evolutions of light flavor are much smaller than top Yukawa. Thus, when we estimate running of λ and top Yukawa, we neglect contributions from light flavor Yukawa RGEs.

The input values of λ and top Yukawa y_t are defined by Higgs and top mass. In the SM, the physical Higgs mass is defined at the tree level by

$$m_H^2 = \frac{1}{4}\lambda v^2$$

as we saw in (2.11). The input value of λ is

$$\lambda(m_Z) = \frac{4m_H^2(m_Z)}{v^2},$$

and the latest data of physical Higgs mass is

$$m_H = \begin{cases} 125.5 \pm 0.2^{+0.5}_{-0.6} \text{ GeV (ATLAS)} \\ 125.6 \pm 0.4 \pm 0.2 \text{ GeV (CMS)} \end{cases} \tag{2.58}$$

as a pole mass [13, 83]. If we neglect mass correction from electroweak interaction, we can make an approximation $m_H \sim m_H(m_Z)$.

Input values of top Yukawa are defined by effective top mass in top pole mass scale, like

$$m_t(M_t) = \frac{v}{\sqrt{2}} y_t(M_t). \tag{2.59}$$

A top pole mass M_t is measured by tevatron and LHC, the current value is

$$M_t = \begin{cases} 173.20 \pm 0.87 \text{ GeV (Tevatron)} \\ 173.29 \pm 0.95 \text{ GeV (LHC combine)} \end{cases}, \tag{2.60}$$

we can find in Ref. [84, 85]. In addition, since top has color charge, we must use imput top mass which contain QCD correction as a input value of RGE. Such a physical top mass is called $\overline{\text{MS}}$ top mass. The value of $\overline{\text{MS}}$ is well studied in Ref. [69, 70, 86] for example. In this section, we employ $\overline{\text{MS}}$ top mass and Higgs mass [70]

$$m_t(M_t) = 163.3 \text{ GeV}, \qquad m_H = 125.6 \text{ GeV}.$$

Let us choose input values of RGE as

$$\lambda(m_H) = \frac{2 \times (125.6(\text{GeV}))^2}{(246(\text{GeV}))^2} \sim 0.521, \quad y_t(M_t) = \frac{\sqrt{2} \times 163.3(\text{GeV})}{246(\text{GeV})} \sim 0.937. \tag{2.61}$$

Figure 2.6 shows the RGE running of top Yukawa and λ in the SM. The blue line shows running of top Yukawa, and the red is running of λ. The vertical axis is the value of

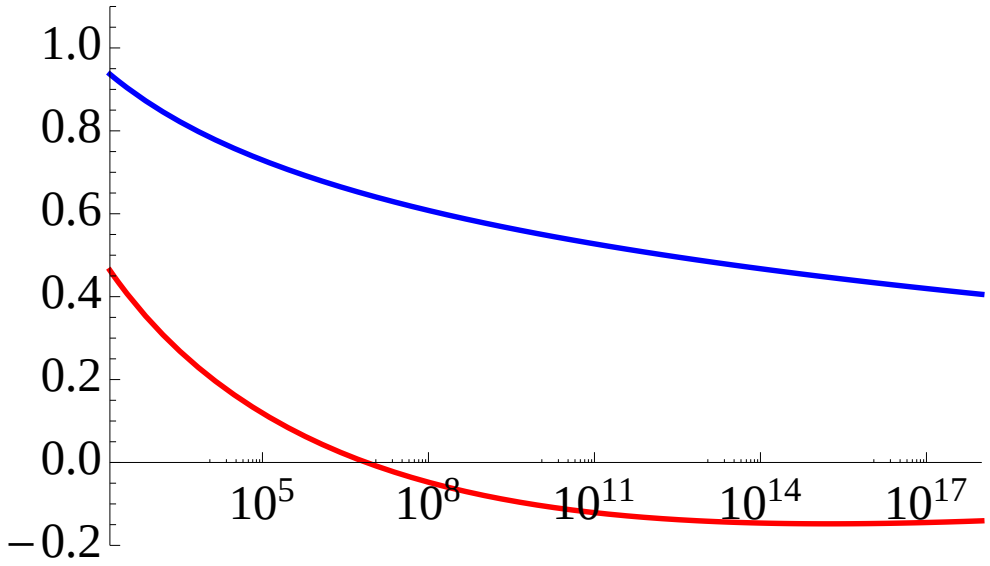

Figure 2.6: RGE running of top Yukawa y_t and Higgs quartic interaction λ. The blue line is y_t, and the red line is λ. Vertical axis is a value of coupling constant, horizontal axis is reference scale which has unit GeV.

couplings, and the horizontal axis is energy scale in GeV. We find that λ becomes negative in around the scale $\sim 10^7$ GeV. This point is quite important when we estimate a stability of vacuum in next chapter. Note that Figure 2.6 is a result of 1-loop RGE and that when we take into account 2-loop RGE, this running raise up from 1-loop RGE case. In 2-loop case, the scale that λ becomes zero appear in higher scale than 1-loop case. λ can be positive up to Planck scale with top pole mass $M_t \sim 171.5$ GeV. In addition, 3-loop RGE has quite small negative contribution to running. Such a result is estimated by [69, 70].

Chapter 3

Phenomenology in electroweak sector

In this section, we review the phenomenology of the electroweak interaction in the SM. First we review the effective potential and vacuum stability bound. A shape of Higgs potential in high energy region is non-trivial even in the SM. We can consider two types of scenario, stable/unstable vacuum, in high energy limit of Higgs potential. We can give various types of constraints for model parameters corresponding to these two scenarios. Next we review Higgs production and decay process at the LHC. We check important value, the signal strength of Higgs boson at the LHC. Finally we review electroweak precision measurement and constraint on new physics from the fit of its experimental result [26, 87]. We will return to these point for point of extra dimensional theory as a candidate beyond the SM in Chapter 4.

3.1 Vacuum stability bound

We can apply the RGE technique to estimate the stability of our electroweak vacuum. In order to calculate vacuum stability, let us consider the effective potential and its quantum correction. Next, we see the effective potential for high field value region in the SM.

3.1.1 Effective potential

We first define the generating functional of generalized Green's functions,

$$\begin{aligned} Z[J] = \exp(iW[J]) &=< 0|T\left[\exp\left(i\int d^4x \sum_i J_i(x)\phi_i(x)\right)\right]|0> \\ &= N\int \mathcal{D}\phi \exp\left(iS[\phi] + \int d^4x \sum_i J_i(x)\phi_i(x)\right), \end{aligned} \tag{3.1}$$

where the square bracket indicates functional nature of Z and W, $W[J]$ is the generating functional of connected Green's functions, $T[\cdot]$ is the time ordering operator, $J_i(x)$ is the external source field of the corresponding field $\phi_i(x)$, and the path integral in the second row is done over all the fields contained in the theory.

Next, we define the effective action $\Gamma[\varphi]$ from Legendre transformation of $W[J]$, that is

$$\Gamma[\varphi] = W[J] - \int d^4x \sum_i J_i(x)\varphi_i(x), \tag{3.2}$$

where $\varphi_i(x)$ is the expectation value, or in other ward classical field, value of the given field $\phi_i(x)$, generated by the source J_i. Explicitly, it is

$$\begin{aligned}\varphi_i(x) &= \frac{\langle 0|T\phi_i(x)\exp\left(i\int d^4x\sum_i J_i(x)\phi_i(x)\right)|0\rangle}{\langle 0|\exp\left(i\int d^4x\sum_i J_i(x)\phi_i(x)\right)|0\rangle} \\ &= \frac{\delta}{\delta J_i(x)}W[J].\end{aligned} \tag{3.3}$$

As the same time, have

$$\begin{aligned}\frac{\delta}{\delta\varphi_i(x)}\Gamma[\varphi_i(x)] &= \frac{\delta J_i(x)}{\delta\varphi_i(x)}\frac{\delta}{\delta J_i(x)}W[J_i(x)] - \left(\frac{\delta}{\delta\varphi_i(x)}J_i(x)\right)\varphi_i(x) - J_i(x) \\ &= -J_i(x)\end{aligned} \tag{3.4}$$

which is a duality relation of Legendre transformation.

We can write a concrete form of the effective action. For a boson system for example, we have

$$\begin{aligned}i\Gamma[\varphi_i(x)] &= -\frac{1}{2}\varphi_i(x)(\Delta_F^{-1})^{ij}\varphi_j(x) + \kappa^{\text{1PI}}[\varphi] \\ &= i\int d^4x\left[-\frac{1}{2}\varphi(x)(\partial^2 + m_\varphi^2)\varphi(x) - \frac{\lambda}{4!}\varphi(x)^4 + (\text{loop-contribution})\right],\end{aligned} \tag{3.5}$$

where κ^{1PI} is the summation of 1 particle irreducible diagrams, $(\Delta_F^{-1})^{ij}$ is the propagator from the boson $\phi_j(x)$ to $\phi_i(x)$, the legs i, j put ϕ_i and ϕ_j for different field.

Next we consider the vacuum expectation value of the field $\phi_i(x)$. In the absence $J(x)$, the definition of the expectation value of the field $\phi_i(x)$ becomes

$$\varphi_i(x) = \langle 0|\phi_i(x)|0\rangle\,,$$

and this imposes

$$\frac{\delta\Gamma[\varphi(x)]}{\delta\varphi_i(x)} = 0, \tag{3.6}$$

This condition is vacuum condition. If the field value $\varphi_i(x)$ does not depend on space-time coordinates, we can rewrite the equation (3.5) as

$$\begin{aligned}\Gamma[\varphi_i(x) = \varphi_i] &= \left[-\frac{1}{2}m_{\varphi_i}^2\varphi_i^2 - \frac{\lambda}{4!}\varphi_i^4\right]\int d^4x \\ &= -V(\varphi_i)\int d^4x. \end{aligned} \tag{3.7}$$

The function $V(\varphi_i)$ is an effective potential. The fact that the effective action generates 1PI vertex functions implies that the effective potential $V(\varphi_i)$ generates 1PI vertex functions with zero momenta in the external lines.

3.1.2 RGE improvement on effective potential

The effective potential generally contains infinite number of loop corrections. Since physical meaning of RGE is the re-summation of logarithms which arise from loop corrections, we can apply the RGE technique to calculate quantum corrections in an effective potential. We write the effective potential in Higgs sector as V_{eff}. We can write the effective potential schematically,

$$V_{eff} = m_{HB}^2 H_B^2 + \lambda_B H_B^4 + (\text{loops}), \tag{3.8}$$

where m_{HB} is the bare Higgs mass, λ_B is the bare coupling in Higgs sector, and H_B is the classical value of bare Higgs field. We can take into account loop corrections (loops) by RGE technique. After a renormalization, we can write (3.8) as

$$V_{eff}(H) = m_H^2(H)H^2 + \lambda_H(H)H^4. \tag{3.9}$$

We chose the renormalization scale to be a scale of renormalized classical field Higgs field value H. When we consider a scale much higher than $m_H(H)$, we can neglect the first term in (3.9). We can estimate the shapes of Higgs potential value in high field value region by running of λ. By the RG evolution of λ, we can consider some futures of electroweak vacuum. It is discriminated by the scale whether $\lambda(H) = 0$ appears or not. First, in the case that $\lambda(H)$ is everywhere positive, the electroweak vacuum is the global minimum, and is stable like a) in Figure 3.1. In the case that we find the scale where $\lambda(H) = 0$, the electroweak vacuum decay into the true vacuum like b) in Figure 3.1. Even if effective potential will not raise up spontaneously in that case, we can raise it up by higher dimensional operators. The important things when discussing a stability of vacuum is that whether vacuum transition rate is smaller than the life time of the universe. In order to avoid the decay of our universe, we must let the vacuum decay rate smaller than the life time of the universe. The vacuum transition rate is calculated by height of the effective potential, and naively the fourth root of height is almost same order with the scale $\lambda = 0$. The topical value of such a scale to avoid vacuum decay is $\sim$100 TeV. Therefore, we must consider whether $\lambda = 0$ appear below $\sim$100 TeV or not. When we consider a new

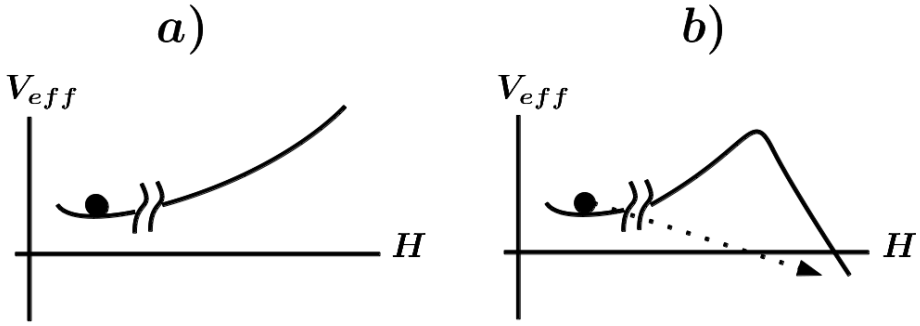

Figure 3.1: The schematic pictures of effective potential. The black point in picture is electroweak vacuum. a) is stable vacuum and b) is unstable vacuum.

physics model. We bound its model parameters whether $\lambda = 0$ or not. Such a bound is vacuum stiability bound.

Note that the Coleman-Weinberg potential [88], which is n-point interaction generated by infinite sum of 1-loop diagram, is also important in high field value region. However in this thesis, we omit a review of Coleman-Weinberg potential. In Ref [69, 70], they analyzed effective potential taking into account the Coleman-Weinberg potential in the SM.

3.2 Higgs production at the LHC

In July 4th 2012, ATLAS and CMS experiments announced that a new particle which has mass around 125 GeV is discovered [5, 6]. About eight month after, in March 2013, it is confirmed that the new particle is the SM Higgs boson [13]. That is, it is a scalar boson, not a pseudo scalar nor other spin particle, it couples with gauge bosons with g_2 and g_Z like values, and couples with top with top Yukawa [89]. Since we discover the Higgs boson with mass $\sim$125 GeV, we can completely calculate a production and decay cross section of the Higgs in the SM.

In this section, we show the Higgs production/decay process in the SM Higgs boson case, and a ratio of cross section in the SM to those in other theories is defined as the signal strength. When a new physics model changes the cross section of the Higgs production and decay process, signal strength can give a bound on new physics model by comparing data with a prediction of new physics model.

3.2.1 Higgs production and decay process at the LHC

The process of Higgs at the LHC can be divided into two parts, Higgs production/decay process. Higgs production at the LHC mainly comes from the gluon fusion through the top loop. Other channels are tree level processes shown in Figure 3.2. Gluon fusion process has about 90 % contribution to Higgs production. Once prodected, Higgs can decay into

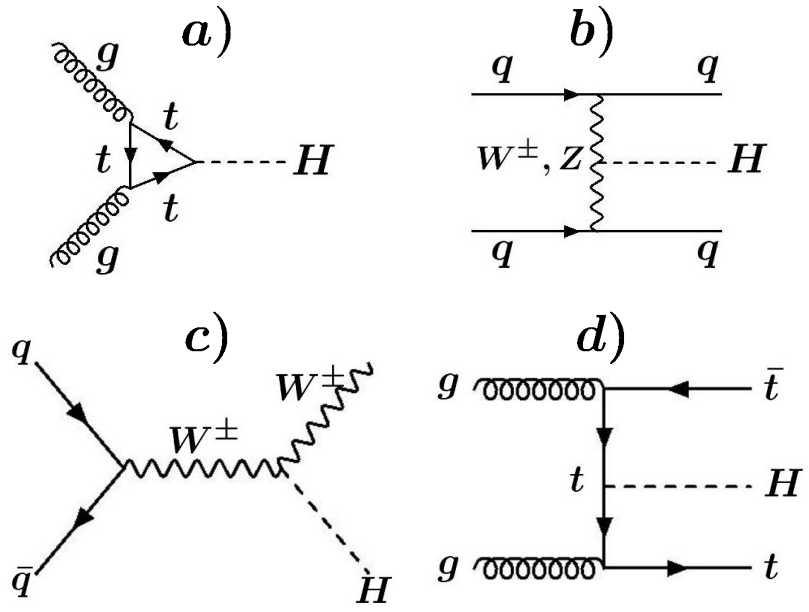

Figure 3.2: Higgs production channel at the LHC. *a*) is gluon fusion process which has about 90 % contribution to Higgs production. *b*) is qqH process mediated by W, Z boson. *c*) is associated production process, and *d*) is $t\bar{t}H$ process.

various channels. The main Higgs decay channel in the SM is $H \to b\bar{b}$. $H \to WW$, $H \to \tau\bar{\tau}$, and $H \to gg$ have almost same branching ratio, and large next to $H \to b\bar{b}$. Higgs to diphoton and digluon decays are also induced through loop processes. $H \to ZZ$ and $H \to c\bar{c}$ have smaller branching ratio than above processes. The rarest possible Higgs decay processes are $H \to \gamma\gamma$ and $H \to Z\gamma$ so far. In these decay processes, just $H \to gg$, $H \to \gamma\gamma$ and $H \to Z\gamma$ are generated by loop processes shown in Figure 3.3. Other decay processes are induced by tree level interaction.

However branching ratio of $H \to ZZ$ and $H \to \gamma\gamma$ is smaller than other channles, signals from these channels are more significant other ones. The expected final state of $H \to ZZ$ decay is multi-jet, or two-lepton plus jets, or four-lepton shown in Figure 3.4. $H \to ZZ \to l\bar{l}l\bar{l}$ can be detected clearly at the LHC.

3.2.2 Signal strength of Higgs boson decay

The signal strength is important and useful value that we can compare the LHC result of Higgs with prediction of new physics models. If we consider a new physics model which contain the SM in low energy limit, an effect of new physics appear through loop contributions in Higgs production and decay process. We show the signal strength in the SM case and some type of new physics case. We will calculate Higgs signal strength in universal extra dimension (UED) case in chapter 4.

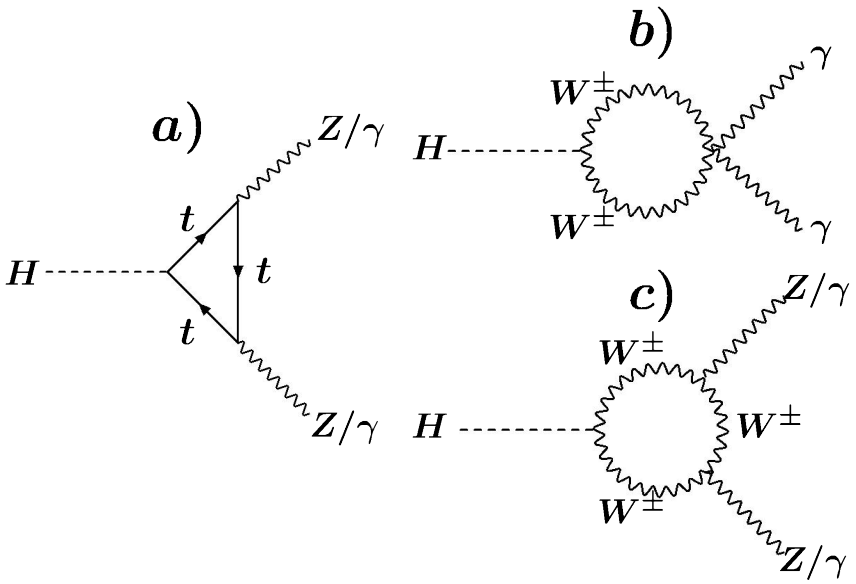

Figure 3.3: Higgs to diphoton and $Z\gamma$ decay processes, that is a) top loop decay process, b) and c) induced by W boson loop. Other than c), since Z and γ are orthogonal mode, these does not interact in tree level vertex. Thus B) does not have $Z\gamma$ decay mode. $H \to gg$ is just inverse process of diagram a) of Figure 3.2. We also need charged Goldstone mode $\phi^{\pm}$ in addition to $W^{\pm}$ in 't Hooft-Feynman gauge.

First let us consider gluon fusion cross section which has 90% contribution of Higgs production at the LHC. The gluon fusion Higgs production cross section in the SM is written by

$$\hat{\sigma}^{SM}_{gg\to H} = \frac{\pi^2}{8M_H}\Gamma^{SM}_{H\to gg}\delta(\hat{s} - M_H^2), \tag{3.10}$$

where $\hat{s}$ is center of mass energy square, $\Gamma^{SM}_{H\to gg}$ is decay width of Higgs to digluon process which is

$$\Gamma^{SM}_{H\to gg} = K\frac{\alpha_s^2}{8\pi^2}\frac{M_H^3}{v^2}|J_t^{SM}|^2. \tag{3.11}$$

K in equation (3.11) is the K-factor which accounts for the higher order QCD corrections, $\alpha_s = g_s^2/4\pi$ is fine structure constant for QCD, and J_t^{SM} is the loop-function induced by top loop which summarized in Appendix D. The experiment report the signal strength which is defined by the ratio of the cross section,

$$\frac{\sigma^{exp}_{pp\to H\to X}}{\sigma^{SM}_{pp\to H\to X}}, \tag{3.12}$$

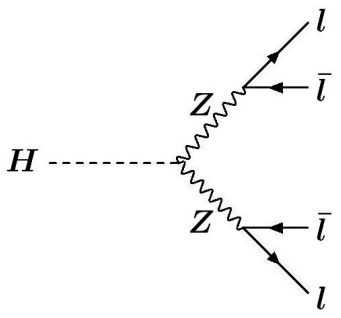

Figure 3.4: $H \to ZZ \to l\bar{l}l\bar{l}$ decay process.

where $X = \gamma\gamma, ZZ, WW$, etc. We compute the signal strength for a new physics (NP) case with gluon fusion production channel as

$$\frac{\sigma^{NP}_{gg\to H\to X}}{\sigma^{SM}_{gg\to H\to X}} \simeq \frac{\Gamma^{NP}_{H\to gg}\Gamma^{NP}_{H\to X}/\Gamma^{NP}_{H}}{\Gamma^{SM}_{H\to gg}\Gamma^{SM}_{H\to X}/\Gamma^{SM}_{H}}, \tag{3.13}$$

where $\Gamma^{NP/SM}_{H}$ is total decay width of the Higgs in NP/SM case and

$$\hat{\sigma}^{NP}_{gg\to H} = \frac{\pi^2}{8M_H}\Gamma^{NP}_{H\to gg}\delta(\hat{s} - M_H^2), \tag{3.14}$$

$$\Gamma^{NP}_{H\to gg} = K\frac{\alpha_s^2}{8\pi^2}\frac{M_H^3}{v_{EW}^2}|J_t^{SM} + J^{NP}|^2. \tag{3.15}$$

K is K-factor which accounts for the higher order QCD corrections, $\alpha_s = g_s^2/4\pi$ is the fine structure constant for QCD, $v_{EW} \simeq 246$ GeV is vacuum expectation value of Higgs in weak scale, J_t^{SM} is SM top loop function, and J^{NP} is loop effects from a new physics which affect gluon fusion process. We can estimate the prediction of signal strength in a NP case by calculating loop contribution J^{NP}.

3.3 Electroweak S, T parameters

The electroweak precision measurement gives one of the tightest constraints on new physics models. It is well known that the LEP experiment determined the several electroweak parameters ; fine structure constant $\alpha \sim 1/137.035999679$, Fermi constant $G_F \sim 1.16637 \times 10^{-5}(\mathrm{GeV}^{-2})$, Z and W boson pole masses $m_Z = 91.1876 \pm 0.0021$ (GeV), $m_W = 80.420 \pm 0.031$(GeV), respectively. These values were given by global fit of precision measurements of lepton four-Fermi interactions which are mediated by Z boson. We can reconstruct electroweak parameters in the SM ; gauge couplings g_2, g_Y and vacuum expectation value of Higgs boson v from these experimental results [90]. In this section, we show some structure of Higgs sector which is related to constraints from electroweak precision measurement not

only in the SM case but also in case with multi Higgses and general representations. Next we show a custodial symmetry which appear accidentally with accidental appear in the SM case. Finally, we show usual parameters which give a bound on models in terms of mass and field renormalization, which are well known S, T parameters proposed by [78, 79].

3.3.1 The ρ parameter

Since the LEP is a weak scale experiment, not a low energy experiment, we must take into account the observable values containing quantum corrections. In other words, the results of the LEP give a upper bound on radiative corrections from a new physics candidate. Such observable values are sensitive to the weak mixing angle s_W whose global fit is

$$s_W^2 \equiv 1 - \frac{m_W^2}{m_Z^2} = 0.22292 \pm 0.00028. \tag{3.16}$$

We must take into account a radiative correction to fit this value. More generally, we can generalize (3.16) into the parameter:

$$\rho \equiv \frac{m_W^2}{m_Z^2 c_W^2}, \tag{3.17}$$

called "ρ parameter". In the SM, $\rho = 1$ at the tree level. The value of ρ parameter strongly depends on $SU(2)_L$ representation of Higgs doublets. Let us check the value of ρ parameter in a case beyond the SM.

Gauge boson mass terms in $SU(2)_L \times U(1)_Y$ sector are simply written by

$$\left(-g_2 I_W^a W_\mu^a \langle\Phi\rangle + i g_Y \frac{Y_\Phi}{2} B_\mu \langle\Phi\rangle\right)^2 \tag{3.18}$$

where $Y_\Phi = 1$ is the hypercharge of Φ. These mass terms are generally written as

$$\left(\frac{g_2^2}{2}\left[I(I+1) - I_3^2\right]\left(W_\mu^{1\,2} + W_\mu^{2\,2}\right) + I_3^2\left(g_2 W_\mu^3 - g_Y B_\mu\right)^2\right)\langle\Phi\rangle^2, \tag{3.19}$$

as we checked previously in (2.12). Therefore the mass terms of gauge bosons are generally written as

$$\begin{aligned} m_W^2 &= g_2^2\left(I(I+1) - I_3^2\right)\langle\Phi\rangle^2 \\ m_Z^2 &= 2\left(g_2^2 + g_Y^2\right) I_3^2 \langle\Phi\rangle^2, \end{aligned} \tag{3.20}$$

and in such a case, the ρ parameter (3.17) is

$$\rho = \frac{g_2^2\left(I(I+1) - I_3^2\right)}{2\left(g_2^2 + g_Y^2\right) I_3^2 c_W^2} = \frac{\left(I(I+1) - I_3^2\right)}{2 I_3^2}, \tag{3.21}$$

where we used $c_W = g_2/g_Z$ and $g_Z^2 = g_2^2 + g_Y^2$. In order to keep $\rho = 1$, we can only choose weak isospins of these Higgs doublets as

$$(I, I_3) = \left(\frac{1}{2}, \pm\frac{1}{2}\right), (3, \pm 2), \cdots. \tag{3.22}$$

Thus, the SM Higgs doublet automatically satisfies $\rho = 1$ since the SM Higgs doublet has $\frac{1}{2}$ representation for $SU(2)_L$ gauge symmetry. When we extend the Higgs sector of the SM, however, the ρ parameter does not take the SM value $\rho = 1$. In such a case, we must consider exotic Higgs fields which satisfy (3.22). When we introduce the i-th Higgs doublet H_i with the vacuum expectation value v_i, weak isospin I_i and hyper charge Y_i, such a Higgs must satisfy a relation

$$\rho = \frac{\sum_i [I_i(I_i+1) - I_{3i}^2]}{\sum_i (2I_{3i}^2)}. \tag{3.23}$$

When we consider a new physics model, it is important that exotic Higgs fields must satisfy (3.23) at the tree level. On the other hand, when we take into account radiative corrections of order $g_2^2 \log(m_H/m_W)$, we write

$$\hat{\rho} \equiv \frac{m_W^2}{m_Z^2 c_W^2(m_W)} = 1 + \Delta\rho, \tag{3.24}$$

where $c_W^2(m_W)$ is running parameter at the m_W scale. Essentially $\Delta\rho$ is the T parameter which we will see a detail in latter subsection.

3.3.2 Custodial symmetry

The SM Higgs potential has mass term and quartic interaction term. The potential is constructed by $(2, 1)$ representation Higgs doublet for $SU(2)_L \times U(1)_Y$ symmetry. However, this potential is accidentally symmetric another hidden global symmetry. This hidden symmetry is called "custodial symmetry". When we introduce custodial symmetry as an exact symmetry into the SM, ρ parameter is ensured to be $\rho = 1$ in all order of loop level. A brief review of custodial symmetry can be found in Refs. [91, 92] for example. Here let us check a property of custodial symmetry.

First, let us return to the SM Higgs potential

$$V(\Phi) = \mu^2|\Phi|^2 + \lambda|\Phi|^4.$$

where we omit factor $\frac{1}{4}$ in quartic term by conversion. It is constructed by requiring gauge invariance under $SU(2)_L \times U(1)_Y$ and renormalizability. We can simply expand this Higgs potential as

$$\begin{aligned} V &= \mu^2 |\Phi|^2 + \lambda |\Phi|^4 \\ &= \mu^2 \left(\phi_1^2 + \phi_2^2 + \phi_3^2 + \phi_4^2\right) + \lambda \left(\phi_1^2 + \phi_2^2 + \phi_3^2 + \phi_4^2\right)^2, \end{aligned} \tag{3.25}$$

by component fields of the Higgs doublet which are

$$\Phi = \frac{1}{\sqrt{2}} \begin{pmatrix} \phi_1 + i\phi_2 \\ \phi_4 + i\phi_3 \end{pmatrix}. \tag{3.26}$$

We see that each term in the potential (3.25) has a form of radius of three-dimensional sphere. Thus (3.25) has $SO(4)$ global symmetry which conserves the absolute value of four-component vector $\phi_{1,2,3,4}$. Mathematically, this group is isomorphic to $SU(2)_L \times SU(2)_R$. In broken phase of $SU(2)_L \times U(1)_Y$, since only physical Higgs field $\phi_4 = H$ gets non-zero vacuum expectation value v, the radius squared becomes

$$\left(\phi_1^2 + \phi_2^2 + \phi_3^2 + \phi_4^2\right) \to \left(\phi_1^2 + \phi_2^2 + \phi_3^2 + (H+v)^2\right). \tag{3.27}$$

We see that the global $SO(4)$ symmetry is already broken in (3.27). Since H is only field which has a vacuum expectation value, H cannot be rotated with $\phi_{1,2,3}$. The global $SO(4)$ is broken down to $SO(3)$ symmetry which rotates only $\phi_{1,2,3}$ and which is isomorphic to $SU(2)$. This survived $SU(2)$ is called custodial $SU(2)_V$ which is diagonal component of $SU(2)_L \times SU(2)_R$.

Let us illustrate operation of $SU(2)_L \times SU(2)_R$ as follows. $SU(2)_L$ rotates two components of Higgs doublet as shown in (3.26). On the other hand, $SU(2)_R$ global symmetry rotates two components of $SU(2)_L$ Higgs doublets;

$$\begin{aligned} \Phi = (\Phi_a, \Phi_b) &= \begin{pmatrix} \phi_a & \phi_b \\ \phi_c & \phi_d \end{pmatrix} \\ &= \frac{1}{\sqrt{2}} \begin{pmatrix} \phi_4 - i\phi_3 & \phi_1 + i\phi_2 \\ -\phi_1 - i\phi_2 & \phi_4 + i\phi_3 \end{pmatrix} \\ &= \frac{1}{\sqrt{2}} \begin{pmatrix} \phi_4 - i\phi_3 & \sqrt{2}\phi^+ \\ -\sqrt{2}\phi^- & \phi_4 + i\phi_3 \end{pmatrix}. \end{aligned} \tag{3.28}$$

This form is called bi-doublet Higgs. $\Phi_{a,b}$ are $SU(2)_L$ doublets which are rotated by an $SU(2)_L$ gauge transformation U_L from left side of bi-doublet, and an $SU(2)_R$ transformation U_R rotates ϕ_a and ϕ_R from right side of bi-doublet, like as

$$\Phi' = U_L \Phi U_R^\dagger \qquad \text{as} \qquad \begin{array}{c} \\ SU(2)_L \end{array} \overset{SU(2)_R}{\begin{pmatrix} \phi_a & \phi_b \\ \phi_c & \phi_d \end{pmatrix}} \quad . \tag{3.29}$$

Such a representation of the Higgs has gauge invariant form

$$\mathrm{Tr}\left(\Phi^\dagger \Phi\right). \tag{3.30}$$

Actually, a Higgs Lagrangian

$$\mathcal{L} = \mathrm{Tr}\left|D_\mu \Phi\right|^2 - \mu^2 \mathrm{Tr}(\Phi^\dagger \Phi) - \lambda \mathrm{Tr}\left[(\Phi^\dagger \Phi)^2\right] \tag{3.31}$$

is $SO(4)$ invariant. After spontaneous symmetry breaking, the vacuum expectation value of bi-doublet Higgs can be written as

$$\langle \Phi \rangle = \frac{1}{\sqrt{2}} \begin{pmatrix} v & \\ & v \end{pmatrix}. \tag{3.32}$$

It breaks both $SU(2)_L$ and $SU(2)_R$ symmetry,

$$U_L \langle \Phi \rangle \neq \langle \Phi \rangle, \qquad \langle \Phi \rangle U_R^\dagger \neq \langle \Phi \rangle. \tag{3.33}$$

However, we can find that there is an unbroken symmetry which leaves diagonal component of VEV (3.32). Such a transformation is realized by the case that there is a parity symmetry P_{LR} which keeps $U_L = U_R$, in such a case

$$U_L \langle \Phi \rangle U_L^\dagger = \langle \Phi \rangle. \tag{3.34}$$

This survived subgroup from $SU(2)_L \times SU(2)_R$ symmetry breaking is the meanings of custodial $SU(2)_V$. Thus, symmetry breaking pattern is

$$SU(2)_L \times SU(2)_R \times P_{LR} \to SU(2)_V. \tag{3.35}$$

The custodial symmetry protects the tree level relation $\rho = 1$ from radiative corrections. We will show some detail of "custodial protection" in next subsection.

3.3.3 S, T parameters

The ρ parameter well explains the structure of the electroweak sector in focus on the weak mixing angle. On the other hand, Peskin and Takeuchi [78, 79] proposed a more convenient form of electroweak parameters, S, T, U. These parameters can be used to show how the electroweak precision measurement restricts the physics beyond the SM through its radiative correction to electroweak precision measurement. The variables are defined by use of the two-point functions of the SM gauge bosons. In an unbroken gauge theory, the two-point function of the gauge bosons in $\xi = 1$ gauge are written as

$$\Pi_{ab}^{\mu\nu}(k) = \left(g_{\mu\nu} - \frac{k_\mu k_\nu}{k^2} \right) \Pi_{ab}(k^2) \tag{3.36}$$

from Ward-Takahashi identity, but in a broken gauge theory, like the SM gauge theory $SU(2)_L \times U(1)_Y \to U(1)_{e.m.}$, only a transverse part satisfies the relation (3.36). In such a case, whole two point function takes the form

$$\Pi_{ab}^{\mu\nu}(k) = i\Pi_{ab}^T(k^2) \left(g_{\mu\nu} - \frac{k_\mu k_\nu}{k^2} \right) + i\Pi_{ab}^L(k^2) \frac{k_\mu k_\nu}{k^2}, \tag{3.37}$$

where index a, b are types of gauge bosons which are $A, Z, W^\pm$, k is external momentum of gauge bosons, the indices $T(L)$ show transverse (longitudinal) part, and $\Pi_{ab}^{T\prime}$ is defined

by $\frac{d}{dk^2}\Pi^T_{ab}(k^2)$. The S, T parameters are defined by the transverse part of the two point function (3.37), and the definition depends on the sign of the weak mixing angle and gauge coupling constants. In our definition (2.3), and (2.13), the S, T parameters are defined by

$$\frac{\alpha S}{4s_W^2 c_W^2} = \Pi^T_{ZZ}{}'(0) + \frac{c_W^2 - s_W^2}{c_W s_W}\Pi^T_{Z\gamma}{}'(0) - \Pi^{\mathrm{T}}_{\gamma\gamma}{}'(0), \tag{3.38}$$

$$\alpha T = \frac{\Pi^T_{WW}(0)}{m_W^2} - \frac{\Pi^T_{ZZ}(0)}{m_Z^2},$$

$$\frac{\alpha U}{4s_W^2} = \Pi^T_{WW}{}'(0) - c_W^2\Pi^T_{ZZ}{}'(0) + 2s_W c_W \Pi_{Z\gamma}{}'(0) - s_W^2\Pi_{\gamma\gamma}{}'(0). \tag{3.39}$$

The physical meaning of the S parameters is the field renormalization of the neutral current at the Z pole scale. The U parameter contain not only field renormalization for neutral current but also charged current. On the other hand, the T parameter constructed by mass corrections for W and Z, thus we can understand the T parameter as the magnitude of weak isospin breaking from radiative corrections. Note that, S and U parameters depend on definition of each other. If we choose $U = 0$, we can enforce the ambiguity of U parameter into S parameter. Hereafter, we assume $U = 0$.

3.3.4 Analysis of S,T parameters

The general shape of the S and T parameters are

$$S = \sum_{M_{\mathrm{NP}}<\Lambda} S^{\mathrm{NP}} + S_{\mathrm{Higgs}} + S_{\mathrm{threshold}}, \tag{3.40}$$

$$T = \sum_{M_{\mathrm{NP}}<\Lambda} T^{\mathrm{NP}} + T_{\mathrm{Higgs}} + T_{\mathrm{threshold}}, \tag{3.41}$$

where the first terms are the contributions from new physics and the last two terms represent, respectively, the effects from Higgs mass calibration and the threshold correction via possible higher-dimensional operators around the UV cutoff scale Λ. The form of first two terms in (3.40),(3.41) depends on models, and we will show the case of Universal Extra Dimension models in chapter 4. The last terms, threshold S, T operators are shown in [25]. These forms are

$$S_{\mathrm{threshold}} = c_S\frac{2\pi v^2}{\Lambda^2}, \quad T_{\mathrm{threshold}} = c_T\frac{m_H^2}{4\alpha\Lambda^2}, \tag{3.42}$$

where c_S and c_T are the parameters in UV cutoff operators, and these must be typically $\mathcal{O}(1)$. The global analysis of S, T parameters assumes a reference Higgs mass to be 117 GeV. Thus, when we estimate the value of S, T parameter, we must take into account a gap of Higgs mass between the discovered Higgs mass $\sim$125 GeV and above value. The second terms in (3.40) and (3.41) come from this gap. The exact form of Higgs calibration

terms is

$$S_{Higgs} = \frac{1}{12\pi} \log\left(\frac{m_H^2}{m_{H,fit}^2}\right), \qquad T_{Higgs} = -\frac{3}{12\pi c_W^2} \log\left(\frac{m_H^2}{m_{H,fit}^2}\right), \tag{3.43}$$

with $m_{H,fit}$ =117 GeV. New physics contributions, the first terms in (3.40) and (3.41) depend on models. We will show the values of these terms in the case of Universal Extra Dimension models in chapter 4. The S and T are also described by combinations of some electroweak variables and their values are calculated in global analysis with experimental results. One of the latest numbers can be found in Ref. [87],

$$S|_{U=0} = 0.05 \pm 0.09, \quad T|_{U=0} = 0.08 \pm 0.07, \quad \rho_{ST} = +0.91, \tag{3.44}$$

with the 126 GeV reference Higgs mass and assuming the U parameter is zero and ρ_{ST} is the correlation coefficient.

Chapter 4

Extra dimensions and their electroweak phenomenology

The extra dimensional theory was first studied by Kaluza in 1921 [20]. The original motivation is unification of gravity and electromagnetic force. Kaluza tried to assign the electromagnetic field as a vector-scalar component of the five dimensional metric. Klein suggested the idea of compactification of fifth direction in 1926 [21]. Now the basic idea of the theory with compactified extra dimension is called Kaluza-Klein theory.

In late 20th century, Antoniadis first pointed out a possibility which realizes a TeV scale extra dimension in viewpoint of string theory [22]. After then, various types of extra dimensional models have been considered. One of a major model, ADD model or "large extra dimensions" was proposed by Arkani-Hamed, Dimopoulos, and Dvali [93]. They suggested that the large hierarchy between weak and Planck scales can be explained by the dilution of coupling constant in extra dimensional theory. The ADD model assumes 2 or more large number of compactified extra spacial dimensions in which only gravity can propagate. Thus only gravitational coupling constant is diluted by extra spacial volume factor in four dimensional effective theory. On the other hand, Randall and Sundrum tried to explain the origin of large hierarchy by a curved spacial dimension [94]. This is RS model or namely "warped extra dimension". RS model explains the large hierarchy by order ten parameter with non-factorized exponential warp factor in extra dimensional space. We can consider a case where not only gravity but also other fields can propagate extra spacial dimension(s). In extra dimensional theory, coupling constants in four-dimensional effective theory is obtained from coupling constants in higher dimensional theory, compactification scale, and the "overlap" of mode functions of Kaluza-Klein (KK) excited modes. In other words, this overlap structure can be an origin of a hierarchical structure in four dimensional effective theory. The other feature of extra dimensional theory is the boundary condition of extra space coordinate. Extra spacial dimension(s) is compacfitied on orbifold space such as S^1/Z_2, T^2/Z_4, etc$\cdots$ to realize four-dimensional chiral structure. The boundary condition on fixed points in these geometry determines the shape of mode functions. In addition, there is a possibility that the boundary condition on fixed points breaks a symmetry.

The extra dimensional theory has been developed with various motivations. The Uni-

versal Extra Dimension (UED) models have phenomenological motivations. The virtue of UED is that the lightest Kaluza-Klein particle (LKP) can be a candidate of dark matter due to the symmetry of extra dimension, and KK parity. The UED assumes that all the SM particles can propagate in extra dimensional bulk. Therefore, all the SM particle have KK excited modes. Such a KK mode changes collider signatures through loop corrections from the SM prediction.

In this chapter, we study not only five-dimensional but also all the known seven types of six-dimensional UED models. We cyclopaedically research the predictions and bounds on UED models in LHC Higgs search and electroweak S, T parameters analysis whose basic idea we reviewed in Chapter 3. In addition, we examine the RGE in six-dimensional models in order to estimate the vacuum stability bound. In general UED models, when we consider a few TeV KK scale, the scale where Higgs quartic interaction λ becomes zero appear in several TeV scale. In such a case, the electroweak vacuum rapidly decays into the true vacuum as we reviewed in Chapter 3. In order to avoid rapid vacuum decay, we require the UV cutoff scale Λ which effective potential becomes negative. Therefore, we regard the scale of $\lambda = 0$ as the upper bound on λ in our analysis.

4.1 RGE and vacuum stability bound in UEDs

4.1.1 RGE in six-dimensional UED models

Considering the RGE is an effective way of probing scale dependence. Its concrete form is derived from the invariance, under the change of the renormalization scale μ, of the bare vertex function Γ_0 , which is a function of bare parameters. The scale invariance requires that

$$\mu \frac{d}{d\mu} \Gamma_0(\{c_0\}, \{m_0\}, \{\Phi_0\}) = 0, \tag{4.1}$$

where $\{c_0\}$, $\{m_0\}$, and $\{\Phi_0\}$ represent sets of bare couplings, masses, and fields, respectively. Since bare parameters and fields are divergent by themselves, we can rewrite the bare ones with finite physical ones (renormalized parameters and fields) and counter terms, which contain divergences. In this paper, we show all the bare/renormalized variables with/without the subscript "0."

In the following, we consider the RGE for the Higgs quartic coupling λ in the six-dimensional models. We obey the convention of Ref. [1] in describing the electroweak (EW) sector. The potential of the Higgs field H at the tree level is depicted as

$$-\frac{M_{H0}^2}{2} H_0^2 + \frac{\lambda_{(6)0}}{4} H_0^4, \tag{4.2}$$

where M_{H0} and $\lambda_{(6)0}$ are the bare Higgs mass and six-dimensional Higgs couplings. After the six-dimensional bare Higgs field H_0 is KK expanded, we can find the zero mode $H_0^{(0)}$, where we use a superscript for a KK index. In considering the one-loop running of λ, we

need not consider the renormalization of the Higgs mass and hence the physical Higgs mass m_H becomes

$$m_H = \sqrt{\lambda_{(6)0}} v_{(6)0} = \sqrt{\lambda_{(6)}} v_{(6)} = \sqrt{\lambda} v, \tag{4.3}$$

where the four-dimensional (4D) Higgs vacuum expectation value $v = 246\,\mathrm{GeV}$ and quartic coupling λ are expressed as $v_{(6)} = v/\sqrt{V}$, $\lambda_{(6)} = \lambda\sqrt{V}$, with V being the volume of the extra dimensions. Let us write

$$H_0^{(0)} = \sqrt{Z_H} H^{(0)}, \quad \lambda_0 = Z_\lambda (Z_H)^{-2} \lambda, \tag{4.4}$$

where Z_λ is the renormalization factor for the Higgs quartic coupling and $\sqrt{Z_H}$ is that for the wave function renormalization of the Higgs zero mode. We also need the information of the RGEs for the gauge and Yukawa couplings to compute the running of λ. We summarize the beta functions ,

$$\mu \frac{d}{d\mu} \mathcal{Q} = \beta_{\mathcal{Q}}, \tag{4.5}$$

where detailed form of $\beta_{\mathcal{Q}}$ can be found in Appendix A.

Let us review how to compute RGEs in a theory with (a) compactified extra dimension(s). We adopt the bottom-up approach discussed in Refs. [95, 96], which takes into account a contribution of a massive particle to the beta functions when the increasing scale μ passes its mass. In the case of the UED, after KK decomposition, the corresponding 4D effective theory contains not only the SM fields but also their KK partners. Following this prescription, we get

$$\beta_{\mathcal{Q}} = \beta_{\mathcal{Q}}^{(\mathrm{SM})} + \sum_{s:\,\text{massive states}} \theta(\mu - M_s) \Big(N_s \beta_{s,\mathcal{Q}}^{(\mathrm{NP})} \Big), \tag{4.6}$$

where $\beta_{\mathcal{Q}}^{(\mathrm{SM})}$ and $\beta_{s,\mathcal{Q}}^{(\mathrm{NP})}$ are the contributions from the SM particles and from the new massive ones with mass M_s, respectively, and N_s is the number of degenerated states. At the tree level, M_s is expressed as

$$M_s^2 = m_{s,(\mathrm{SM})}^2 + M_{s,(\mathrm{KK})}^2, \tag{4.7}$$

where $m_{s,(\mathrm{SM})}$ is the SM mass of the corresponding zero mode and $M_{s,(\mathrm{KK})}$ are KK masses. In general, the value of $M_{s,(\mathrm{KK})}$ is much greater than that of $m_{s,(\mathrm{SM})}$ and M_s^2 can be approximated as $M_s^2 \simeq M_{s,(\mathrm{KK})}^2$.

Let us review the KK expansions in the six-dimensional UED models. In the models on the orbifolded T^2 [namely T^2/Z_2, $T^2/(Z_2 \times Z_2')$, and T^2/Z_4] and the one on RP^2, the KK mass $M_{s,(\mathrm{KK})}^2$ becomes of T^2 type:

$$M_{s,(\mathrm{KK})}^2 \to M_{(m,n)}^2 := \frac{m^2}{R_5^2} + \frac{n^2}{R_6^2}, \tag{4.8}$$

where m (n) is the KK index along the fifth (sixth) direction and $N_{(m,n)} = 1$ irrespective of m and n. We note that the beta functions for gauge, Yukawa , and Higgs self-couplings take the same forms irrespective of the models based on T^2 and are independent of the KK indices. This reason is as follows. Because of the flat profile of the zero modes, the three-point functions with one SM field and the four-point functions with two SM fields become universal at their leading order after using the orthonormality of KK mode functions. In contrast, the value N_s and the summation of the KK index $\sum_s$ in Eq. (4.6) are affected by the difference in the patterns of the orbifolding. Hence , the evolution of λ depends on the choice of the model. The explicit range of m, n summation is shown in Table 4.1.

Let us turn to the model on RP^2. In Fig. 4.1, we show the surviving modes. The surviving modes of KK fermions become the same as in the T^2/Z_2 model. On the other hand, the patterns of the bosonic particles are complicated. The allowed range of m and n is $m \geq 0,\ n \geq 0$, and the type of surviving mode is classified into the following four. In region I, $(m,n) = (0,2),(0,4),(0,6),\ldots$ and $(m,n) = (2,0),(4,0),(6,0),\ldots$; a physical scalar mode coming from the extra component of the six-dimensional gauge boson is projected out. In region II, $(m,n) = (0,1),(0,3),(0,5),\ldots$ and $(m,n) = (1,0),(3,0),(5,0),\ldots$; the only surviving bosonic mode is this scalar that was projected in region I. In region III, $m \geq 1,\ n \geq 1$; all the bosonic modes are left as is, just like in other orbifolded models on T^2. In the last region IV, only fermionic degrees of freedom remain.

Next, we go on to the models based on S^2. The explicit form of the KK mass $M^2_{s,(\mathrm{KK})}$ on S^2 is

$$M^2_{s,(\mathrm{KK})} \to M^2_{(j)} := \frac{j(j+1)}{R^2}, \tag{4.9}$$

with the index $j \geq 1$.

For each jth mode in the S^2, S^2/Z_2, and PS models, respectively, the number of degrees of freedom reads

$$n^{S^2}(j) = 2j+1, \tag{4.10}$$

$$n^{S^2/Z_2}(j) = \begin{cases} j+1 & \text{for } j = \text{even} \\ j & \text{for } j = \text{odd} \end{cases}, \tag{4.11}$$

$$n^{\mathrm{PS}}_{\mathrm{fermion}} = 2j+1, \quad n^{\mathrm{PS}}_{\mathrm{even}}(j) = \begin{cases} 2j+1 \\ 0 \end{cases}, \quad n^{\mathrm{PS}}_{\mathrm{odd}}(j) = \begin{cases} 0 & \text{for } j = \text{even} \\ 2j+1 & \text{for } j = \text{odd} \end{cases}. \tag{4.12}$$

In the cases of S^2 and S^2/Z_2, the number of the surviving degrees of freedom is the same for KK bosons and fermions. On the other hand, the PS is similar to RP^2 ; that is, surviving KK bosons are divided into two categories, even and odd. The even category includes all the KK bosons except for the physical scalar from the six-dimensional gauge boson, while the odd one only contains this one. We note that the number of degenerate

Type of orbifolding	Range of (m, n)
T^2/Z_2	$m + n \geq 1$, or $m = -n \geq 1$
$T^2/(Z_2 \times Z_2')$	$0 \leq m < \infty,\ 0 \leq n < \infty;\ (m, n) \neq (0, 0)$
T^2/Z_4	$1 \leq m < \infty,\ 0 \leq n < \infty$

Table 4.1: The range of the parameters (m, n) except for the zero mode $(m, n) = (0, 0)$ in each case of the orbifolding.

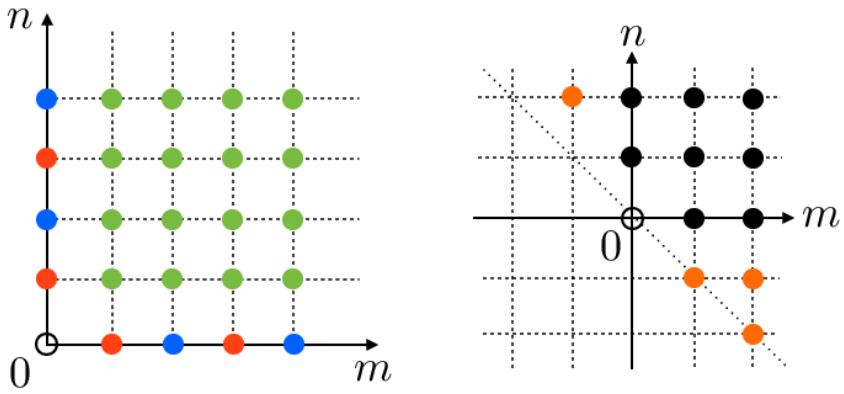

Figure 4.1: *Left*: The patterns of the remaining bosonic modes in the RP^2 model, where blue, red, and green points indicate that they belong to the regions I, II, and III, respectively. The definitions of these regions are found in the text. *Right*: The same as left one for fermionic modes. At the orange points (region IV), there are no bosonic modes. In both pictures, the black circles $(m = n = 0)$ correspond to the SM particles.

states is $2j + 1$, irrespective of the statistics of the particles and their oddness/evenness. Finally, we comment on the beta functions of the S^2-based models. From the surviving bosonic particles in each KK level, we can see that the RGEs in S^2, S^2/Z_2 are similar to those in T^2/Z_2, $T^2/(Z_2 \times Z_2')$, T^2/Z_4, while those in the PS are similar to those in RP^2.

4.1.2 Running of Higgs quartic interaction and Vacuum Stability

Following the discussion in the previous section, we evaluate the constraints on the highest possible UV cutoff scale Λ from vacuum stability of the Higgs potential. In our analysis, we literally evaluate the KK summation in Eq. (4.6), unlike the previous analysis in Ref. [50] where we obtained the UV cutoff scale of the UED models from the perturbativity of the 4D gauge couplings via the RGEs with its KK summation replaced by an integration. In other words, we treat the threshold correction when the reference energy crosses the mass of a KK particle explicitly in our numerical calculation. As it was discussed in the previous section, we can ignore the mass coming from the Higgs mechanism with good precision.

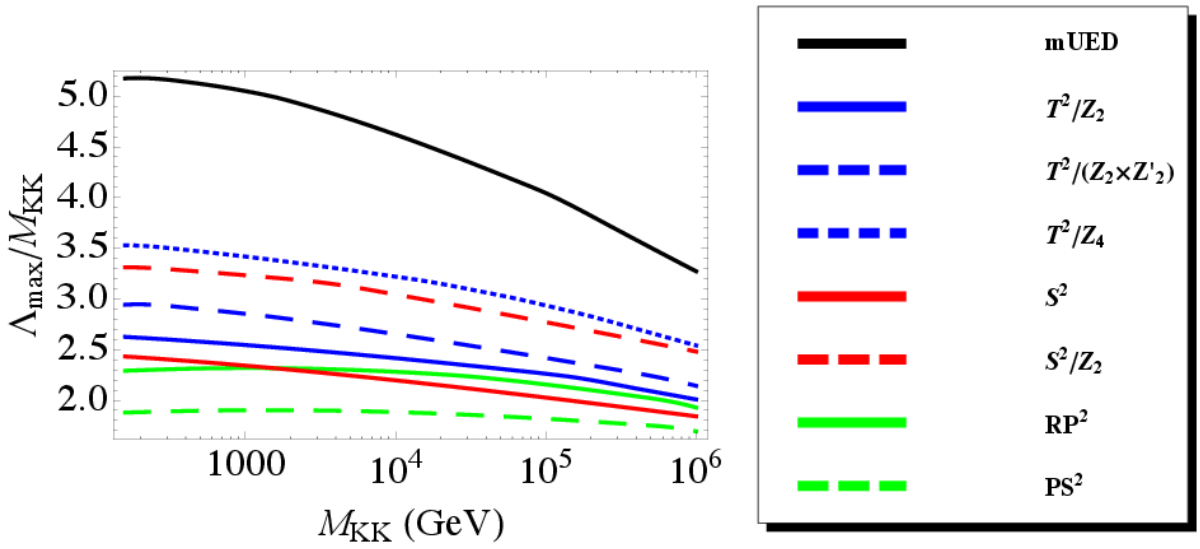

Figure 4.2: *Left*: Upper bounds on the UV cutoff of the UED models as a function of $M_{\rm KK}$, with the initial conditions in Eq. (4.14). *Right*: Our color convention for types of the UED models. The lines in red, blue, and green show the results of T^2-based, S^2-based, and nonorientable-manifold-based UEDs, respectively.

Model	mUED	T^2/Z_2	$T^2/(Z_2 \times Z_2')$	T^2/Z_4	S^2	S^2/Z_2	RP^2	PS
$\tilde{\Lambda}_{\rm max}$	5.0	2.5	2.9	3.4	2.3	3.2	2.3	1.9

Table 4.2: Upper bounds on cutoff scale $\Lambda_{\rm max} = \tilde{\Lambda}_{\rm max} M_{\rm KK}$ with $M_{\rm KK} = 1\,\text{TeV}$ and the initial conditions in Eq. (4.14).

Here, we adopt the following criterion for determining $\Lambda_{\rm max}$:

$$\lambda(\mu = \Lambda_{\rm max}) = 0, \tag{4.13}$$

where the Higgs potential is destabilized.

We note that the vacuum stability bound is sensitive to the differences in the initial condition of the Higgs quartic interaction λ and the top Yukawa coupling y_t [69, 86]. In our analysis, we adopt the following values:

$$\frac{v^2}{2}\lambda(\mu = m_Z) = 126^2\,\text{GeV}^2, \quad \frac{v}{\sqrt{2}}y_t(\mu = 173.5\,\text{GeV}) = 160\,\text{GeV}, \tag{4.14}$$

where m_Z is the Z-boson mass, the 126 GeV is the observed Higgs mass at the LHC, the 173.5 GeV and the 160 GeV are the latest values of the pole and the $\overline{\rm MS}$ masses of the top quark reported by the particle data group [97], respectively.

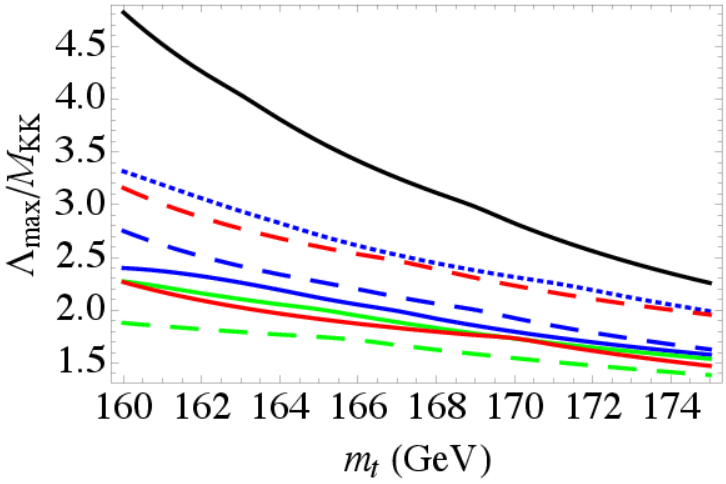

Figure 4.3: Cutoff upper bounds on the six-dimensional UED models and the mUED with the initial condition of the Higgs in Eq. (4.14) and of the top quark in Eq. (4.15) with changing in the region of $[160\,\text{GeV}, 175\,\text{GeV}]$ with $M_{\rm KK} = 1\,\text{TeV}$. Conventions of line colors and shapes are the same as in Fig. 4.2.

The results are summarized in Fig. 4.2, and the values with $M_{\rm KK} = 1\,\text{TeV}$ are also listed in Table 4.2. $M_{\rm KK}$ means the first KK mass: $M_{\rm KK} = 1/R$ for the S^1/Z_2 (mUED) and T^2-based compactifications (namely, T^2/Z_2, $T^2/(Z_2 \times Z_2')$, T^2/Z_4 and RP^2) and $M_{\rm KK} = \sqrt{2}/R$ for the S^2-based ones (namely, S^2/Z_2, PS and S^2), where we assume $R_5 = R_6 = R$. It is noted that the mUED case has been studied in Refs. [98–101] in many contexts, and we find a study in the case of T^2/Z_4 [102].[1] We mention that our conclusion on the mUED is consistent with that in a previous analysis in Ref. [101]. The constraints from vacuum stability, shown in Table 4.2, are tighter than our previous bounds from perturbativity of the gauge couplings: $\Lambda_{\rm max} \sim 5 M_{\rm KK}$ in T^2/Z_2, $T^2/Z_2 \times Z_2'$, T^2/Z_4, RP^2 and $\Lambda_{\rm max} \sim 7 M_{\rm KK}$ in S^2, S^2/Z_2, PS. We note that, in the previous analysis, we ignored differences in types of the compactifications and did not put a bound on the mUED since the KK summations in the single Higgs production and the Higgs decay, which are important in LHC phenomenology and which we consider in the next section, are convergent in this case.

Next, we consider the effects when we change the values of top Yukawa coupling in the initial conditions of the RGEs with $M_{\rm KK} = 1\,\text{TeV}$. We note that, within the SM, various values of $\overline{\rm MS}$ top mass $m_t|_{\overline{\rm MS}}$ have been reported between 160 and 175 GeV [69, 86, 97, 105]. Based on this fact, we calculate the bounds on λ with varying the initial condition of the

[1] We can find some related works on the evolutions of higher-dimensional neutrino operator in the mUED [71, 103] and in the T^2/Z_4 [102] and of the Cabibbo–Kobayashi–Maskawa matrix [104] in the mUED context.

top Yukawa as

$$\frac{v}{\sqrt{2}} y_t(\mu = 173.5\,\mathrm{GeV}) = m_t|_{\overline{\mathrm{MS}}}, \quad \text{for } 160\,\mathrm{GeV} \leq m_t|_{\overline{\mathrm{MS}}} \leq 175\,\mathrm{GeV}. \tag{4.15}$$

Our result, depicted in Fig. 4.3, is sensitive to the value of $m_t|_{\overline{\mathrm{MS}}}$ and is consistent with the analysis in Ref. [100] (mUED) and in Ref. [102] (T^2/Z_4). We cannot avoid the ambiguity originating from the top Yukawa coupling. From Figs. 4.2 and 4.3, we find that the dependence of Λ on M_{KK} and $m_t|_{\overline{\mathrm{MS}}}$ is greater in the mUED than in the six-dimensional UED models. In the latter, the KK threshold corrections are larger than those in the mUED because of their denser KK spectra, and hence the vacuum becomes unstable at a lower energy scale.

4.2 Higgs signals at Large Hadron Collider in UEDs

Equipped with the knowledge for the cutoff scale of UED models in the previous section, we estimate the bound on their KK mass scale from the recent results of Higgs search at the LHC.

4.2.1 Feature of Higgs signals in UED models

The structure of the Higgs signal at the LHC can be divided into the production and decay. The Higgs production is dominated by the gluon fusion process $gg \to H$, which is induced by the top loop. One of the most important Higgs decay channels that lead to its discovery is the diphoton one $H \to \gamma\gamma$, which is induced by the top and W boson loops. The Higgs signal is very sensitive to the contribution of the loop corrections at the LHC. In UED models, a lot of additional KK loops contribute to both $gg \to H(H \to gg)$ and $H \to \gamma\gamma$. The KK top loop contribution to the gluon fusion production cross section takes the following form:

$$\hat{\sigma}^{\mathrm{UED}}_{gg\to H} = \frac{\pi^2}{8m_H} \Gamma^{\mathrm{UED}}_{H\to gg} \delta(\hat{s} - m_H^2), \tag{4.16}$$

$$\Gamma^{\mathrm{UED}}_{H\to gg} = K \frac{\alpha_s^2}{8\pi^2} \frac{m_H^3}{v_{\mathrm{EW}}^2} |J_t^{\mathrm{SM}}(m_H^2) + J_t^{\mathrm{KK}}(m_H^2)|^2, \tag{4.17}$$

where $K \sim 1.5$ is the K factor accounting for the higher-order QCD corrections for the case of the LHC, $\alpha_s = g_s^2/4\pi$ is the fine structure constant for QCD, $v \simeq 246$ GeV is the electroweak scale, and $J_t^{\mathrm{SM/KK}}$ denotes the SM/KK top quark loop function, defined in Refs. [49, 50]. The KK top quark and KK W-boson loop contributions to the Higgs decay into diphoton are written as

$$\Gamma^{\mathrm{UED}}_{H\to\gamma\gamma} = \frac{\alpha^2 G_F m_H^3}{8\sqrt{2}\pi^3} \left| J_W^{\mathrm{SM}}(m_H^2) + J_W^{\mathrm{KK}}(m_H^2) + \frac{4}{3}(J_t^{\mathrm{SM}}(m_H^2) + J_t^{\mathrm{KK}}(m_H^2)) \right|^2, \tag{4.18}$$

where $\alpha = e^2/4\pi$ and G_F are fine structure constants for the QED and Fermi constant, respectively. The SM/KK W-boson loop functions $J_W^{\rm SM/KK}$ are defined in Ref. [49]. We have listed them in Appendix D.

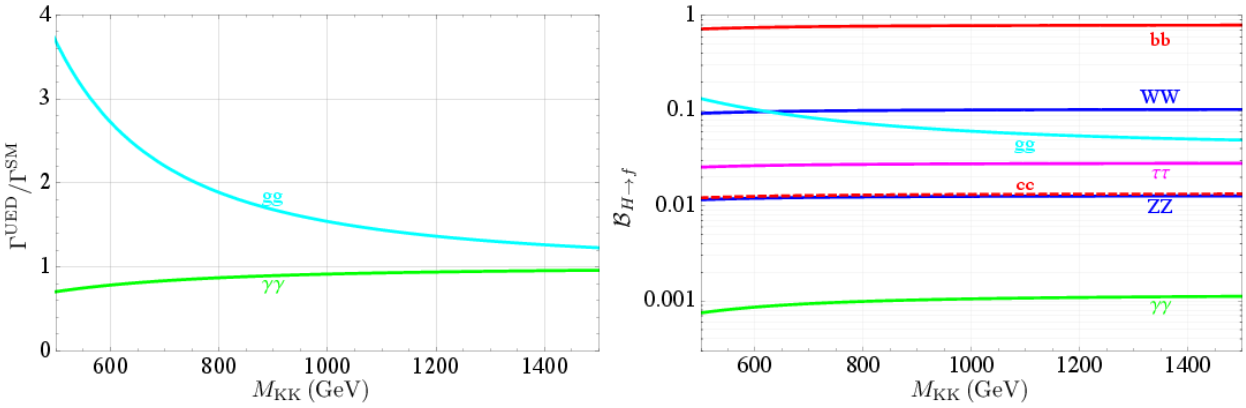

Figure 4.4: For the Higgs decay in the T^2/Z_2 UED model, we show the UED/SM ratio (left) and the branching ratio (right) as a function of $M_{\rm KK}$ for each final state, which is indicated by the caption within Figure; especially we distinguish the almost degenerate cc and ZZ by dashed and solid lines, respectively.

Because of these additional contributions, the loop-induced processes $gg \to H$ ($H \to gg$) and $H \to \gamma\gamma$ receive nontrivial effects, which we compute and use to estimate the branching ratios and the Higgs decay rates into the diphoton and digluon. As an illustration, we show results for the T^2/Z_2 model in Fig. 4.4. The UED/SM ratio of $H \to gg$ is always enhanced while that of $H \to \gamma\gamma$ is suppressed as already seen in Ref. [49]. These behaviors also affect the branching ratios of the Higgs decay as shown in the right panel of Fig. 4.4. The enhancement in $H \to gg$ is straightforwardly understood as the KK top contributions in the loop diagram. The reason for the suppression in $H \to \gamma\gamma$ is as follows. Since the vector-like fermions have twice the degrees of freedom compared with SM fermions, their negative contributions to the Higgs decay rate become larger than the positive ones coming from the KK W loop. Thus, the sum of the KK loops becomes negative, and it overcomes the positive SM contribution. As a consequence, the decay rate of $H \to \gamma\gamma$ is suppressed compared with the SM.

4.2.2 Strategy to constrain the KK mass scale

As shown above, the UED models give different production cross sections in the gluon fusion (GF). On the other hand, the other productions, which are the vector boson fusion (VBF), the Higgs-Strahlung (VH), and the associated production with a $t\bar{t}$ pair (ttH), are the same as the SM. We express the VH production associated with W and Z by WH and ZH, respectively. In the recent analysis, the ATLAS and CMS experiments have reported on ratios of these production channels in $H \to \gamma\gamma, ZZ$, and WW for each category tagging

their decays [73–77, 106].[2] Such ratios are quite important for obtaining the bound on UED models because of the nontrivial effect of the KK loop corrections on both the production and the decay of the Higgs boson. In order to take the different ratios of the production cross section into account, we employ the following quantity [89, 107]:

$$\epsilon_f^{I,X} = \frac{a_f^{I,X}\sigma_X^{\rm SM}}{\sum_Y a_f^{I,Y}\sigma_Y^{\rm SM}}, \tag{4.19}$$

where X and I indicate a production channel and a category tagging the decay $H \to f$, $\sigma_X^{\rm SM}$ is the Higgs production cross section of the channel X in the SM , and $a_f^{I,X}$ is introduced as its acceptance. When the set $\{\epsilon_f^{I,X}\}$ is given in the decay $H \to f$, the signal strength is written as

$$\mu_{H\to f}^I = \sum_X \epsilon_f^{I,X}\,\frac{\sigma_X}{\sigma_X^{\rm SM}}\,\frac{\mathcal{B}_{H\to f}}{\mathcal{B}_{H\to f}^{\rm SM}}, \tag{4.20}$$

where $\sigma_X^{(\rm SM)}$ represents the Higgs production cross section of the channel X , and $\mathcal{B}_{H\to f}^{(\rm SM)} = \Gamma_{H\to f}^{(\rm SM)}/\Gamma_{H\to \rm all}^{(\rm SM)}$ is the branching ratio of the Higgs decay $H \to f$ (in the SM). In the UED model, $\sigma_{\rm GF} = \hat{\sigma}_{gg\to H}^{\rm UED}$, $\Gamma_{H\to\gamma\gamma(gg)} = \Gamma_{H\to\gamma\gamma(gg)}^{\rm UED}$ as in Eqs. (4.16)–(4.18) , and the others are assumed to be the same as the SM in our analysis.

I	$\mu_{H\to\gamma\gamma}^I$	$\epsilon_{\gamma\gamma}^{I,X}$ (%)				
Event category	Signal strength	GF	VBF	VH(WH)	VH(ZH)	ttH
Unconventional central low P_T	0.9 ± 0.7	93.7	4.0	1.4	0.8	0.2
Unconventional central high P_T	$1.0^{+1.1}_{-0.9}$	79.3	12.6	4.1	2.5	1.4
Unconventional rest low P_T	$2.6^{+0.9}_{-1.0}$	93.2	4.0	1.6	1.0	0.1
Unconventional rest high P_T	$2.7^{+1.3}_{-1.2}$	78.1	13.3	4.7	2.8	1.1
Conventional central low P_T	$1.4^{+1.0}_{-0.9}$	93.6	4.0	1.3	0.9	0.2
Conventional central high P_T	$2.0^{+1.5}_{-1.3}$	78.9	12.6	4.3	2.7	1.5
Conventional rest low P_T	$2.2^{+1.2}_{-1.0}$	93.2	4.1	1.6	1.0	0.1
Conventional rest high P_T	1.3 ± 1.3	77.7	13.0	5.2	3.0	1.1
Conventional transition	$2.8^{+1.7}_{-1.6}$	90.7	5.5	2.2	1.3	0.2
Loose high mass 2 jet	$2.8^{+1.7}_{-1.4}$	45.0	54.1	0.5	0.3	0.1
Tight high mass 2 jet	$1.6^{+0.8}_{-0.6}$	23.8	76.0	0.1	0.1	0.0
Low mass 2 jet	$0.3^{+1.7}_{-1.5}$	48.1	3.0	29.7	17.2	1.9
E_T^{miss} significance	$3.0^{+2.7}_{-1.9}$	4.1	0.5	35.7	47.6	12.1
One lepton	$2.7^{+2.0}_{-1.7}$	2.2	0.6	63.2	15.4	18.6

Table 4.3: The ATLAS result of $H \to \gamma\gamma$ analysis. The ATLAS experiment defines these event categories and uses these ratios of the production channels as in Ref. [73].

[2]We use "ZZ" and "WW" as the meaning of $ZZ \to 4\ell$ and $WW \to 2\ell 2\nu$ for simplicity.

I	$\mu^I_{H\to\gamma\gamma}$	$\epsilon^{I,X}_{\gamma\gamma}$ (%)			
Event category	Signal strength	GF	VBF	VH	ttH
Missing E_T	$1.9^{+2.6}_{-2.3}$	22.0	2.6	63.7	11.7
Electron tag	$-0.7^{+2.8}_{-2.0}$	1.1	0.4	78.7	20.8
muon tag	$0.4^{+1.8}_{-1.4}$	0	0.2	79.0	19.8
2-jet loose	$0.8^{+1.1}_{-1.0}$	47.0	50.9	1.7	0.5
2-jet tight	$0.3^{+0.7}_{-0.6}$	20.7	78.9	0.3	0.1
Untag-3	$-0.3^{+0.8}_{-0.9}$	92.5	3.9	3.3	0.3
Untag-2	0.3 ± 0.5	91.6	4.5	3.6	0.4
Untag-1	0.0 ± 0.7	83.5	8.4	7.1	1.0
Untag-0	$2.2^{+0.9}_{-0.8}$	72.9	11.6	12.9	2.6
2-jet (7 TeV)	$4.2^{+2.3}_{-1.8}$	26.8	72.5	0.6	0
Untag-3 (7 TeV)	$1.5^{+1.7}_{-1.8}$	91.3	4.4	4.1	0.2
Untag-2 (7 TeV)	$0.0^{+1.3}_{-1.2}$	91.3	4.4	3.9	0.3
Untag-1 (7 TeV)	$0.2^{+1.0}_{-1.0}$	87.6	6.2	5.6	0.5
Untag-0 (7 TeV)	$3.8^{+2.0}_{-1.7}$	61.4	16.8	18.7	3.1

Table 4.4: The CMS result of $H \to \gamma\gamma$ analysis. The CMS experiment defines these event categories and uses these ratios of the production channels as in Ref. [106].

I	$\mu^I_{H\to ZZ}$	$\epsilon^{I,X}_{ZZ}$ (%)	
Event category	Signal strength	GF	VBF
Untagged	$0.85^{+0.32}_{-0.26}$	95	5
2-jet tag	$1.22^{+0.84}_{-0.57}$	80	20
I	$\mu^I_{H\to WW}$	$\epsilon^{I,X}_{WW}$ (%)	
SF 1 jet (7 TeV)	$0.9^{+2.1}_{-2.2}$	100	0
SF 0 jet (7 TeV)	0.1 ± 1.0	100	0
DF 1 jet (7 TeV)	1.7 ± 1.0	100	0
DF 0 jet (7 TeV)	0.6 ± 0.5	100	0
SF 1 jet (8 TeV)	1.5 ± 0.9	100	0
SF 0 jet (8 TeV)	1.1 ± 0.7	100	0
DF 1 jet (8 TeV)	0.3 ± 0.4	100	0
DF 0 jet (8 TeV)	0.7 ± 0.3	100	0

Table 4.5: The CMS result of $H \to ZZ/WW$ analysis. The CMS experiment defines these event categories and uses these ratios of the production channels as in Ref. [76, 77]. SF and DF denote "same flavor" and "different flavor", respectively.

For the analysis in $H \to \gamma\gamma$, the ATLAS and CMS experiments have shown their results of $\mu^I_{H\to\gamma\gamma}$ and the set $\{\epsilon^{I,X}_{\gamma\gamma}\}$ they used in their analysis [73, 106]. We summarize these values in Tables 4.3 and 4.4. For the analysis in $H \to ZZ/WW$, the CMS result is summarized in Table 4.5. The result of $H \to WW$ in the CMS experiment is given by assuming that all Higgs signals are produced by the GF process [77]. The ATLAS experiment only gives the signal strength for the specific production channels [74, 75], which is written as

$$\mu^X_{H\to ZZ/WW} = \frac{\sigma_X}{\sigma^{\rm SM}_X}\frac{\mathcal{B}_{H\to ZZ/WW}}{\mathcal{B}^{\rm SM}_{H\to ZZ/WW}}. \tag{4.21}$$

The results are given as $\mu^{\rm GF+ttH}_{H\to ZZ} = 1.8^{+0.8}_{-0.5}$, $\mu^{\rm VBF+VH}_{H\to ZZ} = 1.2^{+3.8}_{-1.4}$, $\mu^{\rm GF}_{H\to WW} = 0.82 \pm 0.36$, and $\mu^{\rm VBF}_{H\to WW} = 1.66 \pm 0.79$. In this article, we assume $\mu^{\rm GF+ttH}_{H\to ZZ} \simeq \mu^{\rm GF}_{H\to ZZ}$ for simplicity.

We evaluate a bound on the KK scale in each UED model by performing a χ^2 analysis of the results as shown above. The χ^2 function is represented as

$$\chi^2 = \sum_f \sum_I \left(\frac{\mu^I_{H\to f} - \hat{\mu}^I_f}{\hat{\sigma}^I_f} \right)^2 , \tag{4.22}$$

where we assume the experimental results to be Gaussian distribution $\hat{\mu}^I_f \pm \hat{\sigma}^I_f$.[3] The number of the observables we use in our analysis is 42 in total , and the degree of freedom is also the same number in terms of testing a justification of a model.

4.2.3 Bound on KK scale from the current data

Here we show bounds on several UED models from the Higgs searches at the LHC. For our analysis, we have taken the highest possible UV cutoff scale $\Lambda_{\rm max}$ shown in Table 4.2. The Higgs mass is chosen to be 126 GeV. In Fig. 4.5, we show the exclusion C.L. of each UED model as a function of the KK scale $M_{\rm KK}$ by use of all the ATLAS and CMS results of $H \to \gamma\gamma, WW, ZZ$. The black line indicates the result in the five-dimensional mUED model. The blue solid, dashed, and dotted lines denote those in the T^2-based ones, namely , the T^2/Z_2, $T^2/(Z_2 \times Z_2')$ and T^2/Z_4, respectively. The red solid and dashed lines represent those in the S^2-based ones, namely S^2 and S^2/Z_2, respectively. The green solid and dashed lines show those in the nonorientable ones, namely , RP^2 and PS, respectively.

As can be seen in this graph, we find that the region $M_{\rm KK} \lesssim 600$ GeV is excluded within 95% C.L. in the mUED model. For the six-dimensional models in the T^2-based space, we find the excluded regions $M_{\rm KK} \lesssim 1100$, 1000 , and 800 GeV within 95% C.L. for T^2/Z_2, $T^2/(Z_2 \times Z_2')$, and T^2/Z_4, respectively. For the S^2-based models, we can see that the regions $M_{\rm KK} \lesssim 1300$ and 900 GeV are excluded within 95% C.L. in the S^2 and S^2/Z_2, respectively. For the nonoriented models, the regions $M_{\rm KK} \lesssim 1100$ and 1200 GeV are excluded within 95% C.L. in the RP^2 and PS, respectively. As seen above, the excluded

[3]Note that , since we neglect the correlation among the categories, which is not made public, this analysis should rather be taken as an illustration.

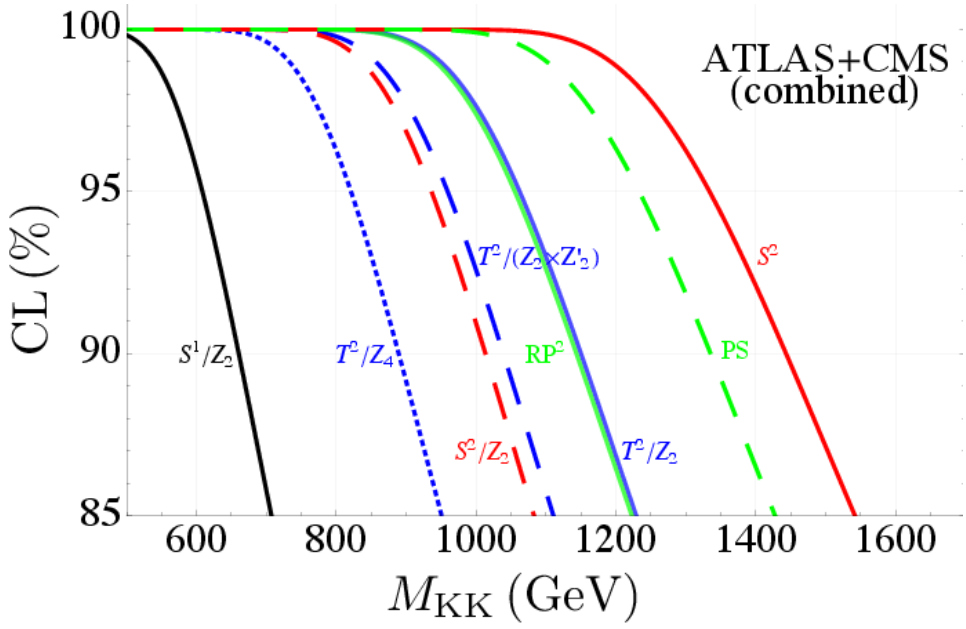

Figure 4.5: Exclusion C.L.s of all the UED models as functions of the KK scale $M_{\rm KK}$ by use of all the ATLAS and CMS results of $H \to \gamma\gamma, WW, ZZ$. Colors denote the same as in Fig. 4.2.

region is different from one model to another in the case for UED. This is because the difference of the KK spectrum has a large impact on the Higgs decays via loop processes. We summarize these bounds and possible highest UV cutoff for each models in Table 4.6.

We compare the bounds obtained from the ATLAS experiment with those from the CMS in Fig. 4.6. We find that the CMS result gives a more stringent bound on the KK scale compared with the ATLAS one. In other words, for now, the UED models are likely to explain the recent ATLAS result, while they are disfavored by the recent CMS result.

Throughout this analysis, we ignore the effects from the higher-dimensional operators around Λ. See Ref. [108] for such an effect.

We also summarized the suppression of BR($H \to \gamma\gamma$) and $\sigma(H \to \gamma\gamma)$ in Table 4.7 assuming possible lowest $M_{\rm KK}$ which is summarized in Table 4.6. The enhancement ratio of $H \to \gamma\gamma$ is a little smaller than $H \to ZZ, WW$ due to $H \to \gamma\gamma$ receive KK loop effects not only in Higgs production process but also in Higgs decay process. The suppression ratio of branching ratio BR($H \to \gamma\gamma$) and cross section $\sigma_{H\to\gamma\gamma}$ are summarized in Table 4.7.

4.2.4 S, T parameters in UEDs

In this section, we formulate the contributions to the S and T parameters in the six-dimensional UED models and in the mUED model. It is well known that the S and T parameters are logarithmically divergent in six dimensions [25]. To have a rough idea of

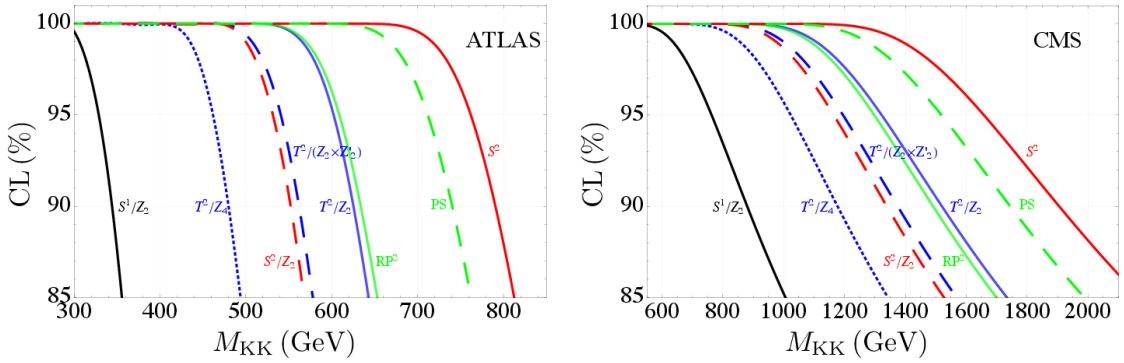

Figure 4.6: The exclusion C.L.s of all UED models as functions of the KK scale $M_{\rm KK}$ obtained from the ATLAS (left) and CMS (right) results of $H \to \gamma\gamma, WW, ZZ$. Colors denote the same as in Fig. 4.2.

	$\Lambda/M_{\rm KK}$ for $M_{\rm KK} \sim O$(TeV)	Higgs signal strength
mUED	5.0	610 GeV
T^2/Z_2	2.5	1060 GeV
$T^2/(Z_2 \times Z_2')$	2.9	960 GeV
T^2/Z_4	3.4	820 GeV
RP^2	2.3	1060 GeV
S^2	2.3	1330 GeV
S^2/Z_2	3.2	940 GeV
PS	1.9	1240 GeV

Table 4.6: Highest possible UV cutoff scales and lower bounds on the KK scale $M_{\rm KK}$ for each model at the 95% C.L.

	UED/SM ratio of BR($H \to \gamma\gamma$)	UED/SM ratio of $\sigma_{\gamma\gamma\to H}$
mUED	0.93	0.94
T^2/Z_2	0.93	0.94
$T^2/(Z_2 \times Z_2')$	0.93	0.94
T^2/Z_4	0.92	0.94
RP^2	0.93	0.94
S^2	0.85	0.88
S^2/Z_2	0.92	0.94
PS	0.90	0.92

Table 4.7: Prediction on the UED/SM ratio of BR($H \to \gamma\gamma$) and $\sigma_{\gamma\gamma\to H}$ with the lowest possible value of the KK scale.

what happens, we employ the following prescription. First, we compute the contributions from each KK mode within four-dimensional field theory employing the dimensional regularization. They are manifestly finite. Then we sum such contributions up to a mode in which the KK mass exceeds the UV cutoff Λ. To estimate the possible effects from the UV theory above Λ, we also put the higher-dimensional operators in six dimensions.

As we shoed in (3.40) and (3.41), the general shape of the S and T parameters are

$$S = \sum_{\substack{s \\ \text{with } M_s<\Lambda}} \left(S^{(\mathrm{KK})}_{s,\mathrm{boson}} + S^{(\mathrm{KK})}_{s,\mathrm{fermion}} \right) + S_{\text{Higgs calibration}} + S_{\mathrm{threshold}}, \tag{4.23}$$

$$T = \sum_{\substack{s \\ \text{with } M_s<\Lambda}} \left(T^{(\mathrm{KK})}_{s,\mathrm{boson}} + T^{(\mathrm{KK})}_{s,\mathrm{fermion}} \right) + T_{\text{Higgs calibration}} + T_{\mathrm{threshold}}, \tag{4.24}$$

where the first terms in parentheses are the contributions of KK particles, and last two terms are the contribution of Higgs calibration and higher dimensional operators.

As we discussed in section 4.1.2, in the configuration of $m_H = 126\,\mathrm{GeV}$, the value of the maximum UV cutoff scale tends to be low, and the threshold corrections possibly become important. We will include these effects below. We find that the effect from the state-s fermion loops takes the following general shapes in every six-dimensional UED model, which is the same as in the mUED and was already calculated in Ref. [25]. We show them in our notation:

$$S^{(\mathrm{KK})}_{\mathrm{fermion},s} \simeq \frac{1}{4\pi}\frac{2}{3} x_{t,s}, \quad T^{(\mathrm{KK})}_{\mathrm{fermion},s} \simeq \frac{1}{\alpha}\left(\frac{m_t^2}{4\pi^2 v^2}\right) x_{t,s}, \tag{4.25}$$

where $x_{t,s}$ is defined with the KK mass of the state "s" M_s as

$$x_{t,s} = \frac{m_t^2}{M_s^2} \tag{4.26}$$

and we ignore their $\mathcal{O}(x_{t,s}^2)$ corrections. In the RP^2 model, we should pay attention to the fact that the summation range differs between bosonic and fermionic sectors.

The bosonic part is highly model dependent. In this paper, we have newly calculated the contributions to S and T in every six-dimensional model. The complete forms of the gauge-boson two-point functions are summarized in Appendix C.

In the cases of T^2/Z_2, $T^2/(Z_2 \times Z_2')$, T^2/Z_4, S^2, and S^2/Z_2, the forms are

$$S^{(\mathrm{KK})}_{\mathrm{boson},s} \simeq \frac{1}{\pi}\left\{ -\frac{5}{36} x_{W,s} + \frac{1}{24} x_{H,s} + \left(\frac{1}{24} - \frac{1}{6c_W^2}\right) x_{Z,s} \right\}, \tag{4.27}$$

$$T^{(\mathrm{KK})}_{\mathrm{boson},s} \simeq \frac{1}{4\pi}\frac{1}{s_W^2}\left\{ \left(\frac{15}{4} - \frac{193}{72}\frac{1}{c_W^2} + \frac{1}{2c_W^4}\right) x_{W,s} + \left(-\frac{85}{72} - \frac{7}{18}\frac{1}{c_W^2}\right) x_{Z,s} + \left(\frac{13}{36} + \frac{5}{36}\frac{1}{c_W^2} - \frac{1}{2c_W^4}\right) x_{H,s} \right\}, \tag{4.28}$$

where we define similar variables as in Eq. (4.26): $x_{i,s} = \frac{m_i^2}{M_s^2}$ with m_W^2, m_Z^2, and m_H^2. Note that the lighter the KK particles are the greater they contribute to S and T. In these models, the result is affected only by the differences in the patterns of the surviving KK modes.

In the cases of the models based on the nonorientable manifolds RP^2 and PS, bosonic contributions are classified into three and two categories, respectively. The details of the following classifications have already been discussed in Sec. 4 and thus we do not explain it here. The results in the PS model are shown :

$$S^{(\mathrm{KK})}_{\mathrm{boson},s:\mathrm{odd}} \simeq 0, \quad T^{(\mathrm{KK})}_{\mathrm{boson},s:\mathrm{odd}} \simeq \frac{1}{4\pi}\frac{1}{s_W^2}\frac{5}{18}\left\{\left(1-\frac{1}{c_W^2}\right)x_{W,s} + \left(\frac{1}{c_W^2}-1\right)x_{Z,s}\right\}, \tag{4.29}$$

$$S^{(\mathrm{KK})}_{\mathrm{boson},s:\mathrm{even}} \simeq \frac{1}{\pi}\left\{-\frac{5}{36}x_{W,s} + \frac{1}{24}x_{H,s} + \left(\frac{1}{24}-\frac{1}{6c_W^2}\right)x_{Z,s}\right\}, \tag{4.30}$$

$$T^{(\mathrm{KK})}_{\mathrm{boson},s:\mathrm{even}} \simeq \frac{1}{4\pi}\frac{1}{s_W^2}\left\{\left(\frac{125}{36}-\frac{173}{72}\frac{1}{c_W^2}+\frac{1}{2c_W^4}\right)x_{W,s} + \left(-\frac{65}{72}-\frac{2}{3}\frac{1}{c_W^2}\right)x_{Z,s} + \left(\frac{13}{36}+\frac{5}{36}\frac{1}{c_W^2}-\frac{1}{2c_W^4}\right)x_{H,s}\right\}. \tag{4.31}$$

The shapes in the RP^2 model are closely related the previous ones in the PS as follows:

$$\{S,\,T\}^{(\mathrm{KK})}_{\mathrm{boson},s:\mathrm{region\ I}} = \{S,\,T\}^{(\mathrm{KK})}_{\mathrm{boson},s:\mathrm{even}}, \tag{4.32}$$

$$\{S,\,T\}^{(\mathrm{KK})}_{\mathrm{boson},s:\mathrm{region\ II}} = \{S,\,T\}^{(\mathrm{KK})}_{\mathrm{boson},s:\mathrm{odd}}, \tag{4.33}$$

$$\{S,\,T\}^{(\mathrm{KK})}_{\mathrm{boson},s:\mathrm{region\ III}} = \{S,\,T\}^{(\mathrm{KK})}_{\mathrm{boson},s}, \tag{4.34}$$

where we note that we should use the form of the KK mass on S^2 instead of on T^2.

The mixing among KK states in the gauge sector is schematically of the form

$$\begin{bmatrix} m_{W,Z}^2 + M_{\mathrm{KK}}^2 & M_{\mathrm{KK}}^2 & m_{W,Z}M_{\mathrm{KK}} \\ M_{\mathrm{KK}}^2 & m_{W,Z}^2 + M_{\mathrm{KK}}^2 & m_{W,Z}M_{\mathrm{KK}} \\ m_{W,Z}M_{\mathrm{KK}} & m_{W,Z}M_{\mathrm{KK}} & m_{W,Z}^2 + M_{\mathrm{KK}}^2 \end{bmatrix}. \tag{4.35}$$

In the calculation of S and T parameters, we adopt the following approximation about the mass mixings of six-dimensional W and Z boson-related sectors:

- We ignore off-diagonal terms with the magnitude $\mathcal{O}(m_{W,Z}M_{\mathrm{KK}})$, which are small compared with the other terms with the magnitude $\mathcal{O}(M_{\mathrm{KK}}^2)$.

- In the diagonal terms, for which the forms are approximately as $m_{W,Z}^2 + M_{\mathrm{KK}}^2$, we do not ignore the small part coming from $m_{W,Z}^2$ since this part can contribute to the T parameter.

Because of this approximation, the small mixings being proportional to $m^2_{W,Z}$ are ignored. As a result, some divergent terms that are proportional to $m^2_{W,Z}$ remain in the T parameter , and we simply discard them. Note that the contribution to T from each KK mode must be manifestly finite since it is computed in four-dimensional field theory with the dimensional regularization. The divergence ($\propto m^2_{W,Z}$) that we encounter here is an artifact coming from the ignorance of the small off-diagonal part in the KK mixing of gauge sector. Indeed, we find that there appears no divergence proportional to m^2_H or m^2_t, as we treat the mixing of the Higgs and top KK sectors exactly. Although there might be a further possible finite correction due to this procedure, the KK gauge contribution is generally subleading compared to the KK top loops, the mixing of which we treat exactly. In the S parameter, we do not see any divergence even after the above approximation. These features are consistent with the general property of S and T.

After we considered radiative corrections, the Weinberg angles of the KK W and Z bosons get to be very small [109]. We assume in this effect that the KK Weinberg angles are zero and that we can simply ignore the mass corrections. Each KK-state contribution should be suppressed by its KK mass, and hence this effect should not affect the leading order of S and T since their contributions are proportional to KK masses (when we ignore the electroweak masses in loop calculation) [109].

Finally we comment on the mUED model, which has been studied extensively [25, 26, 44, 110, 111]. In the χ^2 analysis of Refs. [25, 26], the authors simply ignored the terms being proportional to $m^2_{W,Z}$, possibly because their effects are not significant compared with those that are proportional to m^2_H or m^2_t.

Boson contributions to S and T in the mUED are approximately described with the even part of the PS (or region I of the RP^2) as we already showed in Eqs. (4.30) and (4.31) since the particle content of each KK state is the same. Fermion contributions are the same as in Eq. (4.25). Here , we adopt the form of the KK mass $M_{(n)}$ with a KK number n

$$M^2_{(n)} = n^2 M^2_{\rm KK}, \quad (\text{for } n = 1, 2, 3, \cdots). \tag{4.36}$$

4.2.5 Numerical result of S, T parameters analysis

We also execute a χ^2 analysis for putting indirect constraints on the UED models. χ^2 from S and T is defined as

$$\chi^2_{ST} = \frac{1}{1-\rho^2_{ST}} \left\{ \frac{(S - S_{\rm exp.})^2}{\sigma^2_S} + \frac{(T - T_{\rm exp.})^2}{\sigma^2_T} - \frac{2\rho_{ST}}{\sigma_S \sigma_T} (S - S_{\rm exp.})(T - T_{\rm exp.}) \right\}, \tag{4.37}$$

where S and T are the theoretical inputs in Eqs. (4.23) and (4.24) and the others are the experimental resultants in Eq. (3.44). In this and the next sections, we again adopt the assumption of $R_5 = R_6 = R$.

At first in this section, we consider the possibility without threshold correction to S and T in Eq. (3.42). We consider the maximal cutoffs with $M_{\rm KK} = 1\,\text{TeV}$ irrespective of $M_{\rm KK}$

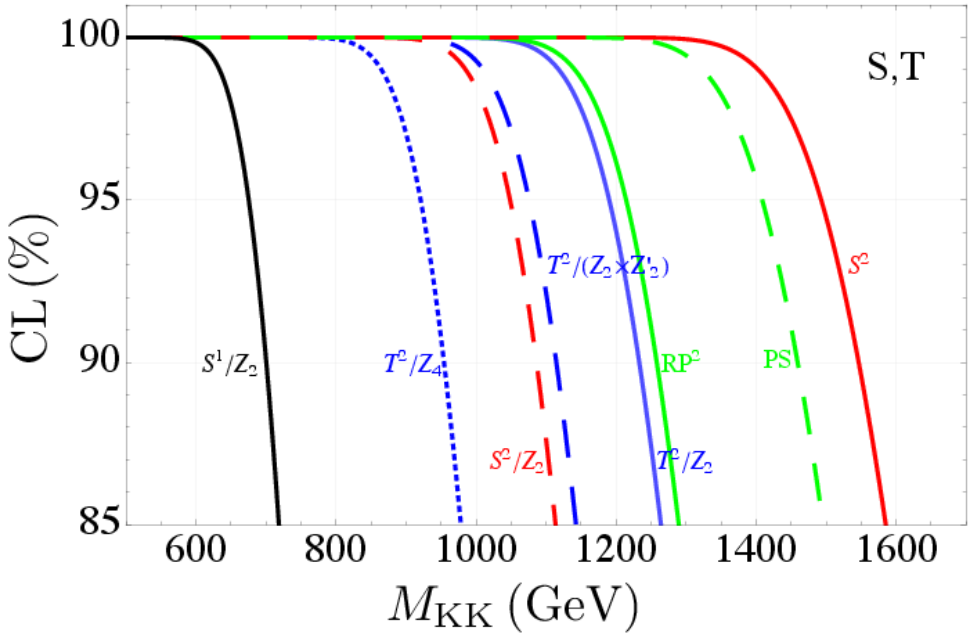

Figure 4.7: The exclusion C.L.s of all the UED models as functions of $M_{\rm KK}$ obtained from the S and T parameters. Colors denote the same as in Figure 4.5.

because our interest is in the case that $M_{\rm KK}$ is about a few TeV, and the values are almost universal as a function of $M_{\rm KK}$ in each model around a few TeV as shown in Fig. 4.2. The result is listed in Fig. 4.7. Each minimum is located around 1700 GeV (T^2/Z_2), 1500 GeV ($T^2/(Z_2 \times Z_2')$), 1300 GeV (T^2/Z_4), 2200 GeV (S^2), 1500 GeV (S^2/Z_2), 1800 GeV (RP^2), 2000 GeV (PS), and 1000 GeV (mUED). Interestingly, these values are somewhat greater than the corresponding 95% C.L. bound from the combined results in the Higgs searches as shown in Fig. 4.5.

We also estimate the 95% C.L. bounds of the models from Fig. 4.7, and the values are about 1200 GeV (T^2/Z_2), 1100 GeV ($T^2/(Z_2 \times Z_2')$), 900 GeV (T^2/Z_4), 1500 GeV (S^2), 1100 GeV (S^2/Z_2), 1200 GeV (RP^2), 1400 GeV (PS), and 700 GeV (mUED). Here, we can notice that these indirect bounds are compatible with the direct bounds via the LHC results discussed in the previous section. We note that our 95% C.L. bound (700 GeV) on the mUED is close to the previous values by the Gfitter group (700 GeV in $m_H = 126$ GeV) in Ref. [26].

We summarize the bounds on $M_{\rm KK}$ for each models in Table 4.8. We have commnets on higer dimensional operators. If Λ is much higher than $M_{\rm KK}$, the contributions of KK loops are much larger than higher dimensional operators. However, we found that possible highest UV cutoff are just a few times larger than $M_{\rm KK}$, especially six-dimensional case. We show the bounds on $M_{\rm KK}$ taking into account the threshold corrections of S, T parameters (3.42) for each models in Figure 4.8. The vertical axis is exclusion confidence level, and the horizontal axis is $M_{\rm KK}$. The blue, black and red lines show the case of $c_S = +1, 0$

	$\Lambda/M_{\rm KK}$ for $M_{\rm KK} \sim O(\text{TeV})$	S and T parameters
mUED	5.0	680 GeV
T^2/Z_2	2.5	1190 GeV
$T^2/(Z_2 \times Z_2')$	2.9	1080 GeV
T^2/Z_4	3.4	920 GeV
RP^2	2.3	1220 GeV
S^2	2.3	1490 GeV
S^2/Z_2	3.2	1050 GeV
PS	1.9	1410 GeV

Table 4.8: Highest possible UV cutoff scales and lower boerunds on the KK scale $M_{\rm KK}$ for each model at the 95% C.L.

and -1, respectivily. The dashed, solid and dotted lines show the case of $c_T = +1, 0$ and -1, respectivily. We can find from Figure 4.8 that the maximal ambiguity of lower bound on $M_{\rm KK}$ is about 300-500 GeV, respectively. In our analysis, we omitted the effects of higher dimensional operators in analysis of Higgs signal strength. It is expected that the ambiguity from higher dimensioal operator becomes large like a case of S, T analysis.

4.3 Five-dimensional limits

Finally, let us show the results of five-dimensional limits $R_5 \gg R_6$ on six-dimensional UED models. If we assume LKP as the dark matter candidate in RP^2 model, the case $R_5 = R_6$ is disfavored because the $R_5 = R_6$ case requires the lower dark matter mass than the case $R_5 \gg R_6$. We show the same exclusion confidence level from the LHC Higgs search and from S, T analysis for five-dimensional limit of RP^2 and $T^2/(Z_2 \times Z_2')$ in Figure 4.9. We can find that the lower bounds on $M_{\rm KK}$ in five-dimensional limit are almost same as mUED case. The small differences comes from the existence of scalar modes of gauge field, A_5, A_6. In addition, RP^2 models does not have specific KK states we had shown in Figure 4.1 in subsection 4.1.1. Such a differences affect the RGE and S, T parameters. Note that, in five-dimensional limit loosens the possible higher KK mode as $\Lambda_{\rm max} = 5.5 M_{\rm KK}$ and $3.9 M_{\rm KK}$ for $T^2/(Z_2 \times Z_2')$ and RP^2, respectively.

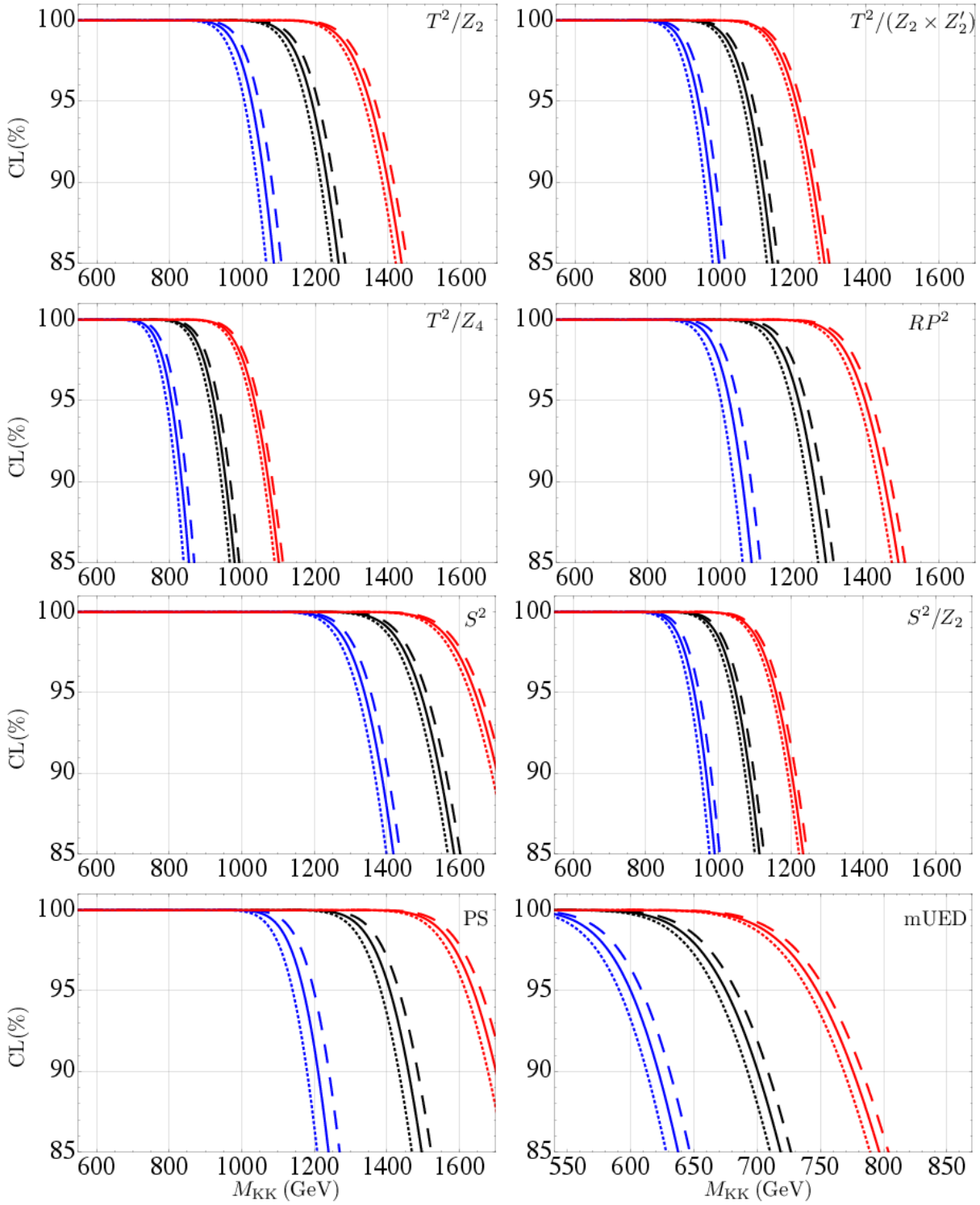

Figure 4.8: The exclusion C.L.s via the χ^2 analysis of S and T parameters as a function of $M_{\rm KK}$ with the maximal cutoffs in the UED models with threshold corrections in Eq. (3.42). In each panel corresponding to each model, the left (blue), center (black), and right (red) bunches of lines are for $c_S = +1$, 0, and -1, respectively. In each bunch, the dotted, solid, and dashed lines correspond to $c_T = -1$, 0, and $+1$, respectively.

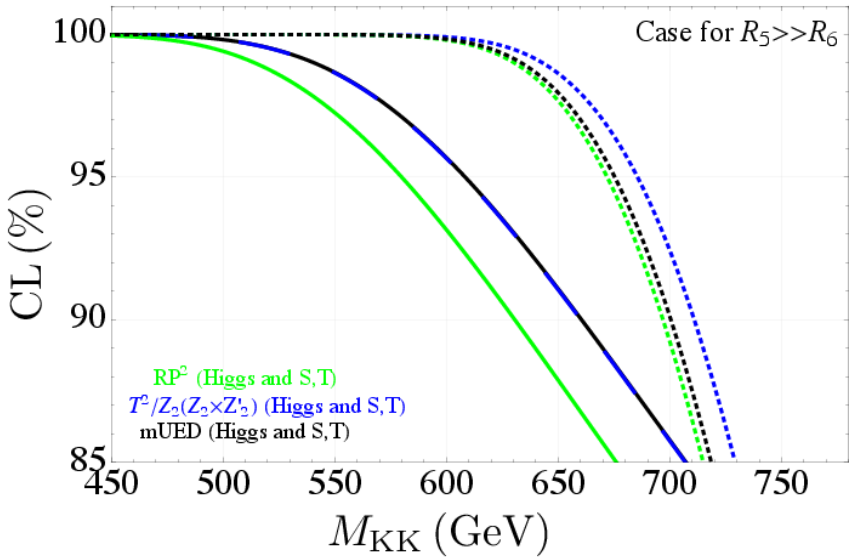

Figure 4.9: The same exclusion C.L.s as above, in the limit $R_5 \gg R_6$. The solid and dotted lines correspond to the bounds from Higgs searches and S, T constraints, respectively. The former Higgs bounds for $T^2/Z_2(Z_2 \times Z_2')$ and mUED are degenerate with each other.

Chapter 5

Summary and overview

We have studied the effects of Kaluza-Klein (KK) loops to Higgs production and decay processes at the LHC and electroweak precision measurement not only for the minimal Universal Extra Dimension (mUED) case but also in all the known six-dimensional UEDs. The total effect of KK loops depends on the UV cutoff Λ of higher dimensional field theory. We estimated the highest Λ by electroweak vacuum stability by analyzing RG evolution of the Higgs quartic interaction.

In the UED models, the contributions from KK top and KK gauge bosons change the Higgs decay rate and production cross section through loop processes. By such KK loop effects, the signal strength at the LHC is generally enhanced. On the other hand, in UED case, electroweak S, T parameters are both enhanced by loop contributions of KK excited mode of heavier SM particles, i.e., top, Higgs, and massive gauge bosons. As a result of our analysis, we found a lower bound on the KK scale $M_{\rm KK}$ for each model that we focus on. The bounds are summarized in Table 4.6 and 4.8 in Chapter 4. The S, T parameters give slightly tight bounds on $M_{\rm KK}$ compared with the bounds from Higgs signal strength. In a few years, however, the constraints from the LHC Higgs search will be stronger than current status. because the LHC will restart in 2015 and new data will be released one after another.

We have some comments on $H \to \gamma\gamma$ coupling. In Table 4.7, we used the values for possible lower bounds on $M_{\rm KK}$ and possible upper bounds on Λ that we found from Higgs signal strength analysis. The KK loop effects on $H \to \gamma\gamma$ will also be tested in a future linear collider [112]. We can find from Table 4.7 that the Higgs production cross section is suppressed about factor 0.9 for each model. This is marginally accessible at the future linear collider with integrated luminosity 500 fb^{-1} at 500GeV for which the expected precision for the BR($H \to \gamma\gamma$) is 23% for $M_h = 120$ GeV [113]. This precision is refined to 5.4% with luminosity 1 ab^{-1} at 1 TeV for the same Higgs mass [114]. When we employ the photon-photon collider option of the linear collider, $H\gamma\gamma$ coupling can be measured more directly from the total production cross section of the Higgs. This is well within the reach for integrated photon-photon luminosity 410 fb^{-1} at a linear e^+e^- collider operated at a $\sqrt{s} = 210$ GeV, which can measure $\Gamma_{H\to\gamma\gamma} \times {\rm BR}(H \to \gamma\gamma)$ with accuracy of 2.1% for $m_H = 120\,{\rm GeV}$ [115].

Finally, we comment on the future of six-dimensional UED models. We found that the possible highest value of the UV cutoff Λ cannot be much larger than the KK scale $M_{\rm KK}$ as the result of RGE and vacuum stability analysis. Therefore, if we consider a small $M_{\rm KK}$, typically of order of 1 TeV, in order to account for the dark matter, possible highest Λ must be of the same order. When we consider the TeV scale Λ, corrections from higher dimensional operators in around Λ may become significant. Actually as we have shown in Chapter 4, such higher dimensional operators can affct the S, T parameters significantly. Thus our result implies that in order to be predictive, the UED models need a concrete UV completion that is consistent with the vacuum stability.

The work of UED models are completed. We found that vacuum stability is a very powerful tool for constraining the models. The analysis of vacuum stability is important for phenomenology in this era. Therefore it is interesting to explore other models for physics beyond the SM in a view point of vacuum stability.

Acknowledgement

The author would like to thank Hiroaki Nakano and Kin-ya Oda as supervisors. The author would like to thank my collaborators, Kenji Nishiwaki, Naoya Okuda, Kin-ya Oda, and Ryotaro Watanabe for fruitful collaboration. The author is grateful to Prof. Morimitsu Tanimoto for continuous encouragement. The author thank Tomohiro Abe for useful comments on oblique corrections and Swarup Kumar Majee for discussions in the early stages of our collaboration.

Appendix A

RGE for SM and UEDs

In this Appendix, we show concrete form of RGEs for gauge, Yukawa, and Higgs quartic coupling. Here, we rewrite the schematic shape of the beta function for a quantity $\mathcal{Q}$ in six-dimensional UED:

$$\beta_{\mathcal{Q}} = \beta_{\mathcal{Q}}^{(\mathrm{SM})} + \sum_{s:\,\mathrm{KK\ states}} \theta(\mu - M_s)\Big(N_s \beta_{s,\mathcal{Q}}^{(\mathrm{KK})}\Big). \tag{A.1}$$

As we have already discussed, the β-functions take different forms depending on the following two categories: UEDs on an orientable space and those on an unorientable one. The former contains T^2/Z_2, $T^2/(Z_2 \times Z_2')$, T^2/Z_4, S^2 and S^2/Z_2 whereas the latter contains the remaining RP^2, PS. The contribution of the KK particles to the beta function $\beta_{s,\mathcal{Q}}^{(\mathrm{KK})}$ is independent of the KK index and we can omit the index s as $\beta_{\mathcal{Q}}^{(\mathrm{KK})}$. We note that in all the RGE analysis in this thesis, we ignore Yukawa couplings except the top quark one.

A.1 UEDs in orientable space

In the following, λ is 4D Higgs self-couplings; g_1, g_2, and g_3 show the 4D $U(1)_Y$, $SU(2)_W$, and $SU(3)_C$ gauge couplings; $y_{\ell_k}, y_{u_k}, y_{d_k}\,(k = 1,2,3)$ represent the 4D (diagonalized) Yukawa couplings of the charged leptons, the up-type quarks, and the down-type quarks, respectively. Here, we adopt the SM normalization in the $U(1)_Y$ gauge coupling g_1. The index k indicates their generations. V_{ij} stand for the Cabibbo–Kobayashi–Maskawa matrix, and $N_{C_{f_i}}$ indicates the color factor of the particle f_i, namely, 3 for quarks and 1 for leptons.

For Higgs quartic interaction $\mathcal{Q} = \lambda$, we have

$$\beta_\lambda^{(\mathrm{SM})} = \frac{1}{(4\pi)^2}\left\{6\lambda^2 - (3g_1^2 + 9g_2^2)\lambda + \frac{3}{2}(g_1^4 + 2g_1^2 g_2^2 + 3g_2^4) + 4\lambda\sum_i N_{C_{f_i}} y_{f_i}^2 - 8\sum_i N_{C_{f_i}} y_{f_i}^4\right\}, \tag{A.2}$$

$$\beta_\lambda^{(\mathrm{KK})} = \frac{1}{(4\pi)^2}\left\{6\lambda^2 - (3g_1^2 + 9g_2^2)\lambda + \left(\frac{5}{2}g_1^4 + 5g_1^2 g_2^2 + \frac{15}{2}g_2^4\right) + 8\lambda\sum_i N_{C_{f_i}} y_{f_i}^2 - 16\sum_i N_{C_{f_i}} y_{f_i}^4\right\}. \tag{A.3}$$

For gauge couplings $\circ\ \mathcal{Q} = g_i\,(i = 1, 2, 3)$,

$$\beta_{g_i}^{(\mathrm{SM})} = \frac{1}{(4\pi)^2} b_{g_i}^{(\mathrm{SM})} g_i^3, \quad \beta_{g_i}^{(\mathrm{KK})} = \frac{1}{(4\pi)^2} b_{g_i}^{(\mathrm{KK})} g_i^3, \tag{A.4}$$

with $b_{g_i}^{(\mathrm{SM})} = (\frac{41}{6}, -\frac{19}{6}, -7)$ and $b_{g_i}^{(\mathrm{KK})} = (\frac{27}{2}, \frac{3}{2}, -2)$ for $g_i = (g_1, g_2, g_3)$, respectively.

For Yukawa couplings $\circ\ \mathcal{Q} = y_{\ell_k}, y_{u_k}, y_{d_k}\,(k = 1, 2, 3)$,

$$\beta_{y_{\ell_k}}^{(\mathrm{SM})} = \frac{1}{(4\pi)^2}\left\{ -\frac{15}{4} g_1^2 - \frac{9}{4} g_2^2 + \frac{3}{2} y_{\ell_k}^2 + \sum_i N_{C_{f_i}} y_{f_i}^2 \right\} y_{\ell_k}, \tag{A.5}$$

$$\beta_{y_{u_k}}^{(\mathrm{SM})} = \frac{1}{(4\pi)^2}\left\{ -\frac{17}{12} g_1^2 - \frac{9}{4} g_2^2 - 8 g_s^2 + \frac{3}{2} y_{u_k}^2 + \sum_j y_{d_j}^2 (V_{kj} V_{jk}^\dagger) + \sum_i N_{C_{f_i}} y_{f_i}^2 \right\} y_{u_k}, \tag{A.6}$$

$$\beta_{y_{d_k}}^{(\mathrm{SM})} = \frac{1}{(4\pi)^2}\left\{ -\frac{15}{12} g_1^2 - \frac{9}{4} g_2^2 - 8 g_s^2 + \frac{3}{2} y_{d_k}^2 + \sum_j y_{u_j}^2 (V_{kj}^\dagger V_{jk}) + \sum_i N_{C_{f_i}} y_{f_i}^2 \right\} y_{d_k}, \tag{A.7}$$

$$\beta_{y_{\ell_k}}^{(\mathrm{KK})} = \frac{1}{(4\pi)^2}\left\{ -\frac{9}{2} g_1^2 - \frac{3}{2} g_2^2 + \frac{3}{2} y_{\ell_k}^2 + 2 \sum_i N_{C_{f_i}} y_{f_i}^2 \right\} y_{\ell_k}, \tag{A.8}$$

$$\beta_{y_{u_k}}^{(\mathrm{KK})} = \frac{1}{(4\pi)^2}\left\{ -\frac{25}{18} g_1^2 - \frac{3}{2} g_2^2 - \frac{32}{3} g_s^2 + \frac{3}{2} y_{u_k}^2 + 2 \sum_i N_{C_{f_i}} y_{f_i}^2 - \frac{3}{2} \sum_j (V_{kj} V_{jk}^\dagger) y_{d_j}^2 \right\} y_{u_k}, \tag{A.9}$$

$$\beta_{y_{d_k}}^{(\mathrm{KK})} = \frac{1}{(4\pi)^2}\left\{ -\frac{1}{18} g_1^2 - \frac{3}{2} g_2^2 - \frac{32}{3} g_s^2 + \frac{3}{2} y_{d_k}^2 + 2 \sum_i N_{C_{f_i}} y_{f_i}^2 - \frac{3}{2} \sum_j (V_{kj}^\dagger V_{jk}) y_{u_j}^2 \right\} y_{d_k}. \tag{A.10}$$

A.2 Projective Sphere case

In the case of PS, the contributions of the bosonic KK particles to the beta functions is classified into two categories as $\beta_{\mathrm{even},\mathcal{Q}}^{(\mathrm{KK})}$ and $\beta_{\mathrm{odd},\mathcal{Q}}^{(\mathrm{KK})}$.

For Higgs quartic interaction $\circ\ \mathcal{Q} = \lambda$,

$$\beta_{\mathrm{even},\lambda}^{(\mathrm{KK})} = \frac{1}{(4\pi)^2}\left\{ 6\lambda^2 - 3\lambda g_1^2 - 9\lambda g_2^2 + 2 g_1^4 + 4 g_1^2 g_2^2 + 6 g_2^4 + 8 \sum_i \lambda N_{C_{f_i}} y_{f_i}^2 - 16 \sum_i N_{C_{f_i}} y_{f_i}^4 \right\}, \tag{A.11}$$

$$\beta_{\mathrm{odd},\lambda}^{(\mathrm{KK})} = \frac{1}{(4\pi)^2}\left\{ + \frac{1}{2} g_1^4 + g_1^2 g_2^2 + \frac{3}{2} g_2^4 + 8 \sum_i \lambda N_{C_{f_i}} y_{f_i}^2 - 16 \sum_i N_{C_{f_i}} y_{f_i}^4 \right\}. \tag{A.12}$$

For gauge couplings $\circ\ \mathcal{Q} = g_i\,(i = 1, 2, 3)$,

$$\beta^{(\mathrm{KK})}_{\mathrm{even},g_i} = \frac{1}{(4\pi)^2} b^{(\mathrm{KK})}_{\mathrm{even},g_i} g_i^3, \quad \beta^{(\mathrm{KK})}_{\mathrm{odd},g_i} = \frac{1}{(4\pi)^2} b^{(\mathrm{KK})}_{\mathrm{odd},g_i} g_i^3, \tag{A.13}$$

with $b^{(\mathrm{KK})}_{\mathrm{even},g_i} = (\frac{27}{2}, \frac{7}{6}, -\frac{5}{2})$ and $b^{(\mathrm{KK})}_{\mathrm{odd},g_i} = (\frac{40}{3}, \frac{25}{3}, \frac{17}{2})$ for $g_i = (g_1, g_2, g_3)$, respectively.

For Yukawa couplings $\circ\ \mathcal{Q} = y_{\ell_k}, y_{u_k}, y_{d_k}$ $(k = 1, 2, 3)$,

$$\beta^{(\mathrm{KK})}_{\mathrm{even},y_{\ell_k}} = \frac{1}{(4\pi)^2} \left\{ -\frac{33}{8} g_1^2 - \frac{15}{8} g_2^2 + \frac{3}{2} y_{\ell_k}^2 + 2 \sum_i N_{C_{f_i}} y_{f_i}^2 \right\} y_{\ell_k}, \tag{A.14}$$

$$\beta^{(\mathrm{KK})}_{\mathrm{even},y_{u_k}} = \frac{1}{(4\pi)^2} \left\{ -\frac{101}{72} g_1^2 - \frac{15}{8} g_2^2 - \frac{28}{3} g_s^2 + \frac{3}{2} y_{u_k}^2 + 2 \sum_i N_{C_{f_i}} y_{f_i}^2 - \frac{3}{2} \sum_j (V_{kj} V_{jk}^\dagger) y_{d_j}^2 \right\} y_{u_k}, \tag{A.15}$$

$$\beta^{(\mathrm{KK})}_{\mathrm{even},y_{d_k}} = \frac{1}{(4\pi)^2} \left\{ -\frac{17}{72} g_1^2 - \frac{15}{8} g_2^2 - \frac{28}{3} g_s^2 + \frac{3}{2} y_{d_k}^2 + 2 \sum_i N_{C_{f_i}} y_{f_i}^2 - \frac{3}{2} \sum_j (V_{kj}^\dagger V_{jk}) y_{u_j}^2 \right\} y_{d_k}, \tag{A.16}$$

$$\beta^{(\mathrm{KK})}_{\mathrm{odd},y_{\ell_k}} = \frac{1}{(4\pi)^2} \left\{ -\frac{3}{8} g_1^2 + \frac{3}{8} g_2^2 + 2 \sum_i N_{C_{f_i}} y_{f_i}^2 \right\} y_{\ell_k}, \tag{A.17}$$

$$\beta^{(\mathrm{KK})}_{\mathrm{odd},y_{u_k}} = \frac{1}{(4\pi)^2} \left\{ +\frac{1}{72} g_1^2 + \frac{3}{8} g_2^2 - \frac{4}{3} g_s^2 + 2 \sum_i N_{C_{f_i}} y_{f_i}^2 \right\} y_{u_k}, \tag{A.18}$$

$$\beta^{(\mathrm{KK})}_{\mathrm{odd},y_{d_k}} = \frac{1}{(4\pi)^2} \left\{ +\frac{13}{72} g_1^2 + \frac{3}{8} g_2^2 - \frac{4}{3} g_s^2 + 2 \sum_i N_{C_{f_i}} y_{f_i}^2 \right\} y_{d_k}. \tag{A.19}$$

A.3 RP^2 case

In the regions having bosonic modes (regions I, II, and III), the following relations are fulfilled for each type of coupling C:

$$\beta^{(\mathrm{KK})}_{\text{region I},C} = \beta^{(\mathrm{KK})}_{\mathrm{even},C}, \quad \beta^{(\mathrm{KK})}_{\text{region II},C} = \beta^{(\mathrm{KK})}_{\mathrm{odd},C}, \quad \beta^{(\mathrm{KK})}_{\text{region III},C} = \beta^{(\mathrm{KK})}_{C}. \tag{A.20}$$

We write down the formula for the region without having a bosonic mode (region IV).

For$\circ\ \mathcal{Q} = \lambda$,

$$\beta^{(\mathrm{KK})}_{\text{region IV},\lambda} = \frac{1}{(4\pi)^2} \left\{ +8 \sum_i \lambda N_{C_{f_i}} y_{f_i}^2 - 16 \sum_i N_{C_{f_i}} y_{f_i}^4 \right\}. \tag{A.21}$$

For $\circ\ \mathcal{Q} = g_i$ $(i = 1, 2, 3)$,

$$\beta^{(\mathrm{KK})}_{\text{region IV},g_i} = \frac{1}{(4\pi)^2} b^{(\mathrm{KK})}_{\text{region IV},g_i} g_i^3, \tag{A.22}$$

with $b^{(\mathrm{KK})}_{\text{region IV},g_i} = (\frac{40}{3}, 8, 8)$ for $g_i = (g_1, g_2, g_3)$, respectively.

For $\circ\ \mathcal{Q} = y_{\ell_k}, y_{u_k}, y_{d_k}$ $(k = 1, 2, 3)$,

$$\beta^{(\mathrm{KK})}_{\text{region IV},y_{\ell_k}} = \frac{1}{(4\pi)^2} \left\{ +2 \sum_i N_{C_{f_i}} y_{f_i}^2 \right\} y_{\ell_k}, \tag{A.23}$$

$$\beta^{(\mathrm{KK})}_{\text{region IV},y_{u_k}} = \frac{1}{(4\pi)^2} \left\{ +2 \sum_i N_{C_{f_i}} y_{f_i}^2 \right\} y_{u_k}, \tag{A.24}$$

$$\beta^{(\mathrm{KK})}_{\text{region IV},y_{d_k}} = \frac{1}{(4\pi)^2} \left\{ +2 \sum_i N_{C_{f_i}} y_{f_i}^2 \right\} y_{d_k}. \tag{A.25}$$

A.4 mUED case

The surviving modes for each KK level in the mUED are totally the same as in region I of the RP^2 or in the "even" region of the PS. Hence, we can use those forms for RGEs in the mUED.

Appendix B

A, B functions

In this Appendix, we give some formula for useful functions in calculating loop corrections. We use the dimensional regularization scheme here.

B.1 A function

First of all, we introduce "A function" which appears in the one-loop self energy in ϕ^4 theory. The definition is

$$A(m_a^2) \equiv \int \frac{d^d k}{(2\pi)^d} \frac{1}{k^2 - m_a^2}, \tag{B.1}$$

where k is unknown momentum of the internal line in a loop, m_a is mass of a particle a in the loop, and $(2\pi)^d$ is the volume factor in d dimensional theory. The value of (B.1) can be calculated by general formula

$$\int \frac{d^d k}{(2\pi)^d} \frac{1}{(k^2 - m_a^2)^\alpha} = i \frac{(-1)^\alpha}{(4\pi)^{d/2}} \frac{\Gamma(\alpha - d/2)}{\Gamma(\alpha)} \frac{1}{(m_a^2)^{\alpha - d/2}}, \tag{B.2}$$

where Γ is the gamma function. In the case of $\alpha = 1$, we find

$$\begin{aligned}
A(m_a^2) &= \frac{-i}{(4\pi)^{d/2}} \frac{\Gamma(1 - d/2)}{\Gamma(1)} \frac{1}{(m_a^2)^{1-d/2}} \\
&= \frac{-i}{(4\pi)^{(2-\epsilon/2)}} \Gamma(\epsilon/2 - 1) \frac{m_a^2}{(m_a^2)^{\epsilon/2}} \\
&= \frac{-i}{16\pi^2} \Gamma(\epsilon/2 - 1) m_a^2 \left(\frac{4\pi}{m_a^2} \right)^{\epsilon/2} \\
&= \frac{i}{16\pi^2} m_a^2 \left[\frac{2}{\epsilon} + 1 - \gamma + \mathcal{O}(\epsilon) \right] \left[1 + \frac{\epsilon}{2} \log \frac{4\pi}{m_a^2} + \mathcal{O}(\epsilon^2) \right] \\
&= \frac{i}{16\pi^2} m_a^2 \left[\frac{2}{\epsilon} + 1 - \gamma + \log 4\pi + \log \frac{\mu^2}{m_a^2} + \mathcal{O}(\epsilon) \right]
\end{aligned} \tag{B.3}$$

where $\epsilon \equiv 4 - d$ which is divergent in 4-dimensional limit, γ is Euler's constant, and μ is momentum scale. Equation B.3 expresses the fact that the terms which do not contain ϵ give the finite correction at the scale μ, and the terms higher order in ϵ will vanish in 4-dimensional limit. The first term should be canceled by renormalization; when we employ $\overline{\text{MS}}$ renormalization scheme, γ and $\log 4\pi$ are also renormalized. Thus, we only have to take into account the term $\log \frac{\mu}{m_a^2}$ as loop correction from ϕ^4 theory:

$$A(m_a^2)_{\text{finite correction part}} = i\frac{m_a^2}{16\pi^2}\log\frac{\mu}{m_a^2}. \tag{B.4}$$

B.2 B functions

B.2.1 B_0 (scalar integral)

Next, we focus on the loop contribution for two point function induced by 3-point interaction. We define the most basic type of loop integral as "B_0 function",

$$B_0(p^2, m_a^2, m_b^2) \equiv \int \frac{d^dk}{(2\pi)^d}\frac{1}{(k^2 - m_a^2)\left((k+p)^2 - m_b^2\right)}, \tag{B.5}$$

where p is the external momentum, and m_a, m_b are the masses of the particles in internal lines. The analytical calculation of (B.5) can be given by Feynman parameter integral

$$\frac{1}{AB} = \int_0^1 dx \frac{1}{(A + (1-x)B)^2}. \tag{B.6}$$

We find

$$\begin{aligned} B_0(p^2, m_a^2, m_b^2) &= \int \frac{d^dk}{(2\pi)^d}\int_0^1 dx \frac{1}{\left(x(k^2 - m_a^2) + (1-x)\left((k+p)^2 - m_b^2\right)\right)^2} \\ &= \int \frac{d^dk'}{(2\pi)^d}\int_0^1 dx \frac{1}{\left(k'^2 + p^2x(1-x) - xm_a^2 - (1-x)m_b^2\right)^2} \\ &= \int \frac{d^dk'}{(2\pi)^d}\int_0^1 dx \frac{1}{\left(k'^2 - M^2\right)^2}, \end{aligned} \tag{B.7}$$

where $k' = k + p(1-x), M^2 = M^2(p^2, m_a^2, m_b^2, x) = -p^2x(1-x) + xm_a^2 + (1-x)m_b^2$. Appling (B.7) to (B.2), we find

$$B_0(p^2, m_a^2, m_b^2) = \int_0^1 dx \frac{i}{16\pi^2}\left(\frac{2}{\epsilon} - \gamma + \log 4\pi - \log\frac{\mu^2}{M^2}\right). \tag{B.8}$$

In a similar (B.4),

$$B_0(p^2, m_a^2, m_b^2)_{\text{finite correction}} = -\int_0^1 dx \frac{i}{16\pi^2}\log\frac{\mu^2}{M^2}. \tag{B.9}$$

We will write the B function as "$B_0(p^2, m_a^2, m_b^2) = B_0, B_0(0, m_a, m_b) = B_0(0)$" and the A function $A(m_x^2) = A_x, A(0) = A_0$ for simplicity.

B.2.2 B_1 (vector integral)

Now we turn to more complicated case of loop integral. "B_1 function" is defined by

$$p^\mu B_1(p^2, m_a^2, m_b^2) \equiv \int \frac{d^dk}{(2\pi)^d} \frac{k^\mu}{(k^2 - m_a^2)\left((k+p)^2 - m_b^2\right)}. \tag{B.10}$$

The left hand side must be proportional to the external momentum p^μ because of there are no other Lorentz vector that we can employ here. We can decompose B_1 into the combination of A and B_0, as we now perform. First, let me multiply $2p_\mu$ to (B.10), so that

$$\begin{aligned}
2p^2 B_1 &\equiv \int \frac{d^dk}{(2\pi)^d} \frac{2p\cdot k}{(k^2 - m_a^2)\left((k+p)^2 - m_b^2\right)} \\
&= \int \frac{d^dk}{(2\pi)^d} \frac{[(k+p)^2 - m_b^2] - k^2 - p^2 + m_b^2}{(k^2 - m_a^2)\left((k+p)^2 - m_b^2\right)} \\
&= \int \frac{d^dk}{(2\pi)^d} \left(\frac{1}{(k^2 - m_a^2)} - \frac{[k^2 - m_a^2] + m_a^2 + p^2 - m_b^2}{(k^2 - m_a^2)\left((k+p)^2 - m_b^2\right)} \right) \\
&= A_a - \int \frac{d^dk}{(2\pi)^d} \frac{1}{\left((k+p)^2 - m_b^2\right)} - \int \frac{d^dk}{(2\pi)^d} \frac{p^2 + m_a^2 - m_b^2}{(k^2 - m_a^2)\left((k+p)^2 - m_b^2\right)} \\
&= A_a - \int \frac{d^dk'}{(2\pi)^d} \frac{1}{\left((k')^2 - m_b^2\right)} - (p^2 + m_a^2 - m_b^2) \int \frac{d^dk}{(2\pi)^d} \frac{1}{(k^2 - m_a^2)\left((k+p)^2 - m_b^2\right)} \\
&= A_a - A_b - (p^2 + m_a^2 - m_b^2) B_0,
\end{aligned} \tag{B.11}$$

where momentum shift $k' = K + p$ is done. We already know the analytical form of A and B_0, and thus we can easily calculate B_1 as

$$B_1(p^2, m_a^2, m_b^2) = \frac{1}{2p^2} \left[A(m_a^2) - A(m_b^2) - (p^2 + m_a^2 - m_b^2) B_0(p^2, m_a^2, m_b^2) \right]. \tag{B.12}$$

The equation (B.12) appears to have a pole in zero momentum limit $p^2 = 0$, but this pole is canceled by that part in A and B_0. We show this cancellation below. Let us expand $B_0(p^2, m_a^2, m_b^2)$ around the low momentum limit $p^2 = 0$,

$$B_0(p^2, m_a^2, m_b^2) = B_0(0, m_a^2, m_b^2) + B_0'(0, m_a^2, m_b^2) p^2 + \frac{1}{2} B_0''(0, m_a^2, m_b^2) p^4 + \mathcal{O}(p^6), \tag{B.13}$$

where $B_0'(p^2, m_a^2, m_b^2) = \frac{\partial}{\partial p^2} B_0(p^2, m_a^2, m_b^2)$. We find

$$\begin{aligned}
B_0(0) &= \int \frac{d^dk}{(2\pi)^d} \frac{1}{(k^2 - m_a^2)(k^2 - m_b^2)} \\
&= \int \frac{d^dk}{(2\pi)^d} \frac{1}{(m_a^2 - m_b^2)} \left(\frac{1}{(k^2 - m_a^2)} - \frac{1}{k^2 - m_b^2} \right) \\
&= \frac{1}{(m_a^2 - m_b^2)} \left(A_a - A_b \right),
\end{aligned} \tag{B.14}$$

Inserting the equation (B.14) into (B.13), and (B.13) into (B.12), we find

$$\begin{aligned} B_1 &= \frac{1}{2p^2}\left\{A_a - A_b - (p^2 + m_a^2 - m_b^2)B_0\right\} \\ &= \frac{1}{2p^2}\left\{A_a - A_b - (m_a^2 - m_b^2)B_0\right\} - \frac{1}{2}B_0 \\ &= \frac{1}{2p^2}\left\{A_a - A_b - (m_a^2 - m_b^2)\left[\frac{A_a - A_b}{m_a^2 - m_b^2} + B_0'(0)p^2 + \frac{1}{2}B_0''(0)p^4 + \mathcal{O}(p^6)\right]\right\} - \frac{1}{2}B_0 \\ &= -\frac{(m_a^2 - m_b^2)}{2}B_0'(0) - \frac{m_a^2 - m_b^2}{4}B_0''(0)p^2 - \frac{1}{2}B_0 + \mathcal{O}(p^4). \end{aligned} \tag{B.15}$$

Equation (B.15) only contains B_0 and its derivative functions,

$$B_0' = -\frac{i}{16\pi^2}\int_0^1 dx\,(-x(1-x))\,\frac{1}{-p^2x(1-x) + xm_a^2 + (1-x)m_b^2} \tag{B.16}$$

$$\begin{aligned} B_0'(0) &= -\frac{i}{16\pi^2}\int_0^1 dx\,(-x(1-x))\,\frac{1}{xm_a^2 + (1-x)m_b^2} \\ &= -\frac{i}{16\pi^2}\frac{m_a^4 - m_b^4 + 2m_a^2m_b^2\log\frac{m_a^2}{m_b^2}}{2(m_b^2 - m_a^2)^3} \end{aligned} \tag{B.17}$$

$$B_0''(0) = \frac{i}{16\pi^2}\frac{(m_a^2 - m_b^2)(m_a^4 + 10m_a^2m_b^2 + m_b^4) - 6m_a^2m_b^2(m_a^2 + m_b^2)\log\frac{m_a^2}{m_b^2}}{3(m_a^2 - m_b^2)^5}. \tag{B.18}$$

Note that we can rewrite B_1 by the combination of A, and B_0 in the equation (B.11) by (B.14) and (B.13), we get

$$\begin{aligned} B_1 = &\frac{1}{2p^2}A_a - A_b - \frac{m_a^2 - m_b^2}{2p^2(m_a^2 - m_b^2)}\,(A_a - A_b) \\ &- \frac{p^2}{2p^2}\left(\frac{1}{(m_a^2 - m_b^2)}\,(A_a - A_b)\right) \\ &+ \frac{p^2}{2p^2}(p^2 + m_a^2 - m_b^2)\left(\frac{i}{16\pi^2}\frac{m_a^4 - m_b^4 + 2m_a^2m_b^2\log\frac{m_a^2}{m_b^2}}{2(m_b^2 - m_a^2)^3} + \mathcal{O}(p^4)\right) \\ = &-\frac{1}{2(m_a^2 - m_b^2)}\,(A_a - A_b) \\ &+ \frac{(p^2 + m_a^2 - m_b^2)}{2}\left(\frac{i}{16\pi^2}\frac{m_a^4 - m_b^4 + 2m_a^2m_b^2\log\frac{m_a^2}{m_b^2}}{2(m_b^2 - m_a^2)^3} + \mathcal{O}(p^4)\right). \end{aligned} \tag{B.19}$$

In the equation (B.15) and (B.19), we find that the pole is canceled out, and we have rewritten B_1 by A or B_0 as the above (B.15) and (B.19). Note that we give another useful relation between A and B_0. Since $A(0) = 0$, the equation (B.14) gives

$$\begin{aligned} A_a &= m_a^2 B_0(0, m_a^2, 0) \\ A_b &= m_b^2 B_0(0, 0, m_b^2). \end{aligned} \tag{B.20}$$

B.2.3 B_{21} and B_{22} (tensor integral)

We must consider another important integral. The tensor type of integral is determined as the combination of two types of the functions "B_{21}" and "B_{22}":

$$p^\mu p^\nu B_{21}(p^2, m_a^2, m_b^2) + g^{\mu\nu} B_{22}(p^2, m_a^2, m_b^2) \equiv \int \frac{d^d k}{(2\pi)^d} \frac{k^\mu k^\nu}{(k^2 - m_a^2)\left((k+p)^2 - m_b^2\right)}. \quad \text{(B.21)}$$

Note that, different from B_0, B_1 and B_{21}, B_{22} has mass dimension 2. We will rewrite B_{21} and B_{22} by A and/or B_0 like the case of sec. B.2.2. For this purpose, we will give the two conditions for (B.21). First, let us multiply (B.21) by $2p_\mu$,

$$2p^2 p^\nu B_{21}(p^2, m_a^2, m_b^2) + 2p^\nu B_{22}(p^2, m_a^2, m_b^2) = \int \frac{d^d k}{(2\pi)^d} \frac{2(p\cdot k)k^\nu}{(k^2 - m_a^2)\left((k+p)^2 - m_b^2\right)}. \quad \text{(B.22)}$$

We can apply the formula (B.11) to (B.22), and get

$$\begin{aligned}
&2p^2 p^\mu B_{21} + 2p^\nu B_{22} \\
&= \int \frac{d^d k}{(2\pi)^d} \left(\frac{1}{k^2 - m_a^2} - \frac{1}{(k^2 + p^2) - m_b^2} - (p^2 + m_a^2 - m_b^2) \frac{1}{(k^2 - m_a^2)\left((k+p)^2 - m_b^2\right)} \right) k^\nu \\
&= -\int \frac{d^d k'}{(2\pi)^d} \frac{(k'-p)^\nu}{k'^2 - m_b^2} - (p^2 + m_a^2 - m_b^2) p^\nu B_1 \\
&= p^\nu A_b - (p^2 + m_a^2 - m_b^2) p^\nu B_1, \qquad \text{(B.23)}
\end{aligned}$$

where k' is shifted momentum $k + p = k'$. The first term in the second row has already vanished in the third row because the integrand of this term is odd function of k. Here we rewrote B_{21} and B_{22} by A and B_1. Next, we give the other condition. By multiplying (B.21) by $g_{\mu\nu}$, we get

$$p^2 B_{21} + d B_{22} = \int \frac{d^d k}{(2\pi)^d} \frac{k^2}{(k^2 - m_a^2)\left((k+p)^2 - m_b^2\right)}, \quad \text{(B.24)}$$

and we also apply (B.11),

$$\begin{aligned}
&p^2 B_{21}(p^2, m_a^2, m_b^2) + d B_{22}(p^2, m_a^2, m_b^2) \\
&= \int \frac{d^d k}{(2\pi)^d} \frac{[k^2 - m_a^2] + m_a^2}{(k^2 - m_a^2)\left((k+p)^2 - m_b^2\right)} \\
&= \int \frac{d^d k}{(2\pi)^d} \frac{1}{\left((k+p)^2 - m_b^2\right)} + \int \frac{d^d k}{(2\pi)^d} \frac{m_a^2}{(k^2 - m_a^2)\left((k+p)^2 - m_b^2\right)} \\
&= A_b + m_a^2 B_0. \qquad \text{(B.25)}
\end{aligned}$$

From the subtraction of (B.23) and (B.25),

$$B_{22} = \frac{1}{2(1-d)} \left[-A(m_b^2) - 2m_a^2 B_0 - (p^2 + m_a^2 - m_b^2) B_1 \right]. \quad \text{(B.26)}$$

From (B.15) and (B.20), we can rewrite (B.26) by A and B_0 for $d = 4$ limit

$$\begin{aligned} B_{22} &= \frac{1}{2(1-d)}\Big\{ - A_b - 2m_a^2 B_0 \\ &\qquad - (p^2 + m_a^2 - m_b^2)\frac{1}{2p^2}\left(A_a - A_b - (m_a^2 - m_b^2)B_0) + \frac{1}{2}(p^2 + m_a^2 - m_b^2)B_0 \right) \Big\} \\ &= \frac{1}{2(1-d)}\Big\{ - A_b - 2m_a^2 B_0 - \frac{1}{2}(A_a - A_b) + \frac{1}{2}(m_a^2 - m_b^2)B_0 \\ &\qquad \frac{m_a^2 - m_b^2}{2p^2}(A_a^2 - A_b^2) + \frac{(m_a^2 - m_b^2)^2}{2p^2}B_0 + \frac{1}{2}(p^2 + m_a^2 - m_b^2)B_0 \Big\}, \end{aligned} \tag{B.27}$$

and in $d = 4$ limit,

$$B_{22} = \frac{1}{12}\left\{ \big(A_a + A_b + 2(m_a^2 - m_b^2)B_0\big) + \frac{m_a^2 - m_b^2}{p^2}\big(A_a - A_b - (m_a^2 - m_b^2)B_0\big) - p^2 B_0 \right\} \tag{B.28}$$

Note that $\frac{1}{p^2}$ in (B.27) is canceled by (B.13).

Similarly, from (B.23) and (B.25),

$$\begin{aligned} B_{21} &= \frac{1}{2(d-1)p^2}\left\{(d-2)A_b - d(p^2 + m_a^2 - m_b^2)B_1 2m_a^2 B_0\right\} \\ &= \frac{1}{2p^2}\Big\{\frac{d-2}{d-1}A_b - \frac{d}{d-1}(p^2 + m_a^2 - m_b^2)\frac{1}{2p^2}\big(A_a - A_b - (m_a^2 - m_b^2)B_0\big) \\ &\quad + \frac{d}{d-1}(p^2 + m_a^2 - m_b^2)\frac{1}{2}B_0 - 2\frac{m_a^2}{d-1}B_0\Big\}, \end{aligned} \tag{B.29}$$

and in the limit $d = 4$,

$$B_{21} = \frac{1}{3p^2}\left\{ -A_a + 2A_b + (m_a^2 - 2m_b^2)B_0 - \frac{m_a^2 - m_b^2}{p^2}\big(A_a - A_b - (m_a^2 - m_b^2)B_0\big) \right\}. \tag{B.30}$$

Again, $\frac{1}{p^2}$ terms in the curly bracket are canceled like (B.28), and overall $\frac{1}{p^2}$ is canceled by definition of B_{21} (B.21). Now we can rewrite B_{21} and B_{22} by A, B_0 and its derivative B_0'.

B.3 Fermion loop

In this section, we consider boson two-point function by fermion loop for convenience to calculate S and T parameters. First, we assume the Feynman rule for gauge-fermion vertex as

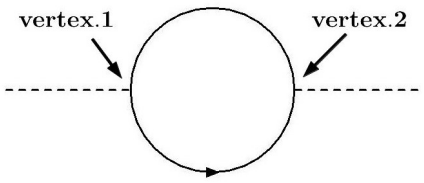

$$\begin{cases} \text{vertex.1} = i\gamma_\mu(C_R^1 P_R + C_L^1 P_L) \\ \text{vertex.2} = i\gamma_\nu(C_R^2 P_R + C_L^2 P_L), \end{cases} \tag{B.31}$$

where P_R, P_L are chiral projections. A two-point function is written as

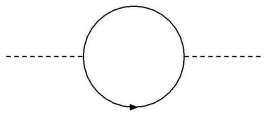

$$= (-1)\int \frac{d^dk}{(2\pi)^d}\frac{\mathrm{Tr}\left[i\gamma_\mu(C_R^1P_R+C_L^1P_L)i\left(\not{k}+\not{p}+m_b\right)i\gamma_\nu(C_R^2P_R+C_L^2P_L)i[\not{k}+m_a]\right]}{[k^2-m_a^2]\left((k+p)^2-m_b^2\right)}. \tag{B.32}$$

The numerator of (B.32) is

$$\begin{aligned}\text{numerator} = &\mathrm{Tr}\left[\gamma_\mu(\not{k}+\not{p})\gamma_\nu\ \not{k}(C_R^1C_R^2P_L+C_L^1C_L^2P_R)\right]\\ &+\mathrm{Tr}\left[\gamma_\mu(\not{k}+\not{p})\gamma_\nu m_a(C_R^1C_R^2P_R+C_L^1C_L^2P_L)\right]\\ &+\mathrm{Tr}\left[\gamma_\mu\gamma_\nu m_b\ \not{k}(C_R^1C_L^2P_R+C_L^1C_R^2P_L)\right]\\ &+\mathrm{Tr}\left[\gamma_\mu\gamma_\nu m_am_b(C_R^1C_L^2P_L+C_L^1C_R^2P_R)\right].\end{aligned} \tag{B.33}$$

The terms which contain $\gamma_\mu\gamma_\nu\gamma_5$ will vanish and in order to calculate S and T we do not have to calculate $\gamma_\mu\gamma_\nu\gamma_\rho\gamma_\sigma\gamma_5$ terms. By using trace technology

$$\begin{aligned}\mathrm{Tr}\left[\gamma_\mu\ \not{k}\gamma_\nu\ \not{k}\right] &= 8k_\mu k_\nu - 4k^2g_{\mu\nu},\\ \mathrm{Tr}\left[\gamma_\mu\ \not{p}\gamma_\nu\ \not{k}\right] &= 4(p_\mu k_\nu + p_\nu k_\mu - g_{\mu\nu}p\cdot k),\\ \mathrm{Tr}\left[\gamma_\mu\gamma_\nu\right] &= 4g_{\mu\nu},\end{aligned} \tag{B.34}$$

we can write (B.32) as

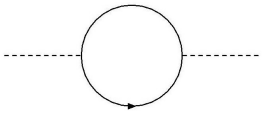

$$\begin{aligned}&= -\int \frac{d^dk}{(2\pi)^d}\frac{(C_R^1C_R^2+C_L^1C_L^2)\left(8k_\mu k_\nu+4(p_\mu k_\nu+k_\mu p_\nu-(k^2+p\cdot kg)_{\mu\nu})\right)+(C_R^1C_L^2+C_L^1C_R^2)4g_{\mu\nu}m_am_b}{[k^2-m_a^2]\left[(k+p)^2-m_b^2\right]}\\ &= -\int \frac{d^dk}{(2\pi)^d}\frac{C_a\left[(8k_\mu k_\nu-4k^2g_{\mu\nu})+4(p_\mu k_\nu+k_\mu p_\nu-p\cdot kg_{\mu\nu})\right]+C_b4g_{\mu\nu}m_am_b}{[k^2-m_a^2]\left[(k+p)^2-m_b^2\right]}\\ &= -\Big\{8C_a(p_\mu p_\nu B_{21}+g_{\mu\nu}B_{22}+g_{\mu\nu}B_{22})-4C_ag_{\mu\nu}(p^2B_{21}+dB_{22})\\ &\qquad\qquad +8C_ap_\mu p_\nu B_1+4C_ag_{\mu\nu}p^2B_1+C_b4g_{\mu\nu}m_am_b\Big\},\end{aligned} \tag{B.35}$$

where $C_a = (C_R^1 C_R^2 + C_L^1 C_L^2), and C_b = (C_R^1 C_L^2 + C_L^1 C_R^2)$. We focus on the coefficient of $g_{\mu\nu}$ to calculate S and T,

$$
\begin{aligned}
(\text{1-loop})|_{g_{\mu\nu}} &= -\left\{8C_a B_{22} - 4C_a(p^2 B_{21} + dB_{22}) + 4C_a p^2 B_1 + 4C_b m_a m_b\right\} \\
&= \frac{8C_a}{12}\left\{A_a + A_b + 2(m_a^2 + m_b^2)B_0 \frac{m_a^2 - m_b^2}{p^2}(A_a - A_b) - \frac{(m_a^2 - m_b^2)^2}{p^2}B_0 - p^2 B_0\right\} \\
&\quad + \frac{4C_a}{3}\left\{-A_a + 2A_b + (m_a^2 - 2m_b^2)B_0 - \frac{m_a^2 - m_b^2}{p^2}\left(A_a - A_b - (m_a^2 - m_b^2)B_0\right)\right\} \\
&\quad + \frac{4dC_a}{12}\left\{A_a + A_b + 2(m_a^2 + m_b^2)B_0 + \frac{m_a^2 - m_b^2}{p^2}(A_a - A_b) - \frac{(m_a^2 - m_b^2)^2}{p^2}B_0 - p^2 B_0\right\} \\
&\quad + \frac{4C_a}{2}\left\{A_a - A_b - (m_a^2 - m_b^2)B_0 - \frac{p^2}{2}B_0\right\} + 4C_b m_a m_b. \qquad \text{(B.36)}
\end{aligned}
$$

Note that $\frac{1}{p^2}$ are canceled by the expansion of B_0. In this way, we get a general form of fermion loop correction.

Appendix C

Two-point functions of gauge bosons in six-dimensional UEDs

In this Appendix, we summarize the two-point functions of photon, W, and Z bosons for calculating Peskin–Takeuchi S and T parameters.

C.1 Notations

First, we summarize our notations for the Passarino–Veltman B function [116]. In this section, we use the following descriptions for masses. The mass squared of the "sth" KK mode of the particle X is represented as

$$M_{X_s}^2 = m_X^2 + M_s^2 \tag{C.1}$$

where m_X is the corresponding zero-mode mass, and M_s is the sth level KK mass. Since only Z, W, H, and top masses are not negligible compared with the KK scale M_s, we use the representations

$$\begin{aligned} M_{W_s}^2 &:= m_W^2 + M_s^2, \quad M_{Z_s}^2 := m_Z^2 + M_s^2 \\ M_{t_s}^2 &:= m_t^2 + M_s^2, \quad M_{H_s}^2 := m_H^2 + M_s^2, \end{aligned} \tag{C.2}$$

and for the other fields,

$$M_{X_s}^2 \simeq M_s^2. \tag{C.3}$$

We will use the Passarino–Veltman loop integral to calculate two-point functions of the gauge bosons with external momentum k below. the definition is

$$\begin{aligned} \frac{1}{(4\pi)^2} B_{X_s,Y_s}(k^2) &= \int \frac{d^d p}{(2\pi)^d} \frac{1}{(p^2 - M_{X_s}^2)((p+k)^2 - M_{Y_s}^2)} \\ &= \frac{i}{(4\pi)^2} \left\{ \frac{1}{\bar{\varepsilon}} - \int_0^1 dx \ln \left[(1-x) M_{X_s}^2 + x M_{Y_s}^2 - x(1-x)k^2 - i\epsilon \right] \right\}, \end{aligned} \tag{C.4}$$

where we use the dimensional regularization in d dimensions and ε is an infinitesimal positive value[1]. $1/\overline{\varepsilon}$ ($:= 1/\varepsilon - \gamma + \ln 4\pi$) means the usual common divergent part with $\varepsilon = 2 - d/2$ and the Euler–Mascheroni constant γ. The following short-hand description is also used later for simplicity:

$$B_{X_s}(k^2) := B_{X_s,X_s}(k^2), \quad \delta B_{X_s,Y_s}(k^2) := \frac{B_{X_s,Y_s}(k^2) - B_{X_s,Y_s}(0)}{k^2}. \tag{C.5}$$

Here, we write down some useful formulas for calculations:

$$B_{X_s,Y_s}(0) \simeq \frac{1}{\overline{\varepsilon}} - \frac{1}{2}\frac{m_X^2 + m_Y^2}{M_s^2}, \tag{C.6}$$

$$B'_{X_s,Y_s}(0) \simeq \frac{1}{6M_s^2}, \tag{C.7}$$

$$B''_{X_s,Y_s}(0) \simeq \frac{2}{3}\frac{1}{(m_X^2 - m_Y^2)^2}\frac{m_X^2 + m_Y^2}{M_s^2}, \tag{C.8}$$

where we assume the hierarchy m_X^2, $m_Y^2 \ll M_s^2$ and values with a prime mean that it is differentiated with respect to k^2 once.

C.2 Gauge boson two-point function in six-dimensional UEDs and mUED : Bosonic contribution

In this subsection, we make a summary of bosonic two-point contributions to two-point function of gauge bosons in the six-dimensional UEDs and the mUED for evaluating S and T parameters. For contributions of fermions, we can use the result in Ref. [25].

The general form of a gauge boson two-point function is as follows:

$$\Pi_{ab}^{\mu\nu}(k^2) = i\Pi_{ab}^{\mathrm{T}}(k^2)\left(g^{\mu\nu} - \frac{k^\mu k^\nu}{k^2}\right) + i\Pi_{ab}^{\mathrm{L}}(k^2)\frac{k^\mu k^\nu}{k^2}, \tag{C.9}$$

where a and b show the type of gauge bosons, and the superscript T (L) indicates the transverse (longitudinal), respectively.

For estimating the S and T parameters, we calculate only the transverse ones. In each following subsection, we show the contributions of KK bosonic particles to the two-point functions from the level-s KK states.

[1]Be careful that "ε" is defined $\varepsilon = 2 - d/2$, and "ϵ" defined as $\epsilon = 4 - d$.

C.2.1 UEDs on oriented geometry case

The gauge boson two-point functions in oriented UED models are summarized as :

$$\Pi^{\mathrm{T},s}_{\gamma\gamma}(k^2) = \frac{\alpha}{4\pi}\left\{ -\frac{4}{9}k^2 + \left(\frac{7}{3}k^2 + \frac{20}{3}M^2_{W_s}\right) B_{W_s}(k^2) - \frac{20}{3}M^2_{W_s}B_{W_s}(0)\right\}, \tag{C.10}$$

$$\begin{aligned}\Pi^{\mathrm{T},s}_{Z\gamma}(k^2) = \frac{\alpha}{4\pi s_W c_W}\Bigg\{ & \left(-\frac{1}{9} + \frac{4}{9}c^2_W\right)k^2 + \left(\frac{20}{3}c^2_W - \frac{2}{3}\right)M^2_{W_s}B_{W_s}(0) \\ & + \left[\left(-\frac{1}{6} - \frac{7}{3}c^2_W\right)k^2 - \left(\frac{20}{3}c^2_W - \frac{2}{3}\right)M^2_{W_s} - 2m^2_W\right]B_{W_s}(k^2)\Bigg\},\end{aligned} \tag{C.11}$$

$$\begin{aligned}\Pi^{\mathrm{T},s}_{ZZ}(k^2) = \frac{\alpha}{4\pi s^2_W c^2_W}\Bigg\{ & \left(\frac{2}{9}c^2_W - \frac{4}{9}c^4_W - \frac{1}{18}\right)k^2 \\ & + \left(-\frac{20}{3}c^4_W + \frac{4}{3}c^2_W - \frac{1}{3}\right)M^2_{W_s}B_{W_s}(0) - \frac{1}{6}M^2_{H_s}B_{H_s}(0) - \frac{1}{6}M^2_{Z_s}B_{Z_s}(0) \\ & + \left[\left(\frac{7}{3}c^4_W + \frac{1}{3}c^2_W - \frac{1}{12}\right)k^2 + \left(\frac{20}{3}c^4_W - \frac{4}{3}c^2_W + \frac{1}{3}\right)M^2_{W_s} - \left(2 - 4c^2_W\right)m^2_W\right]B_{W_s}(k^2) \\ & + \left(-\frac{1}{12}k^2 + \frac{1}{6}M^2_{Z_s} + \frac{1}{6}M^2_{H_s} - \frac{m^2_Z}{c^2_W}\right)B_{H_s,Z_s}(k^2) - \frac{1}{12}(M^2_{H_s} - M^2_{Z_s})^2\delta B_{H_s,Z_s}(k^2)\Bigg\},\end{aligned} \tag{C.12}$$

$$\begin{aligned}\Pi^{\mathrm{T},s}_{WW}(k^2) = \frac{\alpha}{4\pi s^2_W}\Bigg\{ & -\frac{1}{3}k^2 - \frac{1}{6}M^2_{H_s}B_{H_s}(0) - 3M^2_{W_s}B_{W_s}(0) - \frac{17}{6}M^2_{Z_s}B_{Z_s}(0) \\ & + \left[-\frac{1}{12}k^2 + \frac{1}{6}M^2_{H_s} + \frac{1}{6}M^2_{W_s} - m^2_W\right]B_{H_s,W_s}(k^2) \\ & + \left[\frac{31}{12}k^2 + \frac{23}{6}\left(M^2_{W_s} + M^2_{Z_s}\right) - 2M^2_s - m^2_Z\left(c^2_W - 2 + c^{-2}_W\right)\right]B_{W_s,Z_s}(k^2) \\ & - \frac{1}{12}(M^2_{H_s} - M^2_{W_s})^2\delta B_{H_s,W_s}(k^2) - \frac{17}{12}(M^2_{Z_s} - M^2_{W_s})^2\delta B_{Z_s,W_s}(k^2)\Bigg\},\end{aligned} \tag{C.13}$$

C.2.2 RP^2, PS, mUED cases

As we have discussed in Sec. 4, the particle contents of the region III of the RP^2 model is completely the same as those of the six-dimensional UEDs on oriented geometries just as above , and we need not discuss them. Based on the knowledge in Sec. 4, the remaining

boson contributions are written down as follows:

$$\begin{aligned}\Pi^{\mathrm{T},s}_{\gamma\gamma}|_{\text{region II}}(k^2) &= \Pi^{\mathrm{T},s}_{\gamma\gamma}|_{\text{odd}}(k^2)\\ &= \frac{\alpha}{4\pi}\left\{ -\frac{2}{9}k^2 + \left(-\frac{1}{3}k^2 + \frac{4}{3}M^2_{W_s}\right) B_{W_s}(k^2) - \frac{4}{3}M^2_{W_s}B_{W_s}(0)\right\}, \qquad \text{(C.14)}\\ \Pi^{\mathrm{T},s}_{Z\gamma}|_{\text{region II}}(k^2) &= \Pi^{\mathrm{T},s}_{Z\gamma}|_{\text{odd}}(k^2)\\ &= \frac{\alpha}{4\pi}\left[-\frac{c_W}{s_W}\right]\left\{ -\frac{2}{9}k^2 + \left(-\frac{1}{3}k^2 + \frac{4}{3}M^2_{W_s}\right) B_{W_s}(k^2) - \frac{4}{3}M^2_{W_s}B_{W_s}(0)\right\}, \qquad \text{(C.15)}\\ \Pi^{\mathrm{T},s}_{ZZ}|_{\text{region II}}(k^2) &= \Pi^{\mathrm{T},s}_{ZZ}|_{\text{odd}}(k^2)\\ &= \frac{\alpha}{4\pi}\left[\frac{c^2_W}{s^2_W}\right]\left\{ -\frac{2}{9}k^2 + \left(-\frac{1}{3}k^2 + \frac{4}{3}M^2_{W_s}\right) B_{W_s}(k^2) - \frac{4}{3}M^2_{W_s}B_{W_s}(0)\right\}, \qquad \text{(C.16)}\\ \Pi^{\mathrm{T},s}_{WW}|_{\text{region II}}(k^2) &= \Pi^{\mathrm{T},s}_{WW}|_{\text{odd}}(k^2)\\ &= \frac{\alpha}{4\pi s^2_W}\left\{ -\frac{2}{9}k^2 - \frac{2}{3}M^2_{W_s}B_{W_s}(0) - \frac{2}{3}M^2_{Z_s}B_{Z_s}(0)\right.\\ &\quad \left. + \left[-\frac{1}{3}k^2 + \frac{2}{3}\left(M^2_{W_s} + M^2_{Z_s}\right)\right] B_{W_s,Z_s}(k^2) - \frac{1}{3}(M^2_{Z_s} - M^2_{W_s})^2\delta B_{Z_s,W_s}(k^2)\right\}. \qquad \text{(C.17)}\end{aligned}$$

The remaining part can be easily calculated by use of the following relations:

$$\Pi^{\mathrm{T},s}_{ab}|_{\text{region I}}(k^2) = \Pi^{\mathrm{T},s}_{ab}(k^2) - \Pi^{\mathrm{T},s}_{ab}|_{\text{region II}}(k^2), \qquad \text{(C.18)}$$

$$\Pi^{\mathrm{T},s}_{ab}|_{\text{even}}(k^2) = \Pi^{\mathrm{T},s}_{ab}(k^2) - \Pi^{\mathrm{T},s}_{ab}|_{\text{odd}}(k^2), \qquad \text{(C.19)}$$

where ab represents the possible four combinations of gauge bosons.

We can also derive the following relations for the mUED :

$$\Pi^{\mathrm{T},s}_{ab}|_{\text{mUED}}(k^2) \simeq \Pi^{\mathrm{T},s}_{ab}|_{\text{even}}(k^2) \qquad \text{(C.20)}$$

based on the discussions above.

Appendix D

Loop functions in single Higgs production and decay

In this Appendix, we summarize the loop functions that are needed for estimating the single Higgs production through the gluon fusion process and the Higgs decay into a pair of photons. Readers who want more explanations on the above expressions should consult Ref. [50].

For each model, the loop function $J_t^{\rm model}$ describes the contributions of all the zero and KK modes for the top quark in the triangle loops:

$$J_t^{\rm SM}(\hat{s}) = I\left(\frac{m_t^2}{\hat{s}}\right), \tag{D.1}$$

$$J_t^{\rm mUED}(\hat{s}) = \left\{ I\left(\frac{m_t^2}{\hat{s}}\right) + 2\sum_{n\geq 1}\left(\frac{m_t}{m_{t(n)}}\right)^2 I\left(\frac{m_{t(n)}^2}{\hat{s}}\right)\right\}, \tag{D.2}$$

$$J_t^{T^2/Z_2}(\hat{s}) = J_t^{RP^2}(\hat{s}) = \left\{ I\left(\frac{m_t^2}{\hat{s}}\right) + 2\sum_{\substack{m+n\geq 1\\ \text{or } m=-n\geq 1}}\left(\frac{m_t}{m_{t(m,n)}}\right)^2 I\left(\frac{m_{t(m,n)}^2}{\hat{s}}\right)\right\}, \tag{D.3}$$

$$J_t^{T^2/Z_4}(\hat{s}) = \left\{ I\left(\frac{m_t^2}{\hat{s}}\right) + 2\sum_{m\geq 1, n\geq 0}\left(\frac{m_t}{m_{t(m,n)}}\right)^2 I\left(\frac{m_{t(m,n)}^2}{\hat{s}}\right)\right\}, \tag{D.4}$$

$$J_t^{T^2/(Z_2\times Z_2')}(\hat{s}) = \left\{ I\left(\frac{m_t^2}{\hat{s}}\right) + 2\sum_{\substack{m\geq 0, n\geq 0,\\ (m,n)\neq(0,0)}}\left(\frac{m_t}{m_{t(m,n)}}\right)^2 I\left(\frac{m_{t(m,n)}^2}{\hat{s}}\right)\right\}, \tag{D.5}$$

$$J_t^{S^2/Z_2}(\hat{s}) = \left\{ I\left(\frac{m_t^2}{\hat{s}}\right) + 2\sum_{j\geq 1}\left(\frac{m_t}{m_{t(j)}}\right)^2 n^{S^2/Z_2}(j)\, I\left(\frac{m_{t(j)}^2}{\hat{s}}\right)\right\}, \tag{D.6}$$

$$J_t^{\rm PS}(\hat{s}) = J_t^{S^2}(\hat{s}) = \left\{ I\left(\frac{m_t^2}{\hat{s}}\right) + 2\sum_{j\geq 1}\left(\frac{m_t}{m_{t(j)}}\right)^2 (2j+1)\, I\left(\frac{m_{t(j)}^2}{\hat{s}}\right)\right\}, \tag{D.7}$$

where I is given by

$$I(\lambda) = -2\lambda + \lambda(1-4\lambda)\int_0^1 \frac{dx}{x}\ln\left[\frac{x(x-1)}{\lambda} + 1 - i\epsilon\right]. \tag{D.8}$$

The explicit result of the integral is

$$\int_0^1 \frac{dx}{x}\ln\left[\frac{x(x-1)}{\lambda} + 1 - i\epsilon\right] = \begin{cases} -2\left[\arcsin\dfrac{1}{\sqrt{4\lambda}}\right]^2 & (\text{for } \lambda \geq \frac{1}{4}), \\ \dfrac{1}{2}\left[\ln\dfrac{1+\sqrt{1-4\lambda}}{1-\sqrt{1-4\lambda}} - i\pi\right]^2 & (\text{for } \lambda < \frac{1}{4}), \end{cases} \tag{D.9}$$

where this form is related with the Passarino–Veltman's three-point scalar function C_0 [116].

$n^{\text{model}}(j)$ counts the number of degeneracy , and the explicit forms are shown in Eqs. (4.10)–(4.12) and we write the KK top and W masses ($X = t, W$)

$$m_{X(n)} \equiv \sqrt{m_X^2 + \frac{n^2}{R^2}}, \tag{D.10}$$

$$m_{X(m,n)} \equiv \sqrt{m_X^2 + \frac{m^2}{R_5^2} + \frac{n^2}{R_6^2}}, \tag{D.11}$$

$$m_{X(j)} \equiv \sqrt{m_X^2 + \frac{j(j+1)}{R^2}}. \tag{D.12}$$

The range of the KK summation reflects the structure of each extra-dimensional back-

ground. The loop functions which are needed for the process $H \to \gamma\gamma$ are as follows:

$$J_W^{\rm SM}(m_H^2) = L\left(\frac{1}{2}, 3, 3, 6, 0; \frac{m_W^2}{m_H^2}, \frac{m_W^2}{m_H^2}\right), \tag{D.13}$$

$$J_W^{\rm mUED}(m_H^2) = J_W^{\rm SM}(m_H^2) + \sum_{n\geq 1} L\left(\frac{1}{2}, 4, 4, 8, 1; \frac{m_W^2}{m_H^2}, \frac{m_{W(n)}^2}{m_H^2}\right), \tag{D.14}$$

$$J_W^{T^2/Z_4}(m_H^2) = J_W^{\rm SM}(m_H^2) + \sum_{m\geq 1, n\geq 0} L\left(\frac{1}{2}, 5, 4, 10, 1; \frac{m_W^2}{m_H^2}, \frac{m_{W(m,n)}^2}{m_H^2}\right), \tag{D.15}$$

$$J_W^{T^2/(Z_2\times Z_2')}(m_H^2) = J_W^{\rm SM}(m_H^2) + \sum_{\substack{m\geq 0, n\geq 0 \\ (m,n)\neq(0,0)}} L\left(\frac{1}{2}, 5, 4, 10, 1; \frac{m_W^2}{m_H^2}, \frac{m_{W(m,n)}^2}{m_H^2}\right), \tag{D.16}$$

$$J_W^{T^2/Z_2}(m_H^2) = J_W^{\rm SM}(m_H^2) + \sum_{\substack{m+n\geq 1 \\ \text{or } m=-n\geq 1}} L\left(\frac{1}{2}, 5, 4, 10, 1; \frac{m_W^2}{m_H^2}, \frac{m_{W(m,n)}^2}{m_H^2}\right), \tag{D.17}$$

$$\begin{aligned} J_W^{RP^2}(m_H^2) = J_W^{\rm SM}(m_H^2) &+ \sum_{(m,n)}^{A} L\left(\frac{1}{2}, 4, 4, 8, 1; \frac{m_W^2}{m_H^2}, \frac{m_{W(m,n)}^2}{m_H^2}\right) \\ &+ \sum_{(m,n)}^{B} L\left(0, 1, 0, 2, 0; \frac{m_W^2}{m_H^2}, \frac{m_{W(m,n)}^2}{m_H^2}\right), \end{aligned} \tag{D.18}$$

$$J_W^{S^2/Z_2}(m_H^2) = J_W^{\rm SM}(m_H^2) + \sum_{j\geq 1} n^{S^2/Z_2}(j)\, L\left(\frac{1}{2}, 5, 4, 10, 1; \frac{m_W^2}{m_H^2}, \frac{m_{W(j)}^2}{m_H^2}\right), \tag{D.19}$$

$$J_W^{S^2}(m_H^2) = J_W^{\rm SM}(m_H^2) + \sum_{j\geq 1} (2j+1)\, L\left(\frac{1}{2}, 5, 4, 10, 1; \frac{m_W^2}{m_H^2}, \frac{m_{W(j)}^2}{m_H^2}\right), \tag{D.20}$$

$$\begin{aligned} J_W^{\rm PS}(m_H^2) = J_W^{\rm SM}(m_H^2) + \sum_{j\geq 1} \Bigg[& n_{\rm even}^{\rm PS}(j)\, L\left(\frac{1}{2}, 4, 4, 8, 1; \frac{m_W^2}{m_H^2}, \frac{m_{W(j)}^2}{m_H^2}\right) \\ & + n_{\rm odd}^{\rm PS}(j)\, L\left(0, 1, 0, 2, 0; \frac{m_W^2}{m_H^2}, \frac{m_{W(j)}^2}{m_H^2}\right) \Bigg], \end{aligned} \tag{D.21}$$

with

$$L(a, b, c, d, e; \lambda_1, \lambda_2) = a + b\lambda_1 - [\lambda_1(c - d\lambda_2) - e\lambda_2] \int_0^1 \frac{dx}{x} \ln\left[\frac{x(x-1)}{\lambda_2} + 1 - i\epsilon\right]. \tag{D.22}$$

The A summation for RP^2 is over the region that satisfies both $m \geq 1$ and $n \geq 1$ as well as over the ranges $(m, n) = (0, 2), (0, 4), (0, 6), \ldots$ and $(m, n) = (2, 0), (4, 0), (6, 0), \ldots$. Similarly, the B summation is over $m \geq 1$ and $n \geq 1$ as well as over $(m, n) = (0, 1), (0, 3), (0, 5), \ldots$ and $(m, n) = (1, 0), (3, 0), (5, 0), \ldots$.

Bibliography

[1] A. Denner, *Techniques for calculation of electroweak radiative corrections at the one loop level and results for W physics at LEP-200*, Fortsch.Phys. **41** (1993), 307–420, 0709.1075.

[2] S. Weinberg, *A Model of Leptons*, Phys.Rev.Lett. **19** (1967), 1264–1266.

[3] UA1 Collaboration, G. Arnison et al., *Experimental Observation of Isolated Large Transverse Energy Electrons with Associated Missing Energy at s**(1/2) = 540-GeV*, Phys.Lett. **B122** (1983), 103–116.

[4] UA1 Collaboration, G. Arnison et al., *Experimental Observation of Lepton Pairs of Invariant Mass Around 95-GeV/c**2 at the CERN SPS Collider*, Phys.Lett. **B126** (1983), 398–410.

[5] ATLAS Collaboration, G. Aad et al., *Observation of a new particle in the search for the Standard Model Higgs boson with the ATLAS detector at the LHC*, Phys.Lett. **B716** (2012), 1–29, 1207.7214.

[6] CMS Collaboration, S. Chatrchyan et al., *Observation of a new boson at a mass of 125 GeV with the CMS experiment at the LHC*, Phys.Lett. **B716** (2012), 30–61, 1207.7235.

[7] ATLAS Collaboration, *Study of the spin of the new boson with up to 25 fb^{-1} of ATLAS data*, (2013).

[8] CMS Collaboration, S. Chatrchyan et al., *Study of the Mass and Spin-Parity of the Higgs Boson Candidate Via Its Decays to Z Boson Pairs*, Phys.Rev.Lett. **110** (2013), 081803, 1212.6639.

[9] ATLAS Collaboration, *Combined coupling measurements of the Higgs-like boson with the ATLAS detector using up to 25 fb^{-1} of proton-proton collision data*, (2013).

[10] T. A. collaboration, *Evidence for Higgs Boson Decays to the $\tau^+\tau^-$ Final State with the ATLAS Detector*, (2013).

[11] T. A. collaboration, *Differential cross sections of the Higgs boson measured in the diphoton decay channel using 8 TeV pp collisions*, (2013).

[12] CMS Collaboration, *Search for the Higgs boson decaying to invisible particles produced in association with Z bosons decaying to bottom quarks*, (2013).

[13] CMS Collaboration, S. Chatrchyan et al., *Measurement of the properties of a Higgs boson in the four-lepton final state*, (2013), 1312.5353.

[14] CMS Collaboration, S. Chatrchyan et al., *Measurement of Higgs boson production and properties in the WW decay channel with leptonic final states*, JHEP **1401** (2014), 096, 1312.1129.

[15] S. Perlmutter, M. S. Turner, and M. J. White, *Constraining dark energy with SNe Ia and large scale structure*, Phys.Rev.Lett. **83** (1999), 670–673, astro-ph/9901052.

[16] F. Zwicky, *On the Masses of Nebulae and of Clusters of Nebulae*, Astrophys.J. **86** (1937), 217–246.

[17] A. Sakharov, *Violation of CP Invariance, c Asymmetry, and Baryon Asymmetry of the Universe*, Pisma Zh.Eksp.Teor.Fiz. **5** (1967), 32–35.

[18] Super-Kamiokande Collaboration, Y. Fukuda et al., *Measurement of a small atmospheric muon-neutrino / electron-neutrino ratio*, Phys.Lett. **B433** (1998), 9–18, hep-ex/9803006.

[19] Super-Kamiokande Collaboration, Y. Fukuda et al., *Measurements of the solar neutrino flux from Super-Kamiokande's first 300 days*, Phys.Rev.Lett. **81** (1998), 1158–1162, hep-ex/9805021.

[20] T. Kaluza, *On the Problem of Unity in Physics*, Sitzungsber.Preuss.Akad.Wiss.Berlin (Math.Phys.) **1921** (1921), 966–972.

[21] O. Klein, *The Atomicity of Electricity as a Quantum Theory Law*, Nature **118** (1926), 516.

[22] I. Antoniadis, *A Possible new dimension at a few TeV*, Phys.Lett. **B246** (1990), 377–384.

[23] G. Servant and T. M. Tait, *Is the lightest Kaluza-Klein particle a viable dark matter candidate?*, Nucl.Phys. **B650** (2003), 391–419, hep-ph/0206071.

[24] G. Belanger, M. Kakizaki, and A. Pukhov, *Dark matter in UED: The Role of the second KK level*, JCAP **1102** (2011), 009, 1012.2577.

[25] T. Appelquist and H.-U. Yee, *Universal extra dimensions and the Higgs boson mass*, Phys.Rev. **D67** (2003), 055002, hep-ph/0211023.

[26] M. Baak, M. Goebel, J. Haller, A. Hoecker, D. Ludwig, et al., *Updated Status of the Global Electroweak Fit and Constraints on New Physics*, Eur.Phys.J. **C72** (2012), 2003, 1107.0975.

[27] U. Haisch and A. Weiler, *Bound on minimal universal extra dimensions from $\overline{B} \to X_s\gamma$*, Phys.Rev. **D76** (2007), 034014, hep-ph/0703064.

[28] T. G. Rizzo, *Probes of universal extra dimensions at colliders*, Phys.Rev. **D64** (2001), 095010, hep-ph/0106336.

[29] C. Macesanu, C. McMullen, and S. Nandi, *Collider implications of universal extra dimensions*, Phys.Rev. **D66** (2002), 015009, hep-ph/0201300.

[30] H.-C. Cheng, K. T. Matchev, and M. Schmaltz, *Bosonic supersymmetry? Getting fooled at the CERN LHC*, Phys.Rev. **D66** (2002), 056006, hep-ph/0205314.

[31] C. D. Carone, J. M. Conroy, M. Sher, and I. Turan, *Universal extra dimensions and Kaluza-Klein bound states*, Phys.Rev. **D69** (2004), 074018, hep-ph/0312055.

[32] G. Bhattacharyya, P. Dey, A. Kundu, and A. Raychaudhuri, *Probing universal extra dimension at the international linear collider*, Phys.Lett. **B628** (2005), 141–147, hep-ph/0502031.

[33] B. Bhattacherjee and A. Kundu, *The International linear collider as a Kaluza-Klein factory*, Phys.Lett. **B627** (2005), 137–144, hep-ph/0508170.

[34] J. A. Cembranos, J. L. Feng, and L. E. Strigari, *Exotic Collider Signals from the Complete Phase Diagram of Minimal Universal Extra Dimensions*, Phys.Rev. **D75** (2007), 036004, hep-ph/0612157.

[35] B. Bhattacherjee and A. Kundu, *Production of Higgs boson excitations of universal extra dimension at the large hadron collider*, Phys.Lett. **B653** (2007), 300–306, 0704.3340.

[36] B. Bhattacherjee, A. Kundu, S. K. Rai, and S. Raychaudhuri, *Universal Extra Dimensions, Radiative Returns and the Inverse Problem at a Linear e+e- Collider*, Phys.Rev. **D78** (2008), 115005, 0805.3619.

[37] P. Konar, K. Kong, K. T. Matchev, and M. Perelstein, *Shedding Light on the Dark Sector with Direct WIMP Production*, New J.Phys. **11** (2009), 105004, 0902.2000.

[38] S. Matsumoto, J. Sato, M. Senami, and M. Yamanaka, *Productions of second Kaluza-Klein gauge bosons in the minimal universal extra dimension model at LHC*, Phys.Rev. **D80** (2009), 056006, 0903.3255.

[39] G. Bhattacharyya, A. Datta, S. K. Majee, and A. Raychaudhuri, *Exploring the Universal Extra Dimension at the LHC*, Nucl.Phys. **B821** (2009), 48–64, 0904.0937.

[40] P. Bandyopadhyay, B. Bhattacherjee, and A. Datta, *Search for Higgs bosons of the Universal Extra Dimensions at the Large Hadron Collider*, JHEP **1003** (2010), 048, 0909.3108.

[41] D. Choudhury, A. Datta, and K. Ghosh, *Deciphering Universal Extra Dimension from the top quark signals at the CERN LHC*, JHEP **1008** (2010), 051, 0911.4064.

[42] B. Bhattacherjee and K. Ghosh, *Search for the minimal universal extra dimension model at the LHC with $\sqrt{s}$=7 TeV*, Phys.Rev. **D83** (2011), 034003, 1006.3043.

[43] H. Murayama, M. M. Nojiri, and K. Tobioka, *Improved discovery of a nearly degenerate model: MUED using MT2 at the LHC*, Phys.Rev. **D84** (2011), 094015, 1107.3369.

[44] T. Appelquist, H.-C. Cheng, and B. A. Dobrescu, *Bounds on universal extra dimensions*, Phys.Rev. **D64** (2001), 035002, hep-ph/0012100.

[45] B. A. Dobrescu and E. Ponton, *Chiral compactification on a square*, JHEP **0403** (2004), 071, hep-th/0401032.

[46] G. Burdman, B. A. Dobrescu, and E. Ponton, *Six-dimensional gauge theory on the chiral square*, JHEP **0602** (2006), 033, hep-ph/0506334.

[47] R. N. Mohapatra and A. Perez-Lorenzana, *Neutrino mass, proton decay and dark matter in TeV scale universal extra dimension models*, Phys.Rev. **D67** (2003), 075015, hep-ph/0212254.

[48] N. Maru, T. Nomura, J. Sato, and M. Yamanaka, *Higgs Production via Gluon Fusion in a Six Dimensional Universal Extra Dimension Model on S**2/Z(2)*, Eur.Phys.J. **C66** (2010), 283–287, 0905.4554.

[49] K. Nishiwaki, K.-y. Oda, N. Okuda, and R. Watanabe, *A Bound on Universal Extra Dimension Models from up to 2fb-1 of LHC Data at 7TeV*, Phys.Lett. **B707** (2012), 506–511, 1108.1764.

[50] K. Nishiwaki, K.-y. Oda, N. Okuda, and R. Watanabe, *Heavy Higgs at Tevatron and LHC in Universal Extra Dimension Models*, Phys.Rev. **D85** (2012), 035026, 1108.1765.

[51] G. Cacciapaglia, A. Deandrea, and J. Llodra-Perez, *A Dark Matter candidate from Lorentz Invariance in 6D*, JHEP **1003** (2010), 083, 0907.4993.

[52] H. Dohi and K.-y. Oda, *Universal Extra Dimensions on Real Projective Plane*, Phys.Lett. **B692** (2010), 114–120, 1004.3722.

[53] B. A. Dobrescu and E. Poppitz, *Number of fermion generations derived from anomaly cancellation*, Phys.Rev.Lett. **87** (2001), 031801, hep-ph/0102010.

[54] G. Burdman, B. A. Dobrescu, and E. Ponton, *Resonances from two universal extra dimensions*, Phys.Rev. **D74** (2006), 075008, hep-ph/0601186.

[55] B. A. Dobrescu, K. Kong, and R. Mahbubani, *Leptons and photons at the LHC: Cascades through spinless adjoints*, JHEP **0707** (2007), 006, hep-ph/0703231.

[56] K. Ghosh and A. Datta, *Phenomenology of spinless adjoints in two Universal Extra Dimensions*, Nucl.Phys. **B800** (2008), 109–126, 0801.0943.

[57] K. Ghosh and A. Datta, *Probing two Universal Extra Dimensions at International Linear Collider*, Phys.Lett. **B665** (2008), 369–373, 0802.2162.

[58] K. Ghosh, *Probing two Universal Extra Dimension model with leptons and photons at the LHC and ILC*, JHEP **0904** (2009), 049, 0809.1827.

[59] D. Choudhury, A. Datta, D. K. Ghosh, and K. Ghosh, *Exploring two Universal Extra Dimensions at the CERN LHC*, JHEP **1204** (2012), 057, 1109.1400.

[60] G. Cacciapaglia, A. Deandrea, and J. Llodra-Perez, *The Universal Real Projective Plane: LHC phenomenology at one Loop*, JHEP **1110** (2011), 146, 1104.3800.

[61] G. Cacciapaglia, R. Chierici, A. Deandrea, L. Panizzi, S. Perries, et al., *Four tops on the real projective plane at LHC*, JHEP **1110** (2011), 042, 1107.4616.

[62] G. Cacciapaglia and B. Kubik, *Even tiers and resonances on the Real Projective Plane*, JHEP **1302** (2013), 052, 1209.6556.

[63] G. Cacciapaglia, A. Deandrea, J. Ellis, J. Marrouche, and L. Panizzi, *LHC Missing-Transverse-Energy Constraints on Models with Universal Extra Dimensions*, (2013), 1302.4750.

[64] B. Bhattacherjee, *Universal extra dimension: Violation of Kaluza-Klein parity*, Phys.Rev. **D79** (2009), 016006, 0810.4441.

[65] N. Haba, K.-y. Oda, and R. Takahashi, *Top Yukawa Deviation in Extra Dimension*, Nucl.Phys. **B821** (2009), 74–128, 0904.3813.

[66] S. C. Park and J. Shu, *Split Universal Extra Dimensions and Dark Matter*, Phys.Rev. **D79** (2009), 091702, 0901.0720.

[67] T. Kakuda, K. Nishiwaki, K.-y. Oda, and R. Watanabe, *Universal extra dimensions after Higgs discovery*, Phys.Rev. **D88** (2013), 035007, 1305.1686.

[68] C. Froggatt and H. B. Nielsen, *Standard model criticality prediction: Top mass 173 +- 5-GeV and Higgs mass 135 +- 9-GeV*, Phys.Lett. **B368** (1996), 96–102, hep-ph/9511371.

[69] G. Degrassi, S. Di Vita, J. Elias-Miro, J. R. Espinosa, G. F. Giudice, et al., *Higgs mass and vacuum stability in the Standard Model at NNLO*, JHEP **1208** (2012), 098, 1205.6497.

[70] Y. Hamada, H. Kawai, and K.-y. Oda, *Bare Higgs mass and potential at ultraviolet cutoff*, (2013), 1305.7055.

[71] G. Bhattacharyya, S. Goswami, and A. Raychaudhuri, *Power law enhancement of neutrino mixing angles in extra dimensions*, Phys.Rev. **D66** (2002), 033008, hep-ph/0202147.

[72] F. J. Petriello, *Kaluza-Klein effects on Higgs physics in universal extra dimensions*, JHEP **0205** (2002), 003, hep-ph/0204067.

[73] The ATLAS Collaboration, *ATLAS-CONF-2013-012 (2013)*.

[74] The ATLAS Collaboration, *ATLAS-CONF-2013-013 (2013)*.

[75] The ATLAS Collaboration, *ATLAS-CONF-2013-030 (2013)*.

[76] The CMS Collaboration, *CMS PAS HIG-13-002 (2013)*.

[77] The CMS Collaboration, *CMS PAS HIG-13-003 (2013)*.

[78] M. E. Peskin and T. Takeuchi, *A New constraint on a strongly interacting Higgs sector*, Phys.Rev.Lett. **65** (1990), 964–967.

[79] M. E. Peskin and T. Takeuchi, *Estimation of oblique electroweak corrections*, Phys.Rev. **D46** (1992), 381–409.

[80] P. W. Higgs, *Broken symmetries, massless particles and gauge fields*, Phys.Lett. **12** (1964), 132–133.

[81] T. Cheng, E. Eichten, and L.-F. Li, *Higgs Phenomena in Asymptotically Free Gauge Theories*, Phys.Rev. **D9** (1974), 2259.

[82] D. J. Gross and F. Wilczek, *Ultraviolet Behavior of Nonabelian Gauge Theories*, Phys.Rev.Lett. **30** (1973), 1343–1346.

[83] ATLAS Collaboration, *Combined measurements of the mass and signal strength of the Higgs-like boson with the ATLAS detector using up to 25 fb^{-1} of proton-proton collision data*, (2013).

[84] T. A. collaboration, *Combination of ATLAS and CMS results on the mass of the top-quark using up to 4.9 fb^{-1} of $\sqrt{s} = 7$ TeV LHC data*, (2013).

[85] Tevatron Electroweak Working Group, CDF Collaboration, D0 Collaboration, M. Muether and CDF, *Combination of CDF and DO results on the mass of the top quark using up to 8.7 fb^{-1} at the Tevatron*, (2013), 1305.3929.

[86] S. Alekhin, A. Djouadi, and S. Moch, *The top quark and Higgs boson masses and the stability of the electroweak vacuum*, Phys.Lett. **B716** (2012), 214–219, 1207.0980.

[87] M. Baak, M. Goebel, J. Haller, A. Hoecker, D. Kennedy, et al., *The Electroweak Fit of the Standard Model after the Discovery of a New Boson at the LHC*, Eur.Phys.J. **C72** (2012), 2205, 1209.2716.

[88] S. R. Coleman and E. J. Weinberg, *Radiative Corrections as the Origin of Spontaneous Symmetry Breaking*, Phys.Rev. **D7** (1973), 1888–1910.

[89] P. P. Giardino, K. Kannike, M. Raidal, and A. Strumia, *Is the resonance at 125 GeV the Higgs boson?*, Phys.Lett. **B718** (2012), 469–474, 1207.1347.

[90] J. Drees, *Review of final LEP results, or, A Tribute to LEP*, Int.J.Mod.Phys. **A17** (2002), 3259–3283, hep-ex/0110077.

[91] R. Sekhar Chivukula, S. Di Chiara, R. Foadi, and E. H. Simmons, *The Limits of Custodial Symmetry*, Phys.Rev. **D80** (2009), 095001, 0908.1079.

[92] R. A. Diaz and R. Martinez, *The Custodial symmetry*, Rev.Mex.Fis. **47** (2001), 489–492, hep-ph/0302058.

[93] N. Arkani-Hamed, S. Dimopoulos, and G. Dvali, *The Hierarchy problem and new dimensions at a millimeter*, Phys.Lett. **B429** (1998), 263–272, hep-ph/9803315.

[94] L. Randall and R. Sundrum, *A Large mass hierarchy from a small extra dimension*, Phys.Rev.Lett. **83** (1999), 3370–3373, hep-ph/9905221.

[95] K. R. Dienes, E. Dudas, and T. Gherghetta, *Extra space-time dimensions and unification*, Phys.Lett. **B436** (1998), 55–65, hep-ph/9803466.

[96] K. R. Dienes, E. Dudas, and T. Gherghetta, *Grand unification at intermediate mass scales through extra dimensions*, Nucl.Phys. **B537** (1999), 47–108, hep-ph/9806292.

[97] Particle Data Group, J. Beringer et al., *Review of Particle Physics (RPP)*, Phys.Rev. **D86** (2012), 010001.

[98] G. Bhattacharyya, A. Datta, S. K. Majee, and A. Raychaudhuri, *Power law blitzkrieg in universal extra dimension scenarios*, Nucl.Phys. **B760** (2007), 117–127, hep-ph/0608208.

[99] A. Cornell and L.-X. Liu, *Scaling of the Higgs Self-coupling and bounds on the Extra Dimension*, Phys.Rev. **D84** (2011), 036002, 1105.1132.

[100] M. Blennow, H. Melbeus, T. Ohlsson, and H. Zhang, *RG running in a minimal UED model in light of recent LHC Higgs mass bounds*, Phys.Lett. **B712** (2012), 419–424, 1112.5339.

[101] A. Datta and S. Raychaudhuri, *Vacuum Stability Constraints and LHC Searches for a Model with a Universal Extra Dimension*, Phys.Rev. **D87** (2013), 035018, 1207.0476.

[102] T. Ohlsson and S. Riad, *Running of Neutrino Parameters and the Higgs Self-Coupling in a Six-Dimensional UED Model*, Phys.Lett. **B718** (2013), 1002–1007, 1208.6297.

[103] M. Blennow, H. Melbeus, T. Ohlsson, and H. Zhang, *Renormalization Group Running of the Neutrino Mass Operator in Extra Dimensions*, JHEP **1104** (2011), 052, 1101.2585.

[104] A. Cornell and L.-X. Liu, *Evolution of the CKM Matrix in the Universal Extra Dimension Model*, Phys.Rev. **D83** (2011), 033005, 1010.5522.

[105] F. Jegerlehner, M. Y. Kalmykov, and B. A. Kniehl, *On the difference between the pole and the MSbar masses of the top quark at the electroweak scale*, (2012), 1212.4319.

[106] The CMS Collaboration, *CMS PAS HIG-13-001 (2013)*.

[107] T. Abe, R. Kitano, Y. Konishi, K.-y. Oda, J. Sato, et al., *Minimal Dilaton Model*, Phys.Rev. **D86** (2012), 115016, 1209.4544.

[108] K. Nishiwaki, *Higgs production and decay processes via loop diagrams in various 6D Universal Extra Dimension Models at LHC*, JHEP **1205** (2012), 111, 1101.0649.

[109] H.-C. Cheng, K. T. Matchev, and M. Schmaltz, *Radiative corrections to Kaluza-Klein masses*, Phys.Rev. **D66** (2002), 036005, hep-ph/0204342.

[110] T. Flacke, D. Hooper, and J. March-Russell, *Improved bounds on universal extra dimensions and consequences for LKP dark matter*, Phys.Rev. **D73** (2006), 095002, hep-ph/0509352.

[111] I. Gogoladze and C. Macesanu, *Precision electroweak constraints on Universal Extra Dimensions revisited*, Phys.Rev. **D74** (2006), 093012, hep-ph/0605207.

[112] T. Kakuda, K. Nishiwaki, K.-y. Oda, N. Okuda, and R. Watanabe, *Higgs at ILC in Universal Extra Dimensions in Light of Recent LHC Data*, (2012), 1202.6231.

[113] Higgs Working Group of the Extended ECFA/DESY Study, K. Desch, *Higgs boson precision studies at a linear collider*, (2003), hep-ph/0311092.

[114] S. Heinemeyer, S. Kanemura, H. Logan, A. Raspereza, T. M. Tait, et al., *Toward high precision higgs-boson measurements at the international linear e+ e- collider*, (2005), hep-ph/0511332.

[115] T. L. Barklow, *Higgs coupling measurements at a 1-TeV linear collider*, (2003), hep-ph/0312268.

[116] G. Passarino and M. Veltman, *One Loop Corrections for e+ e- Annihilation Into mu+ mu- in the Weinberg Model*, Nucl.Phys. **B160** (1979), 151.